UNIVERSITAT POLITÈCNICA DE CATALUNYA BARCELONATECH

PhD program in Geotechnical Engineering

Monitoring and analysis of soil-vegetation-atmosphere interactions at slope and catchment scale

Implications for mass-wasting in natural and man-made slopes

Doctoral thesis by:

Raül Oorthuis Gómez

Thesis advisors:

Marcel Hürlimann and Jean Vaunat

Department of Civil and Environmental Engineering

Division of Geotechnical Engineering and Geosciences

Universitat Politècnica de Catalunya

Barcelona, April 2022

ABSTRACT

Slope mass-wasting (SMW) due to shallow landslides or debris flows is one of the most important erosional processes in many mountainous regions together with surficial erosion by rainfall runoff. These erosive processes cause great socio-economic and environmental impacts. SMW is affected by soil-vegetation-atmosphere (SVA) interactions and is mainly triggered by climatic actions such as rainfall. SVA interactions involve many factors (e.g. soil type, slope topography, slope hydrological conditions and cover (e.g. bare or vegetated)) that are closely linked to slope thermo-hydro-mechanical response, and hence, to slope stability and erosion. The main aim of this work is to improve the knowledge on SVA interactions through two monitoring systems at slope and catchment scale.

At slope scale, an embankment divided in four partitions with North and South orientations and bare/vegetated slopes in each orientation has been monitored. This work has analyzed four years (2017-2020) of soil hydro-thermal and atmospheric parameters related to SVA interactions. The results show that vegetation increases rainfall infiltration, which suggests a decrease in runoff. In addition, vegetation transpiration increases soil drying rates and states, which favors slope stability. Regarding the thermal response, orientation plays an important role with higher temperatures on the South slopes. However, vegetation diminishes the incidence of solar radiation, which reduces soil heat flux up to 75% on the South-facing slopes, and hence, reduces evaporation and daily temperature fluctuations. Nevertheless, the effect of vegetation transpiration is more important than orientation in developing drier soil conditions. This is clearly observed by comparing the drying rates and hydrologic conditions of the North-vegetated slope, which are higher and dryer, with those of the South-bare slope, which are lower and wetter. The results show that vegetation has effects on the hydrologic and thermal response of slopes that may be positive or negative for SMW.

At catchment scale, a monitoring system for torrential flows (debris flows and debris floods) detection and characterization has been maintained and further developed in the

Rebaixader catchment (Central Pyrenees). 12 years of rainfall and torrential flows occurrence (2009-2020) and 8 years of soil hydrological parameters (2013-2020) have been analyzed to characterize both hydrological soil conditions and rainfall characteristics necessary for torrential flows triggering. Most torrential flows are triggered by short duration (<3 hours) and high intensity (4-10 mm in 5 minutes) rainfalls. Furthermore, the rainfall intensity for torrential flow initiation must be higher when the soil is dryer, and vice versa. First, rainfall thresholds based on rainfall mean intensity (I_{mean}) and maximum intensity (I_{max}) are defined by means of Receiver Operating Characteristics and Precision-Recall curves. The I_{mean} threshold predicted 2 false negatives and 73 false positives for the 2013-2020 dataset, which includes 15 torrential flow events. This results in a low precision of 15%, since only 13 torrential flow out of 86 issued alarms are correctly predicted. Contrarily, the best I_{max} threshold reduced the false positives to 11 and predicted also 2 false negatives, increasing the precision to 54%. Then, the hydro-meteorological thresholds were defined by combining I_{max} and volumetric water content. The best hydro-meteorological threshold reduced the false positives to 8 and the false negatives to 1, increasing the precision to 63%. This confirms that soil hydrological conditions play an important role in torrential flows triggering and may improve early warning predictions.

This work significantly contributed to improve our understanding on SVA interactions and its coupling with slope thermo-hydro-mechanical response, which is strongly related to SMW, by means of in-situ monitoring at slope and catchment scale.

RESUMEN

La pérdida de suelo en laderas (PSL) por deslizamientos de tierra superficiales o corrientes de derrubios es uno de los procesos erosivos más importantes en muchas regiones montañosas junto con la erosión superficial por escorrentía de lluvia. Estos procesos provocan grandes impactos socioeconómicos y ambientales. Las interacciones suelo-vegetación-atmósfera (SVA) afectan a la PSL y se desencadena principalmente por acciones climáticas como la lluvia. Las interacciones SVA implican muchos factores (tipo de suelo, topografía del talud, condiciones hidrológicas y de cubierta (desnuda o vegetada) del talud, etc.) estrechamente relacionados con la respuesta termo-hidromecánica del talud y, por tanto, con su estabilidad y erosión. El objetivo principal es mejorar el conocimiento de las interacciones SVA con dos sistemas de monitorización a escala de talud y de cuenca.

A escala de talud se ha instrumentado un terraplén dividido en 4 partes orientadas al norte y al sur y con un talud con cubierta vegetada y desnuda en cada orientación. Se han analizado cuatro años (2017-2020) de parámetros atmosféricos e hidrotermales del suelo relacionados con interacciones SVA. Los resultados muestran que la vegetación aumenta la infiltración de la lluvia, lo que sugiere una disminución de la escorrentía. Además, la transpiración de la vegetación aumenta las tasas y el estado de secado del suelo, lo que favorece la estabilidad del talud. En cuanto a la respuesta termal, la orientación es importante con temperaturas más elevadas en los taludes sur. Sin embargo, la vegetación disminuye la incidencia de radiación solar reduciendo así el flujo de calor en el suelo hasta un 75% en los taludes sur y disminuyendo la evaporación y las oscilaciones de temperatura diarias. Sin embargo, el efecto de la transpiración de la vegetación es más importante que el de la orientación en el desarrollo de condiciones de suelo más secas. Esto se observa claramente al comparar las tasas de secado y las condiciones hidrológicas del talud norte vegetado, más elevadas y secas, con las del sur no vegetado, más bajas y húmedas. Los resultados demuestran que la vegetación tiene efectos en la respuesta hidro-termal de la ladera que pueden ser positivos o negativos para la PSL.

A escala de cuenca se ha mantenido y mejorado la instrumentación para detectar y caracterizar flujos torrenciales en la cuenca del Rebaixader (Pirineo Central). Se han analizado 12 años de ocurrencia de flujos torrenciales y de lluvia (2009-2020) y 8 años de parámetros hidrológicos del suelo (2013-2020) para definir tanto las condiciones hidrológicas del suelo como las de lluvia necesarias para desencadenar estos flujos. La mayoría de flujos torrenciales se desencadenan por lluvias de corta duración (< 3 horas) y de alta intensidad (4-10 mm en 5 minutos). Además, la intensidad de lluvia para iniciar un flujo torrencial es mayor cuando el suelo está más seco, y viceversa. Primeramente se han definido umbrales de lluvia basados en intensidad media (I_{mean}) y máxima (I_{max}) de lluvia con las curvas de Característica Operativa del Receptor (ROC) y de Precisión-Exhaustividad. El umbral de I_{mean} predice 2 falsos negativos y 73 falsos positivos para el conjunto de datos 2013-2020, que incluye 15 flujos torrenciales. Esto representa una precisión baja del 15%, puesto que sólo se prevén correctamente 13 flujos torrenciales de las 86 alarmas emitidas. Por el contrario, el mejor umbral I_{max} reduce los falsos positivos a 11 y también predice 2 falsos negativos, aumentando la precisión al 54%. A continuación se han definido umbrales hidro-meteorológicos combinando I_{max} y contenido volumétrico de agua. El mejor umbral hidro-meteorológico reduce los falsos positivos a 8 y los falsos negativos a 1, lo que aumenta la precisión al 63%. Esto confirma que las condiciones hidrológicas del suelo juegan un papel importante en el desencadenamiento de flujos torrenciales y pueden mejorar las predicciones de alerta temprana.

Este trabajo ha contribuido significativamente a mejorar la comprensión de las interacciones SVA y su acoplamiento con la respuesta termo-hidro-mecánica del talud, fuertemente relacionada con la PSL, mediante la monitorización in-situ a escala de talud y a escala de cuenca.

RESUM

La pèrdua de sòl en vessants (PSV) per lliscaments de terra superficials o corrents d'arrossegalls és un dels processos erosius més importants a moltes regions muntanyoses junt amb l'erosió superficial per escorrentia de pluja. Aquests processos provoquen grans impactes socioeconòmics i ambientals. Les interaccions sòl-vegetació-atmosfera (SVA) afecten la PSV i es desencadena principalment per accions climàtiques com ara la pluja. Les interaccions SVA impliquen molts factors (tipus de sòl, topografia del talús, condicions hidrològiques i de coberta (nues o vegetades)del talús, etc.) estretament relacionats amb la resposta termo-hidro-mecànica del talús i, per tant, amb la seva estabilitat i erosió. L'objectiu principal és millorar el coneixement de les interaccions SVA amb dos sistemes de monitorització a escala de talús i de conca.

A escala de talús s'ha instrumentat un terraplè dividit en 4 parts orientades al nord i al sud i amb un talús amb coberta vegetada i nua a cada orientació. S' han analitzat quatre anys (2017-2020) de paràmetres atmosfèrics i hidro-termals del sòl relacionats amb interaccions SVA. Es veu que la vegetació augmenta la infiltració de la pluja, suggerint una disminució de l'escorrentia. A més, la transpiració de la vegetació augmenta les taxes i l'estat d'assecat del sòl, el que afavoreix l'estabilitat del talús. Pel que fa a la resposta termal, l'orientació és important amb temperatures més elevades als talussos sud. Tanmateix, la vegetació disminueix la incidència de radiació solar reduint així el flux de calor al sòl fins un 75% als talussos sud i disminuint l'evaporació i les oscil·lacions de temperatura diàries. Tot i això, l'efecte de la transpiració de la vegetació és més important que el de l'orientació per desenvolupar condicions de sòl més seques. Això s'observa comparant les taxes d'assecatge i condicions hidrològiques del talús nord vegetat, més elevades i seques, amb les del sud no vegetat, més baixes i humides. Els resultats mostren que la vegetació té efectes en la resposta hidro-termal dels vessants que poden ser positius o negatius per la PSV.

A escala de conca s'ha mantingut i millorat la instrumentació per detectar i caracteritzar fluxos torrencials a la conca del Rebaixader (Pirineu Central). S'han analitzat 12 anys d'ocurrència de fluxos torrencials i de pluja (2009-2020) i 8 anys de paràmetres hidrològics del sòl (2013-2020) per caracteritzar tant les condicions hidrològiques del sòl com les de pluja necessàries per desencadenar aquests fluxos. La majoria de fluxos torrencials es desencadenen per pluges curtes (< 3 hores) i d'alta intensitat (4-10 mm en 5 minuts). A més, la intensitat de pluja per iniciar un flux torrencial és més elevada quan el sòl està més sec, i viceversa. Primerament s'han definit llindars de pluja basats en intensitat mitja (I_{mean}) i màxima (I_{max}) de pluja amb les corbes de rendiment diagnòstic (ROC) i de Precisió-Reclam. El llindar d' I_{mean} prediu 2 falsos negatius i 73 falsos positius per al conjunt de dades 2013-2020, que inclou 15 fluxos torrencials. Això representa una precisió baixa del 15%, ja que només es preveuen correctament 13 fluxos torrencials de 86 alarmes emeses. En canvi, el millor llindar I_{max} redueix els falsos positius a 11 i també prediu 2 falsos negatius, augmentant la precisió al 54%. A continuació s'han definit llindars hidro-meteorològics combinant I_{max} i contingut volumètric d'aigua. El millor llindar hidro-meteorològic redueix els falsos positius a 8 i els falsos negatius a 1, augmentant la precisió al 63%. Això confirma que les condicions hidrològiques del sòl juguen un paper important en el desencadenament de fluxos torrencials i poden millorar les prediccions d'alerta primerenca.

Aquest treball ha contribuït significativament a millorar la comprensió de les interaccions SVA i el seu acoblament amb la resposta termo-hidro-mecànica del talús, fortament relacionada amb la PSV, mitjançant monitorització a escala de talús i de conca.

ACKNOWLEDGMENTS

Vull agrair l'ajuda a totes les persones que durant el transcurs i desenvolupament de la tesi doctoral han estat al meu costat, d'una manera o altra. Gràcies a tots vosaltres per ajudar-me en els bons moments, però sobretot per ajudar-me durant els moments més difícils.

M'agradaria donar les meves sinceres gràcies als meus tutors, el Marcel Hürlimann i el Jean Vaunat, per haver-me guiat tan bé durant aquests anys. Gràcies a la vostra paciència i als bons consells que m'heu donat he aprés a ser més rigorós a l'hora d'analitzar un problema, i sobretot a no donar les coses per fetes. Gràcies també als dos per ajudar-me a centrar en aquells moments en els que semblava que perdia una mica el nord o el fil de la tesi, això m'ha permès finalitzar-la en bon port. Marcel, gràcies per ensenyar-me aquest món de la recerca, m'ha encantat, però sobretot per voler compartir sempre la teva experiència i vivències. N'he après, i molt. També per ensenyar-me el que era el món del treball de camp, portant-me a la muntanya, i haver-me permès ajudar-vos en questa tasca que m'omplia tant. Jean, gràcies a tu he après a ser molt més clar, sobretot a la hora d'expressar conceptes i resultats a simple vista complicats. Les teves aportacions sempre han estat excel·lents i m'han ajudat molt a ser més precís a l'hora de treure conclusions i a millorar la tesi en general.

Vull donar les gràcies en especial als meus pares, Ángeles i Felix, i a la meva germana Marina, per donar-me sempre suport i aguantar-me, sobretot en el transcurs d'aquest darrer any i quan semblava que no podria acabar. També a tots els meus amics del dia a dia i fora de l'àmbit de la universitat, per haver aguantat les meves xapes i mogudes.

Vull agrair també el finançament rebut per part dels projectes SMUCPHY i EROSLOP i del contracte predoctoral FPI, que m'han permès desenvolupar aquesta tesi doctoral durant aquests anys.

També vull anomenar especialment els membres i amics del projecte SMUCPHY i EROSLOP, per tots aquells moments que hem pogut compartir plegats: al Toni Lloret, al

José Moya, a l'Alessandro Fraccica, a la Càrol Puig-Polo, Vicente Medina, i per descomptat el Jean Vaunat i el Marcel Hürlimann. Gràcies Toni per haver-me endinsat en aquest món de la recerca al final del Màster en Geotècnia iper parlar-me dels contractes predoctorals FPI., a banda dels coneixements que sempre m'has transmès. Segurament sense tu no hagués començat ni conegut realment el que és la recerca, moltes gràcies Toni. José, gràcies per totes les converses que hem tingut durant aquesta tesi (i no sempre sobre recerca), per "perdre" el teu temps en ensenyar-me tot allò que consideraves que em podia ser útil. José, tampoc oblidaré els bons moments treballant a Senet, amb totes les qüestions tècniques (i no tant tècniques) que poc a poc anàvem resolent, i les dificultats afegides que comporta treballar a l'alta muntanya. Alessandro, ha sigut un plaer conèixer-te i poder treballar plegats en aquest projecte, per les sortides a Agròpolis i pels dinars que fèiem plegats i on compartíem els problemes que anaven sorgint durant la tesi. Càrol, gràcies per estar-hi sempre, preguntant-me si tenia alguna dificultat, per interessar-te en com m'anava i voler-me ajudar. Vicente, moltes gràcies per la teva simpatia, per preocupar-te per com avançava la tesis i pels consells que m'has donat. Tampoc em puc oblidar de la Nieves Lantada, que junt amb la Càrol m'ha fet passar molts bons moments, per exemple fent aixecaments topogràfics o escanejos LASER en llocs més o menys complicats. Gràcies Nieves per confiar en mi, per fer-me sentir sempre còmode treballant amb tu, i per haver-me ofert la possibilitat de col·laborar amb vosaltres en el projecte ROCKMODELS. D'igual manera no em puc oblidar del Jordi Corominas, també he aprés molt amb tu i has sigut un referent. També a la Marta Gonzalez i al Jordi Pinyol de l'ICGC, al Joan Martínez de Geomar, al Felipe Buill de la UPC, i al Miquel Massip del Parc UPC Agròpolis. Amb tot ells he pogut compartir xerrades, excursions, conferències i/o dinars, etc. Gràcies a tots!

Gràcies a tots els companys i amics de la UPC que no he anomenat abans i que he conegut durant la tesi doctoral, i amb els que he compartit moltes converses i bones experiències. Sense vosaltres aquests anys no haguessin sigut tant amens!: Gerard Matas, Roger Ruiz, Abdallah Najdi, Stefano Collico, Rosa Mª Palau, Ferran Parera, Clàudia Abancó, Agustín Cuadrado, Riccardo Rorato, David Encalada, Lluís Saló-Salgado, Gaia Di Carluccio, Ningning Zhang, Lu He, Arisleidy Mesa Alcantara, Jattna Sánchez, Clara Alvarado i Miquel. Espero no deixar-me ningú. També a tota la gent del Departament d'Enginyeria Civil i

Ambiental que m'han ajudat amb temes administratius, amb problemes tècnics o amb temes generals de la recerca.

Per últim, no oblidaré mai les sortides per fer recerca al Pirineu i Prepirineu, amb els seus trajectes amb el Nissan, el material que traginàvem, tota la logística, la meteorologia que no sempre ens deixava fer la feina amb comoditat, els problemes tècnics que sempre sorgien "d'imprevist"... però sobretot per la satisfacció que em generava sempre aquest treball. He gaudit molt amb l'oportunitat d'haver treballat en aquests paratges, per mi, idíl·lics, el que m'ha fet sentir com un privilegiat. Gràcies. En aquest context vull agrair a les Pilis i al Mario per fer-me sentir com a casa quan m'allotjava a l'Hostal Casa Moliné, al poble Aneto, després de treballar tot el dia al barranc del Rebaixader.

TABLE OF CONTENTS

LIST OF FIGURES AND TABLES

CHAPTER 1: INTRODUCTION

CHAPTER 2: MONITORING OF A FULL-SCALE EMBANKMENT EXPERIMENT REGARDING SOIL–VEGETATION–ATMOSPHERE INTERACTIONS

CHAPTER 3: SLOPE ORIENTATION AND VEGETATION EFFECTS ON SOIL THERMO-HYDRAULIC BEHAVIOR. AN EXPERIMENTAL STUDY

Chapter 1
INTRODUCTION

1.1. Motivation

Soil-vegetation-atmosphere (SVA) interactions are important for many natural processes like slope mass-movement or soil erosion. SVA interactions are complex and involve many processes which play an important role in slope stability [Tang et al., 2018]. Both the soil properties, as well as the characteristics of vegetation cover and the atmospheric conditions affect the hydrological slope conditions. Hydrological slope conditions define in turn the slope hydrologic response to precipitation events and its coupling with mechanical effects and initiation of slope mass-movements, which is controlled by SVA interactions.

Slope mass-movements are commonly classified based on the involved materials (rock and soil) and by the type of movement (fall, topple, slide, spread, flow) [Hungr et al., 2014]. Within slide, spread and flow, there exist shallow movement occurring mainly in mountainous regions with steep slopes, both in natural slopes and, sometimes, on man-made slopes like the ones build in transportation infrastructures. These processes, in addition to others such as surficial soil erosion, are referred as slope mass-wasting (SMW) in the present work.

The increase in human activities and settlements in recent years has augmented the number of elements exposed to SMW hazards, which in turn increases the probability of a landslide to cause damage. Although SMW is related to natural processes (mainly triggered by climatic and seismic actions), human interaction can increase the occurrence of these phenomena. Land use change, such as deforestation or vegetation removal, the increase of built up and urbanized areas, fillings and cuts for transportation lines and infrastructures, are some examples of human interaction that may influence the triggering of landslides [van Beek et al., 2008].

In addition, several studies have reported a raise in global temperature and extreme weather events, such as prolonged droughts and increment of severe precipitation episodes, which will increase the triggering and impact of SMW in many regions of the world [IPCC, 2014; Stoffel et al., 2014; Gariano & Guzzetti, 2016]. This raise on average global temperature might increase evaporation and accelerate desertification, especially in arid and semi-arid zones, and consequently may increase SMW [Goyal, 2004].

The socio-economic and environmental impacts of SMW are diverse and with many direct and indirect consequences, such as fatalities, damage to buildings or infrastructures, reduction of reservoirs capacity, loss of agricultural lands due to soil degradation, pollution or change in water quality of rivers and streams, etc. [Schuster & Highland, 2001; Kjekstad & Highland, 2009]. Impacts are not limited to erosion or deposition zone, but can also indirectly affect large areas of territory due to interruption of economic activities and environmental impacts [Remondo et al., 2008; J. Zhang et al., 2021].

The increase in human activities and extreme precipitation events, coupled with limited resources, turns SMW in an important threat for sustainable development and with many environmental and socio-economic implications. Just between 1998 and 2017, landslides affected more than 4.8 million people worldwide and resulted in more than 8 billion US$ in economic losses and circa 18,400 fatalities [Wallemacq, 2018]. Other studies increase the death toll at global scale to 56,000 people in the period 2004-2016 due to 4862 non-seismic landslides, of which 79% where triggered by rainfall [Froude & Petley, 2018].

In any case, in order to reduce the risk and losses, and to promote sustainable mitigation strategies with an efficient use of raw materials and resources, it is necessary to understand the predisposing factors of SMW, as well as the initiation or triggering mechanisms. Thus, it is essential to understand SVA interactions and its coupling with thermo-hydro-mechanical slope response to comprehend the triggering mechanisms and for better assessing the hazards related to SMW. It is evident that there is a coupling of complex processes between the soil-vegetation-atmosphere interface, which deserve to be studied, despite the complexity and scarcity of considering all these processes in modeling and field or laboratory settings.

1.2. Soil-vegetation-atmosphere interactions and slope mass-wasting

Slope mass-wasting (SMW) describes a wide variety of processes that result in the downslope movement of rock, soil, or a combination of earth materials. Depending on the type of movement, SMW can be classified as topple, fall, slide, spread, flow or surficial erosion (Figure 1.1) [Hungr et al., 2014]. Moreover, SMW can be defined as a complex landslide if it combines more than one type of movement.

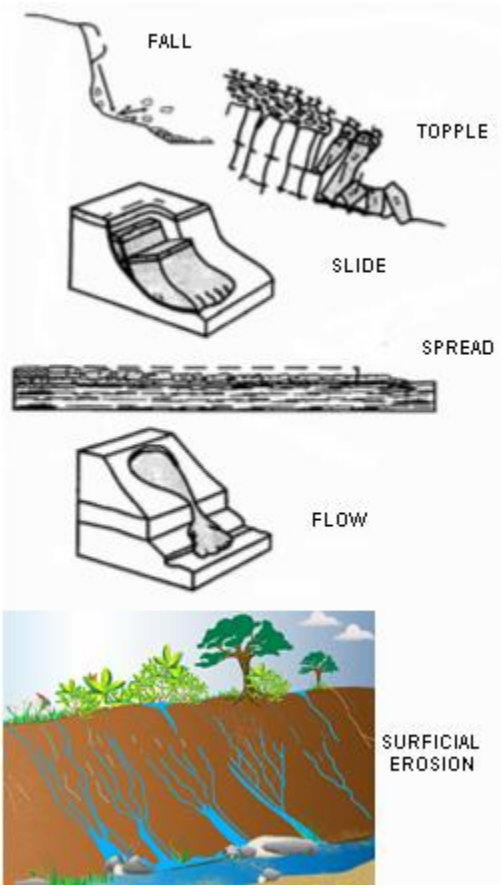

Figure 1.1: Slope mass-wasting (SMW) including landslides and surficial erosion classified by type of movement (modified from Hungr et al. 2014 and Evelpidou 2012). The scale of each diagram can vary from a few meters to hundreds of meters.

SMW is closely related to the hydrological slope conditions, and hence, to SVA interactions, regardless of the precise initiation mechanisms. For instance, a slide occurs when a mass of soil or rocks fails across a rupture surface or weaker layer (usually due to

soil saturation by rainfall infiltration), and moves downslope at slow to high velocities. Slides represent one of the largest, in terms of volume of mobilized mass, and most damaging SMW processes on Earth, like the catastrophic slide event of Vaiont (Italy) in October 1963 which caused more than 2000 causalities [Alonso et al., 2010].

On the other hand, flows are generally mixed loose soils and rocks with abundant water characterized by their extremely rapid velocities, large entrainments, long runout distance, and great impact forces [Iverson, 1997; McDougall, 2017]. These intrinsic characteristics turns flows events into very dangerous mass-wasting phenomena that can lead to devastating consequences. This is the case of the torrential flow event of 1996 in Biescas (Figure 1.2a), which buried a camping site in the Central Pyrenees (Spain) by debris and resulted in almost 100 deaths [Alcoverro et al., 1999]. Another example of a torrential flow that occurred in the Pyrenees was the debris flood on 1 August 2008 between the border of Andorra and Spain (Figure 1.2b). Although there were no fatalities, the border was closed for about 12 hours and both the facilities and parked vehicles were rendered useless.

a)  b) 

Figure 1.2: Large slope mass-wasting events in the Pyrenees. a) Catastrophic debris flow event in Biescas on 8 August 1996 (87 fatalities, source: cope.es). b) Debris flow event between the border of Andorra and Spain on 1 August 2008 (no fatalities, source: Euroconsult).

In addition, surficial erosion involves the detachment, transportation and deposition of soil or geological material by physical forces or erosive agents such as rainfall (raindrop impact and rainfall runoff), water flow, ice, wind, or other natural or anthropogenic factors. Soil erosion by rainfall runoff is one of the most important and widespread mechanisms of erosion in Europe [Olsson et al. 2019], both in natural and engineered slopes. In fact, engineered slopes such as transportation embankments or dams are frequent subjected to erosion due to rainfall runoff flowing from the crest of slopes, which can develop on

temporary or permanently eroded gullies or channels. This is a major problem in man-made or engineered slopes since it directly affects its serviceability and safety [Tang et al., 2018].

Important damage and the associated risk for society due to SMW affected by SVA interactions have been discussed in many studies. For man-made slopes in partially saturated and compacted embankments, increasing soil moisture controlled by SVA interaction is known to have a negative impact on slope stability [Vardon, 2015]. Furthermore, climate interactions such as prolonged drying periods can desiccate and crack clayey embankments, enhancing rainfall infiltration, and consequently jeopardize the embankment stability and serviceability [Dyer et al., 2009; Tang et al., 2018]. Regarding natural slopes, infrastructures and buildings are often threatened by debris flows mainly triggered by intense precipitation and rainfall infiltration controlled by SVA interactions. In order to better understand the triggering mechanisms and better assessing the hazards related to SMW, it is essential to understand SVA interactions and the thermo-hydro-mechanical slope conditions. Figure 1.3 represents a conceptualization of the SVA interactions; note that due the complexity of all the involved interactions some of the processes may be missing.

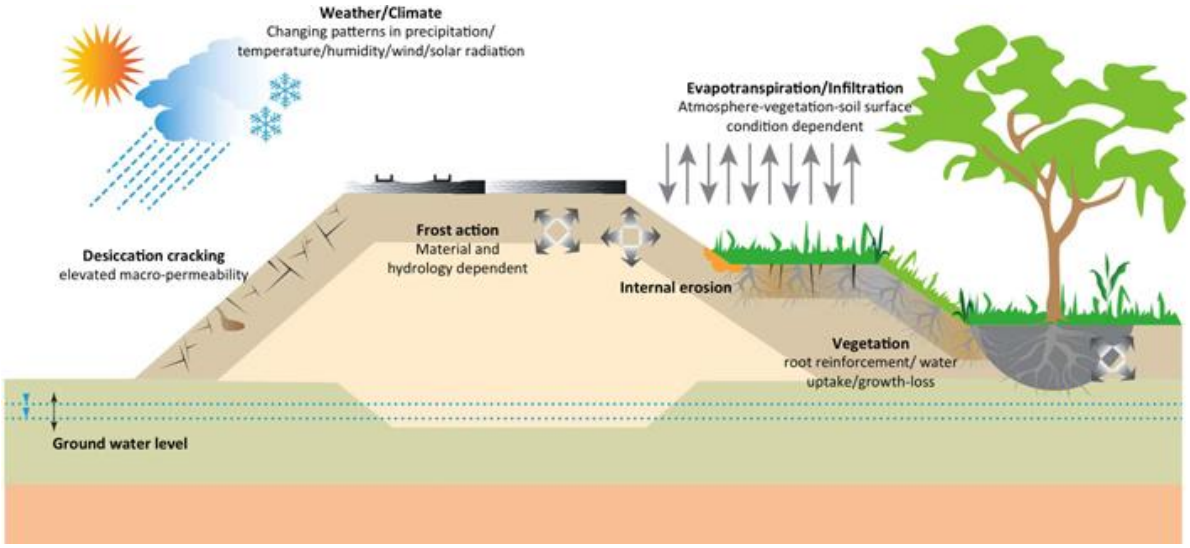

Figure 1.3: Schematic view of the soil–vegetation–atmosphere interactions [Tang et al., 2018].

The physical characteristics that predispose or favor slope instability and erosion are mainly the soil type (e.g. hydraulic conductivity), the hydrological soil conditions of the soil (e.g. moisture content), the slope topography, and the slope cover and land use (bare, vegetated, urbanized, etc.). All these characteristics affect the SVA interactions and are

closely related to the hydrologic slope response, and hence, to its mechanical behavior and subsequent triggering of slope mass-wasting processes. On the one hand, it is known that infiltration capacity decreases with time during a rainfall event as the soil becomes saturated [Horton, 1939; Ran et al., 2012; Kirkham, 2014;]. Therefore, if rainfall intensity exceeds the soil infiltration capacity runoff develops [Xue & Gavin, 2008], which may result in surficial erosion [Ran et al., 2012]. On the other hand, rainfall infiltration into an unsaturated soil decreases the matric suction, which further affects the shear strength and may result in slope instability [Fourie et al., 1999]. If infiltration persists, positive pore water pressures may develop due to increased water level in the soil. This in turn decreases shear strength, which further accentuates the instability of the slope [Gofar & Rahardjo, 2017]. It is worth mentioning that both atmospheric conditions (e.g. relative humidity, temperature and wind velocity) and soil properties (thermal and hydraulic conductivity, soil porosity and vapor diffusivity) influence soil evaporation rates and, therefore, affect the hydrological conditions of the slope and its hydrological response to precipitation [Sakai et al., 2011].

Regarding ground cover, vegetation is known to affect the hydro-mechanical soil conditions and have implications on slope stability. The effects of vegetation on soil hydro-mechanical response are complex and not straightforward, since there can be positive and negative effects regarding slope stability and erosion [Coppin & Richards, 1990; Wu et al., 2015]. Vegetation cover plays an important role in slope stability and its removal may accelerate the erosion rates. For instance, it protects the surface from the kinetic energy of raindrop impacts, which may prevent the detachment of soil particles and downslope erosion by runoff [Kinnell, 2005; Vaezi et al., 2017]. Furthermore, there is consensus about the fact that roots enhances soil mechanical properties by contributing to the shear strength due to root tensile strength [Gray & Barker, 2004; De Baets et al., 2008; Mickovski et al., 2009]. Concerning soil hydrological effects, root-growth can increment or clog the soil pores and therefore its effects on soil porosity, permeability and hydrologic behavior is not straightforward [Hua et al., 2014; Fraccica et al., 2019]. While many studies report an increase of infiltration on vegetated slopes compared to bare slopes (which decreases runoff and hence surficial erosion, whereas increases the probability of slope failure) [Casermeiro et al., 2004; Ludwig et al., 2005; Saco et al., 2007; J. H. Li et al., 2016], others describe lower

infiltration rates [Rahardjo et al., 2014; Garg, Coo, et al., 2015]. On the other hand, plant transpiration is known to accelerate drying rates and increase soil suction, which in turn increases shear strength and enhances slope stability [Simon & Collison, 2002; Greenwood et al., 2004; Pollen-Bankhead & Simon, 2010; Pathirage et al., 2019]. Last but not least, vegetation can intercept solar radiation and decrease the thermal fluxes between soil-atmosphere interface and, hence, evaporation rates and soil hydrologic conditions [Zha et al., 2010; Wang et al., 2018]. Figure 1.4 summarizes some effects of vegetation on the soil regarding SVA interactions.

These examples confirm that the SVA interactions affect the response of the slope to rainfall, and thus the triggering of SMW processes. In front of all these highly coupled input, impervious surfaces or traditional engineering solutions can be unsustainable, costly and difficult to construct compared to solutions based on the use of vegetation at slope surface. Furthermore, these traditional engineering solutions may reduce the infiltration rates and increase both runoff velocity and erosion capacity during heavy rainfalls.

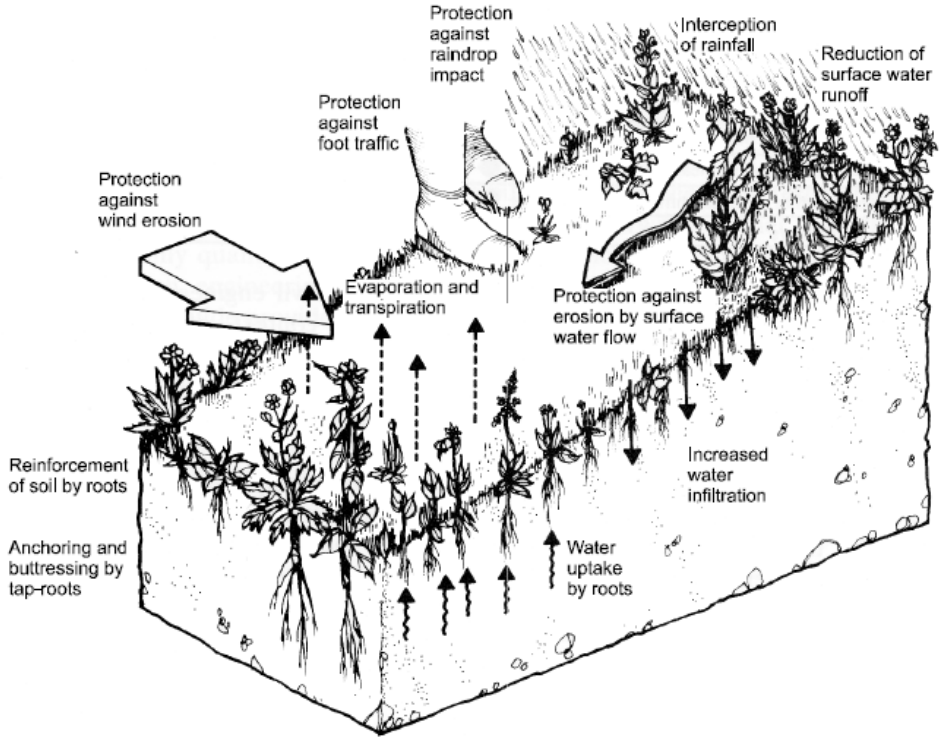

Figure 1.4: Some effects of vegetation on soil-vegetation-atmosphere (SVA) interactions [Coppin & Richards, 1990].

As a summary, SMW triggering mechanisms are mainly driven by climatic actions, where water energy in the form of rainfall plays the most important role [Wieczorek, 1996; Iverson, 2000]. Meteorological or atmospheric factors influencing the initiation of these erosive processes are the type of precipitation (rainfall, snow, etc.), the rainfall intensity, the amount of rainfall and duration, among others. Other meteorological variables such as air temperature, relative humidity, wind, and solar radiation, have direct implications on evapotranspiration and hence on the hydrological soil conditions. Hydrological slope conditions define in turn the slope hydrologic response to precipitation events and its coupling with mechanical effects, which is controlled by soil-vegetation-atmosphere (SVA) interactions. The effects of vegetation on slope hydrologic response and its effects on slope stability are not straightforward. Therefore, understanding the SVA interactions and the thermo-hydro-mechanical slope conditions is crucial for mitigating the risk and losses associated with SMW phenomena.

The hydrological and thermal settings can be obtained principally by field monitoring, remotely sensed, or estimated from models or indirect variables like antecedent rainfall. For example, antecedent or current precipitation may be considered for estimating the hydrologic state of the soil by simple infiltration or hydrological regional models, although this method is not fully reliable since evapotranspiration can play an important role depending on the season, climatology, and other variables such as vegetation cover. Moreover, in recent years the estimation of soil hydrologic state with remote measurements (e.g. satellite measurements of rainfall intensity) has greatly improved, despite the fact of underestimating particularly strong intensity or convective rainstorms compared to direct rain gauge measurements [Hur et al., 2016].

1.3. Monitoring soil-vegetation-atmosphere interactions and slope mass-wasting

Instrumental or in-situ monitoring is a valuable tool for better comprehending SVA interactions and thermo-hydro-mechanical slope response leading to SMW processes. Field monitoring, either at slope or catchment scale, is thus necessary to provide accurate and precise observations on SVA interactions concerning the soil conditions or predisposing

factors for SMW initiation (e.g. pore water pressure, soil moisture) and/or the triggering conditions (e.g. rainfall intensity). Therefore, understanding SVA interactions is especially relevant for the management and maintenance of infrastructure and transportation embankments (cuttings and fillings) [Glendinning et al., 2014; Tang et al., 2018]. Furthermore, it is necessary for minimizing the risk associated with SMW processes, such as rapid mass-movements (e.g. debris flows).

Although remote or satellite techniques and measurements can cover large areas of territory and be very useful for SMW risk assessment at regional scale, they are not as accurate as in-situ slope instrumentation. In addition, frequency or recording rate of remote monitoring is much lower than in-situ instrumentation. For example, rain rate of local or highly convective rainfalls in mountainous regions (at high-altitude), which have an important influence on the triggering processes of SMW [Valenzuela et al., 2018; Rivas et al., 2020], may be underestimated with remote instrumentation techniques [Germann et al., 2006; Brunetti et al., 2018; Sun et al., 2018]. In contrast, field monitoring at smaller scales, at slope and catchment scale, allows characterizing the precise triggering conditions and soil thermo-hydrologic conditions linked to SVA interactions and SMW phenomena.

Field monitoring provides high quality measurements that are essential for the calibration and validation of physical models [Y. J. Cui et al., 2010], which are necessary to simulate SVA interactions and predict SMW phenomena. Furthermore, and besides serving for research purposes, monitoring of in-situ rainfall and/or soil parameters is necessary for the definition of thresholds for SMW initiation based on the recordings of past events. Landslide thresholds are widely used for the definition of early warning and alarm systems (EWASs) in areas where it is necessary to establish alarm or forecast systems for risk reduction. Therefore, monitoring is essential when it comes to alert people or authorities if some critical conditions for landslide initiation are exceeded (e.g. high rainfall intensity), or to early warn people if the conditions for landslide initiation are favorable (e.g. a very high soil moisture or pore water pressure).

Instrumental monitoring systems may focus on different parameters, which depend on the required complexity, the scale to be monitored (regional, catchment or slope), the type of SMW phenomena, among others. Monitoring SVA interactions and SMW processes may

rely on meteorological variables (e.g. mean or peak rainfall intensity), on soil hydrologic (e.g. moisture, pore water pressure) and thermal (temperature, heat flux) variables, ground displacements (e.g. inclinometers, extensometers), flow height (e.g. radar, ultrasound), ground vibrations (e.g. geophones), among others, or with a combination of different approaches. However, the installation and maintenance of systems monitoring SVA interactions can be costly and difficult, especially in mountainous regions, and in the source area of SMW, due to harsh conditions and, sometimes, remote locations.

Last but not least, monitoring and interpretation of soil hydro-thermal parameters require a broader knowledge due to soil heterogeneity, which may complicate obtaining reliable measurements regarding SVA interactions and their coupling with mechanical effects for the initiation of SMW phenomena. In contrast, rainfall monitoring and interpretation is less complex and more widespread compared to more sophisticated monitoring systems based on soil hydro-thermal conditions (e.g. suction, moisture, temperature, etc.), or other parameters such as ground vibration or displacements. This may explain why many approaches to slope stability and SMW phenomena rely on monitoring atmospheric parameters, generally rainfall, and frequently neglect other variables such as the amount of water infiltrating into the soil. Nevertheless, the importance of measuring both rainfall and soil hydrological properties for correctly assessing slope instability and SMW processes, in comparison to stability analysis based exclusively on rainfall parameters, has been widely accepted [Bittelli et al., 2012; Mirus, Becker, et al., 2018].

The elevated number of processes involved in SVA interactions turns instrumental monitoring and the formulation of hydro-thermo-mechanical models capable to relate SVA interactions with the mechanical response of the soil in a complicated task. This is probably why most research focus on soil-atmosphere interactions and studies considering the overall effects of SVA interactions are rather scare. The present research addresses the problem of SVA interactions and SMW based on the integration of information and approaches at two different scales: slope and catchment. For this purpose, long-term monitoring of atmospheric and soil hydro-thermal variables at the source area of SMW is presented and discussed with the aim to gain insight on SVA interactions. In the following we will focus on long-term monitoring at slope (> 4 years) and catchment scale (> 12 years).

1.3.1. Slope scale monitoring

There are several studies monitoring SVA interactions such as soil hydrological (e.g. soil water content, pore-water pressure) and meteorological parameters (e.g. rainfall, air temperature). These studies focus mostly on rainfall infiltration and hydrologic soil response on vegetated natural slopes [Rahardjo, Leong, et al., 2008; Bittelli et al., 2012; Damiano et al., 2012; Cotecchia et al., 2014; Bordoni et al., 2015] and man-made slopes or embankments [A. G. Li et al., 2005; Smethurst et al., 2012; Glendinning et al., 2014]. Other experiments conducted in the laboratory relate rainfall infiltration and slope failure mechanisms, either at full-scale slope experiments [Moriwaki et al., 2004] or model slopes of smaller scale [P. Orense et al., 2004; C.-C. Huang & Yuin, 2010;]. However, these studies do not consider the effects of soil temperature on soil hydrologic conditions, neither the effects of a vegetated slope compared to a bare slope with the same settings.

A small number of studies considers the effects of SVA interactions on slope thermo-hydraulic response over a long-period of time (e.g. more than one year recordings); either on physical experiments [Pagano et al., 2019], full-scale experimental embankments [Y. J. Cui et al., 2005, 2010; Garg, Coo, et al., 2015; Yoshioka et al., 2015; Bicalho et al., 2018] or natural slopes [Enrique et al., 1999; Hemmati et al., 2012; Askarinejad et al., 2018]. Nevertheless, there is a lack of research related to SVA interactions that quantitatively asses the effects of vegetation on slope hydro-thermal response when compared to a bare slope affected by same atmospheric conditions. The monitoring of full-scale embankments is a method to achieve precise and complete observations on SVA interactions related to SMW phenomena. Nevertheless, the design of large embankment experiments in order to monitor both the atmospheric and soil hydro-thermal conditions, as well to evaluate the effects of vegetation on the thermo-hydro-mechanical response of the soil, is not very common although necessary to adopt sustainable engineering solutions for slope stabilization.

1.3.2. Catchment scale monitoring

Herein data short literature review on the monitoring at catchment scale is presented, emphasizing on ground-based or in-situ monitoring of rapid landslides, such as torrential flows (e.g. debris flows and debris floods), and on SVA interactions. Torrential flows are one

of the most hazardous phenomena in mountainous regions. The monitoring of torrential catchments provides very valuable information about the triggering conditions and SVA interactions for torrential flow initiation. Furthermore, it is necessary to improve both the understanding on debris flows dynamics and the implementation of mitigation measures such as early warning and alarm systems (EWASs). EWASs are an important and necessary tool to minimize the risk associated with these rapid mass-movements. Nevertheless, monitoring at catchment scale requires continuous and careful maintenance of instrumentation, and is therefore, a time consuming activity. Indeed, the presence of a warning system induces a feeling of safety only justified if the warning system is maintained and operates properly.

The installation of torrential flows monitoring and observation stations started in 1964 in Asia in the Guxiang gully [Ma, 1994], southeastern Tibet, China, followed in 1969 by the Osawa monitoring station in Mount Fuji, Japan [Imaizumi et al., 2021]. Since then, several monitoring stations have been installed in torrential catchments in Asia, for example in Kamikamihorizawa creek at Mount Yakedake in Japan in 1970, where long-term observations of debris flows triggering rainfall conditions and flow dynamics has been studied for more than 40 years [Suwa et al., 2009]. In the same way, other long-term monitoring stations where installed later in 1973 in Mount Sakurajima in Japan [Takeshi, 2011] and in the Jiangjia gully in China [Scott & Yuyi, 2004; P. Cui et al., 2005; Hong et al., 2015]. China and Japan have pioneered on debris flow monitoring and have provided long-time series of torrential flow occurrence, which are necessary in debris flow research.

The installation of monitoring systems was followed in the southern slopes of Mount Thomas in New Zealand [Pierson, 1980], on the Namekawa catchment in Japan in 1982 [Arisawa & Suzuki, 2013], and in 1988 in the MiDui glacier in Tibet [Kogelnig et al., 2011]. As seen, most of these studies were developed and initiated in Asia. Other torrential catchments monitored in Asia are the Ichinosawa catchment in 1988 [Imaizumi et al., 2005] and Mizunashigawa watershed in Mout Unzen in 1991 [Tsunetaka et al., 2021], both in Japan, or the instrumentation of 15 debris flow monitoring stations (13 on-site and 2 mobile monitoring cars) in Taiwan since 2002 [Yin et al., 2011]. The number of monitoring stations has grown worldwide and includes many sites in Europe since that time. Special mention to the first monitoring site in Europe in the Moscardo Torrent since 1989 [Marchi et al., 2002,

2021; Tecca et al., 2003; Scotton et al., 2011], or the Acquabona watershed since 1996 [Berti et al., 2000; Genevois et al., 2000; Tecca et al., 2003; Scotton et al., 2011], both in the Italian Alps. Other monitoring stations were installed in 1996 along the Óshlíð hillside in the West Fjords region of Iceland, one of the most hazardous roads in Iceland due to avalanches, rockfalls and debris flows [Bessason et al., 2007]. Followed by this, the Dorfbach and Schipfenbach catchments were instrumented in the Swiss Alps in 1997 [Hürlimann, Rickenmann, et al., 2003], followed in 2000 by the instrumentation of the Illgraben catchment [Hürlimann, Rickenmann, et al., 2003; McArdell & Badoux, 2007; Badoux et al., 2009] which is one of the most active debris flow systems in the Alps. Later in 2002, the Lattenbach watershed in Austria was monitored [Hübl & Kaitna, 2010]. More recently, monitoring sites were equipped in the Eastern Pyrenees: in 2005 in the Erill catchment [Raïmat, 2018], in Ensija [Hürlimann et al., 2011] and Rebaixader catchment [Hürlimann et al., 2014; Abancó et al., 2016] in 2009, and in Portainé in 2015 [Palau et al., 2017; Pinyol et al., 2017].

Other sites were instrumented in USA: since 2004 there are two permanent and extensive monitoring sites in Colorado in the Chalk Cliffs [Coe et al., 2008, 2010; McCoy et al., 2010], and 5 temporal systems monitoring debris flows in wild-fire affected watersheds in South-California since 2009 [Kean et al., 2011]. Other catchments instrumented for debris flow research or warning purposes are the Dimai torrent in the Italian Alps [Gregoretti, 2012], and the Manival and Réal Torrent in the French Alps [Navratil et al., 2012], which started in 2010. More examples in the Alps are the Gadria catchment starting in 2011 [Marchi et al., 2012; Comiti et al., 2014], followed by Marderello in 2013 [Coviello et al., 2015; Turconi et al., 2015], the Rovina di Cancia in 2014 [Bernard, 2018; Simoni et al., 2020], and the Rio Rudan in 2019 [INADEF project]. Last but not least, the Dawinbach ravine was instrumented in the Austrian Alps in 2020 [Schöffl et al., 2021]. One can see that most of the listed torrential catchments are located in the European Alps [Hürlimann, Coviello, et al., 2019].

Besides serving for research purposes, instrumental monitoring is essential to reduce the risk in areas affected by these flows, such as populations or infrastructures. It should be noted that most of the sensors used for debris flow monitoring are similar or were developed for lahars detection systems at volcanoes around the world [Hürlimann, Coviello, et al.,

2019]. Monitoring systems generally focus in the characterization of the rainfall triggering conditions, flow dynamics, hydrological soil conditions, or a combination of these approaches in more complex monitoring systems. A summary of sensors employed in torrential flow monitoring are listed in Table 1.1, while more extended information on debris flow monitoring and methods can be found in Itakura et al. [2005]. Sensors systems for debris flow monitoring and warning are diverse and can be divided into early-warning or event-alarm systems [Hungr et al., 1987; Arattano & Marchi, 2008], as detailed below.

Early-warning systems focus on monitoring hydrometeorological conditions initiating debris flows or debris floods, generally by characterizing the triggering rainfall conditions [Wieczorek & Glade, 2005] or watershed discharge [Coe et al., 2008], with the aim of warning before the event is triggered or in an early stage after its development. For this reason, early-warning systems can be very useful, for example when used in conjunction with rainfall forecasts, to warn before the triggering of a torrential flow. Nevertheless, early-warning systems are more prone to false positives, despite providing more lead-time, in comparison to event-alarm systems. In contrast, event-alarm systems are designed to detect torrential flows as they pass through the sensor network and warn the stakeholders before the arrival of the incoming flow (Figure 1.5). Event-alarm systems are diverse and may include several types of ground vibration or acoustic sensors, mainly installed along the channel, such as trip wires or pendulums, video cameras and ultrasonic or radar sensors for monitoring the change in flow dynamics (flow type, height and velocity), among others. Some examples of operating EWASs for torrential flows detection are installed in the Illgraben catchment (based on rainfall, flow depth and ground vibrations, [Badoux et al., 2009]), in Óshlíð (based on ground vibrations, [Bessason et al., 2007]) or in Taiwan (based on rainfall recordings, [Yin et al., 2011]).

Table 1.1: Debris flow parameters and sensors employed for their measurement (modified from Arattano and Marchi 2008), including sensors monitoring meteorological and hydrological conditions for debris flow triggering.

Process measurement	***Parameter***	***Sensor employed for the measurement***
Flow dynamics	Peak flow depth	Direct post-event observation through theodolite or GPS, wire sensors, photocells, ultrasonic sensors
	Flow depth as function of time	Ultrasonic sensors, radar sensors
	Ground vibration	Seismometer or geophones (velocimeters, accelerometers)
	Underground sound	Microphones
	Mean flow velocity	Ultrasonic sensors, geophones
	Surface velocity	Electromagnetic Doppler speedometers, video recordings, speed sensors based on spatial filtering velocimetry
	Basal forces (normal and shear stress)	Load cells
	Fluid pore pressure	Pressure sensors
	Impact force	Pressure mark gauges, piezoelectric sensors
Meteorological	Rainfall conditions (e.g. rainfall intensity, total precipitation)	Rain gauges, radar
	Air temperature	Thermistors
Hydrological	Pore water-pressure (positive and negative)	Tensiometers, piezometers
	Soil moisture	Volumetric water content sensors (e.g. Time Domain Transmission (TDT) and Time Domain Reflectometry (TDR) sensors)

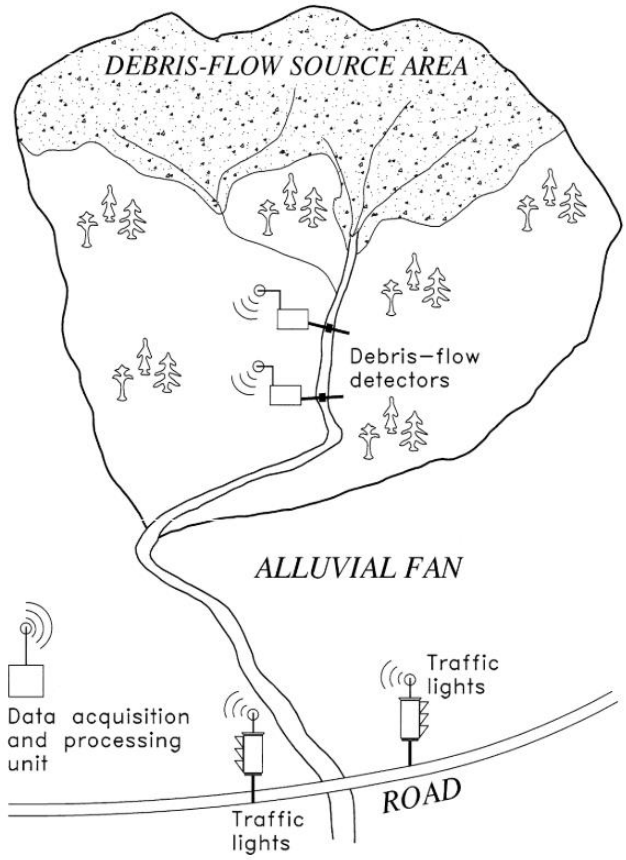

Figure 1.5: Sketch of the components of a debris-flow event-alarm system [Arattano & Marchi, 2008].

Early-warning sensors usually characterize the meteorological conditions for the initiation of torrential flows (e.g. rainfall intensity), although hydrological instrumentation, such as piezometers or suction measurements, may also be of interest for defining the hydrological conditions prone to debris flow triggering (e.g. pore water-pressure or soil moisture). Nevertheless, the majority of these studies and monitoring systems rely on sensors measuring flow dynamics and critical rainfall conditions, and thus neglecting soil hydrological conditions; although it is known that soil hydrology plays an important role in rainfall infiltration and slope stability, and therefore, affects the triggering of torrential flows. There are limited studies monitoring soil hydrologic conditions and its relation with debris flow initiation and magnitude, mainly in the channel-bed [Berti et al., 2000; McCoy et al., 2012; Simoni et al., 2020] or hillslopes at the flanks of the channel [Kean et al., 2011], or in

natural slopes at the initiation zone of debris flows [Comiti et al., 2014; Hürlimann et al., 2014; Raïmat, 2018].

1.4. Objectives

The overall aim of this thesis is to increase our knowledge regarding soil-vegetation-atmosphere (SVA) interactions and its implications on slope mass-wasting (SMW) phenomena. More specifically, it addresses the problem of SMW due to shallow failures in hilly and mountainous areas considering a multi-scale approach: monitoring at slope and catchment scale. In the following, the specific objectives regarding slope and catchment scale are listed.

The specific objectives at slope scale are:

- Development, setup, and maintenance of a sophisticated monitoring system (> 60 sensors) in a full-scale embankment experiment focusing on meteorological and soil hydro-thermal parameters. This objective also include the seeding and maintenance of vegetation (turf grass species) at North/South slopes.
- Calibration, programming and testing of sensors and data acquisition system at laboratory, previous to field installation.
- Recording and management of accurate and long-term time series of SVA interactions (>2 years).
- Basic and hydro-mechanical test program at our geotechnical laboratory on partially saturated soil samples of the soil used in this experimental embankment: granulometry (particle size), Atterberg limits, permeability, soil water retention curve, direct shear tests, etc.
- Analysis of slope hydro-thermal response to natural climatic actions considering different orientations (North and South) and slope covers (bare and vegetated). Specifically:
    - Comparison of orientation and slope cover effects on:
        - Rainfall infiltration (wetting) and soil drying rates (evaporation and evapotranspiration on bare and vegetated

slopes, respectively): soil hydrologic conditions (in terms of soil moisture and suction).

- Soil heat flux and soil temperature: soil thermal conditions

The specific objectives at catchment scale are:

- Maintenance and improvement of the Rebaixader monitoring system, which started in 2009, in order to detect debris flows and debris floods.
- Recording and management of accurate and long-term time series (>4 years) of debris flows and debris floods occurrence and soil-atmosphere interactions in order to characterize:
  - Critical rainfall conditions for torrential flows initiation.
  - Effects of soil hydrology (soil moisture) on necessary rainfall conditions for the triggering of torrential flows.
- Update previous defined rainfall thresholds for torrential flow initiation in the Rebaixader catchment (intensity-duration thresholds).
- Define and develop new hydro-meteorological thresholds for torrential flow initiation considering both rainfall characteristics and soil hydrologic conditions (intensity-soil moisture thresholds).
- Comparison of rainfall thresholds and hydro-meteorological thresholds in terms of predictability using the receiver operating characteristics (ROC) and precision-recall curves (PRC) analysis.

1.5. Thesis structure and content

The thesis work has been structured in the following way: an introduction, four main chapters (each main chapter has been prepared in the form of a scientific paper), and conclusions.

The introduction presents a general state-of-the art about soil-vegetation-atmosphere (SVA) interactions and its effects on slope mass-wasting (SMW). This section describes the main physical mechanisms involved in SMW at slope and catchment scale. At slope scale, several experiments developed to monitor SVA interactions are presented. At catchment

scale, different instrumental techniques and monitoring systems for torrential flows detection and research, such as debris flows and debris floods, are listed.

Chapter 2 and 3 analyze SVA interactions and its implications on slope hydro-thermal response to natural climatic actions considering the slope scale of a full-scale experimental embankment with different orientations (North and South) and covers (bare and vegetated). One of the main goals of these chapters is to understand the effects of orientation on slope hydro-thermal response. A clayey sand with a relative low permeability was used for this experiment.

- Chapter 2 describes the design, construction, and sensors setup of a full-scale experimental embankment. The monitoring system is thoroughly described and includes sensors technical specifications and installation details and procedures. In addition, the results of a basic, mechanic and hydraulic laboratory geotechnical test program of the soil used in this experimental embankment are presented.
- Chapter 3 putts its effort in the comparison of slope hydro-thermal response when different covers (bare and vegetated) and orientations (North and South) are analyzed, and thus not only focusing on orientation effects as in Chapter 2. Specially, the hydrological effects of vegetation on soil drying and infiltration are compared with a bare slope. In addition, the effects of vegetation on soil heat fluxes and temperature are analyzed.

Chapter 4 and 5 focus on SVA interactions and SMW phenomena at catchment scale. Specifically, it presents the results gathered in the Rebaixader catchment (Central Pyrenees), which is monitored for torrential flow research (mainly debris flows and debris floods). These chapters mostly focus on the characterization of the triggering rainfall conditions and the effects of soil hydrology in torrential flow initiation. The soil at the initiation zone of torrential flows consists of sandy gravel with a relative high permeability.

- In chapter 4, the Rebaixader catchment in the Central Pyrenees and its monitoring system for debris flows and debris floods research is presented. This chapter mainly characterizes the critical rainfall conditions and the soil moisture

dynamics (in terms of soil moisture) influencing the triggering of torrential flows. Soil moisture is measured in the initiation zone of torrential flows.

- Chapter 5 further analyses the critical rainfall conditions and the effects of soil hydrology (in terms of soil moisture and suction) for torrential flows initiation. The main results focus on the definition and performance comparison (in terms of predictability) of rainfall thresholds (based on rainfall measurements) and hydro-meteorological thresholds (considering both rainfall and soil moisture conditions) for debris flow triggering. The definition of hydro-meteorological thresholds for debris flows and debris floods prediction is a novel topic in torrential flows research.

Finally, general conclusions are presented in Chapter 6, as well as future research proposals.

Chapter 2

MONITORING OF A FULL-SCALE EMBANKMENT EXPERIMENT REGARDING SOIL–VEGETATION–ATMOSPHERE INTERACTIONS

This chapter reproduces the article published in the *Water* journal on May 25, 2018. The article focusses on the setup and monitoring of a full-scale experimental embankment developed for soil-vegetation-atmosphere interactions research comparing different slope orientations (North and South) and slope covers (bare and vegetated).

Publication reference:

Oorthuis, R., Hürlimann, M., Fraccica, A., Lloret, A., Moya, J., Puig-Polo, C., & Vaunat, J. (2018). Monitoring of a Full-Scale Embankment Experiment Regarding Soil–Vegetation–Atmosphere Interactions. *Water*, *10*(6), 688. https://doi.org/10.3390/w10060688.

Abstract

Slope mass-wasting like shallow slides are mostly triggered by climate effects, such as rainfall, and soil–vegetation–atmosphere (SVA) interactions play a key role. SVA interactions are studied by a full-scale embankment with different orientations (North and South) and vegetation covers (bare and vegetated) in the framework of the prediction of climate change effects on slope stability in the Pyrenees. A clayey sand from the Llobregat river delta was used for the construction of the embankment and laboratory tests showed the importance of suction on the strength and hydraulic conductivity. Sixty sensors, which are mostly installed at the upper soil layer of the embankment, registered 122 variables at four vertical profiles and the meteorological station with a 5 min scan rate. Regarding temperature, daily temperature fluctuation at the shallow soil layer disappeared at a depth of about 0.5 m.

There was great influence of orientation with much higher values at the South-facing slope (up to 55 °C at −1 cm depth) due to solar radiation. Regarding rainfall infiltration, only long duration rainfalls produced an important increase of soil moisture and pore water pressure, while short duration rainfalls did not trigger significant variations. However, these changes mostly affected the surface soil layer and decreased with depth.

Keywords: monitoring; embankment; rainfall infiltration; heat flux

2.1. Introduction

The understanding of soil–vegetation–atmosphere interactions is fundamental for the correct assessment of rainfall-induced slides and other slope mass-wasting processes [Gabarrón-Galeote et al., 2013]. These interactions are of great importance due to future global changes associated with climate changes [Imeson & Lavee, 1998; Corominas, 2000; Coyle et al., 2017; Drabo, 2017]. The fifth assessment report of the Intergovernmental Panel on Climate Change [IPCC, 2014] states that number of warm days has likely increased at the global level and that extreme precipitation events have increased in Europe since 1950. All these effects will largely affect the soil–vegetation–atmosphere interactions and also influence the mechanisms of slope mass-wasting in the future [Panagos et al., 2014; Nearing et al., 2017].

Mass-wasting due to shallow slope failures represents one of the most important erosional process in many mountainous regions and may also be the most dangerous [Hovius et al., 1997]. In addition, superficial failures in artificial slopes are a particularly important issue at transportation embankments [Alonso et al., 1999; Sajjan et al., 2013; Briggs et al., 2017].

Soil–vegetation–atmosphere (SVA) models have generally received little attention in geotechnical engineering, maybe due to the absence of thermo-hydro-mechanical formulations able to couple all the processes with the soil mechanical response. With the exception of some pioneering work such as Blight [1997], it is only in recent years that research has developed on the overall effect of the SVA interactions on responses of natural and artificial slopes [Tsiampousi et al., 2016; Elia et al., 2017; Tang et al., 2018]. However, most studies focus on the infiltration processes in unsaturated soils by performing laboratory

tests on slopes with limited extension [P. Orense et al., 2004; Tohari et al., 2007; C.-C. Huang & Yuin, 2010]. There are also some large-scale experiments [Moriwaki et al., 2004] and a few studies that constructed a full-scale embankment in order to monitor the soil–atmosphere interactions [Cooper et al., 1998; Y. J. Cui et al., 2010; Glendinning et al., 2014]. Finally, multiple research studies have been performed on the monitoring of natural slopes affected by different types of slope mass-wasting mechanisms [Bogaard & van Asch, 2002; Springman et al., 2003; Ng et al., 2008; Rahardjo, Rezaur, et al., 2008;].

The preceding state-of-the-art techniques show that most research focuses on the soil–atmosphere interaction and studies on SVA mechanisms are rather scare. There are studies regarding soil–vegetation interactions [Cassiani et al., 2016], but principally neglecting geotechnical aspects. These aspects, such as the effect of suction and root reinforcement on the shear strength, are important to evaluate the engineering behavior of earth materials and the stability of natural and man-made slopes [Schmidt et al., 2001]. Therefore, the principal goal of our study is to achieve detailed data on the SVA interactions by performing an extensive monitoring of a full-scale physical embankment located close to our university. The registered data will improve our understanding about the thermo-hydraulic processes occurring at the soil–plants–atmosphere interface and their coupling with mechanical effects. In the present publication, we describe the monitoring set-up and present the first monitoring results on the heat and water flow across the upper soil layer of the test embankment.

2.2. Methods

2.2.1. Construction of embankment

At the end of 2016, the test embankment was built with help of a backhoe loader at the ParcUPC Agròpolis, which includes outdoor experimental facilities for research purposes. It is situated on the deltaic floodplain of the Llobregat River about 20 km southwest from Barcelona downtown. The embankment was made using a clayey sand of the zone.

The embankment measures 18 m long, 12 m wide, and 2.5 m high, which incorporates a total volume of about 326 m^3. The slopes are built at 33.7 degrees, corresponding to 3H:2V. The construction phases included three steps: first, the core was built; then an irregular, studded structured, and impermeable polyethylene geomembrane was laid out; and finally, a

50–70 cm thick soil layer was accumulated on the geomembrane. A shallow soil layer on an impermeable bedrock is a very common condition in many mountainous areas including the Pyrenees or the Catalan Coastal Ranges, where multiple slope rainfall-induced failures have occurred in the past [Gallart & Clotet, 1988; Corominas & Moya, 1999; Portilla et al., 2010]. Figure 2.1a shows a photograph of the embankment during the accumulation of the surficial soil layer on the geomembrane.

The surficial soil layer includes four monitored slope partitions, which are laterally separated by the geomembrane: a vegetated and a bare slope at the South side of the embankment and another two partitions with and without vegetation at the North-facing slope. This set-up provided information on the effect of orientation (solar radiation) and of vegetation, two fundamental aspects in the evaluation of the influence of future changes on slope mass-wasting. The growth of vegetation was impeded in two partitions by the periodic application of herbicide, while Cynodon Dactylon and Festuca Arundinacea seeds were sowed in the other two partitions. These species are common in the application of slope revegetation, are resistant against drought, and increase soil strength due to their roots [Katritzidakis et al., 2007; M. Zhang et al., 2013; F. Chen et al., 2015; Garg, Coo, et al., 2015].

In addition, displacement measurements by different geomatic techniques are performed periodically to observe ground movements. At the moment, terrestrial laser scanning (Figure 2.1b) and dual constellation real-time kinematic positioning with GPS were used. In the future, digital photogrammetry using data of time-lapse cameras is planned to achieve movements with a smaller time interval.

(a)

(b)

Figure 2.1: (a) Photograph of the embankment during the construction. ; (b) 3D view of the point cloud obtained by terrestrial laser scanning.

2.2.2. Soil sampling and laboratory tests

Different soil samples of the material used for the construction of the embankment from the Llobregat river delta were taken prior to and during the development of the experiment. A detailed test program was performed at a geotechnical laboratory focusing on the basic, hydraulic, and mechanical characterization of the soil. The different laboratory tests included: (i) particle-size distribution by sieve and sedimentation methods [ASTM International, 2017b, 2017c], (ii) Atterberg limits [ASTM International, 2017a], (iii) permeability, (iv) specific gravity (by pycnometer method) [ASTM International, 2014], (v) direct shear tests (in shear box device) [ASTM International, 2011], and (vi) soil–water retention curve.

Estimation of the soil permeability is important for the correct understanding of the hydro-mechanical behavior of the embankment. However, it must be stated that laboratory measurements of a small sample may be different from field permeability, where heterogeneities in the soil mostly exist [Day & Daniel, 1985]. For example, small movements in the slope can produce cracks that greatly increase vertical permeability.

The saturated hydraulic conductivity was determined in the laboratory by different tests: (i) triaxial tests with constant back pressure, (ii) constant and variable head

permeameter tests, and (iii) consolidation tests in saturated consolidation by using the oedometer apparatus.

Multiple direct shear tests were performed to determine the strength parameters of the soil including four consolidated drained (CD) tests in saturated conditions, and 15 CD tests at constant water content under partially saturated conditions. Normal stress applied to the samples was up to about 30 kN/m^2, which roughly corresponds to a 1.7 m thick soil layer, using the density of the materials under consideration. Samples were statically compacted until they reached the specified dry density (ρ_d = 15.5 ± 0.7 Mg/m^3) using three different water contents (15, 19, and 25%).

The soil–water retention curve (SWRC) was achieved by different methods. The relation between soil suction and soil volumetric water content is important information to understand the hydro-mechanical behavior of unsaturated soils [Fredlund et al., 1996]. The SWRC was measured in the laboratory using drying/wetting cycles on samples with a dry density of 1.62 Mg/m^3. On one side, a standard ceramic tip laboratory tensiometer (T5x, UMS , München, Germany) was used for low suction values up to 200 kPa. On the other side, a dielectric water potential sensor (MPS-6, Decagon Devices, Pullman, WA, USA) and a chilled mirror dew point hygrometer (WP4, Decagon Devices, Pullman, WA, USA) were applied to measure high suction values up to 100 and 300 MPa respectively.

After constructing the embankment, in situ undisturbed soil block samples were taken at several depths between 5 and 20 cm, in order to determine moisture and natural/dry bulk density. These undisturbed soil samples were obtained from thin-walled sampling tubes and clods. Since the monitoring is installed at the two principal orientations (North and South) of the embankment, material was sampled at these two slope faces. The paraffin method [ASTM International, 2018] was applied to measure the density of these undisturbed samples.

2.2.3. Monitoring set-up

The sensors were installed at vertical infiltration profiles inside the upper soil layer of each of the four partitions. In addition, a meteorological station was fixed at the top of the embankment. All the sensors are connected by wires to a datalogger (CR1000, Campbell Scientific, Logan, UT, USA) that was used in combination with two multiplexers due to the

large amount of sensors. The data of all sensors are recorded at a constant sampling rate of 5 min. Every 24 h, the data files are sent via FTP to the university sever. The power supply of the entire monitoring system is provided by solar panels and batteries.

The experiment includes four different zones: (i) South slope with vegetation (SV), (ii) South slope without vegetation (SnV), (iii) North slope with vegetation (NV), (iv) North slope without vegetation (NnV). Each of the four zones is equipped by a vertical profile of different sensors (Figure 2.2) and the devices that measure the surface runoff and seepage. Thus, a complete analysis of the soil–vegetation–atmosphere interaction is possible by incorporating observations gathered by the meteorological station. The installation of the sensors was performed in two main phases. First, the setup of the non-vegetated profiles (SnV and NnV) was performed in spring 2017. Second, the vegetated profiles (SV and NV) were installed in autumn 2017. Finally, some complementary sensors were mounted at the beginning of 2018. Figure 2.3 shows a photograph of the embankment after the installation of the sensors looking towards the North-faced slope.

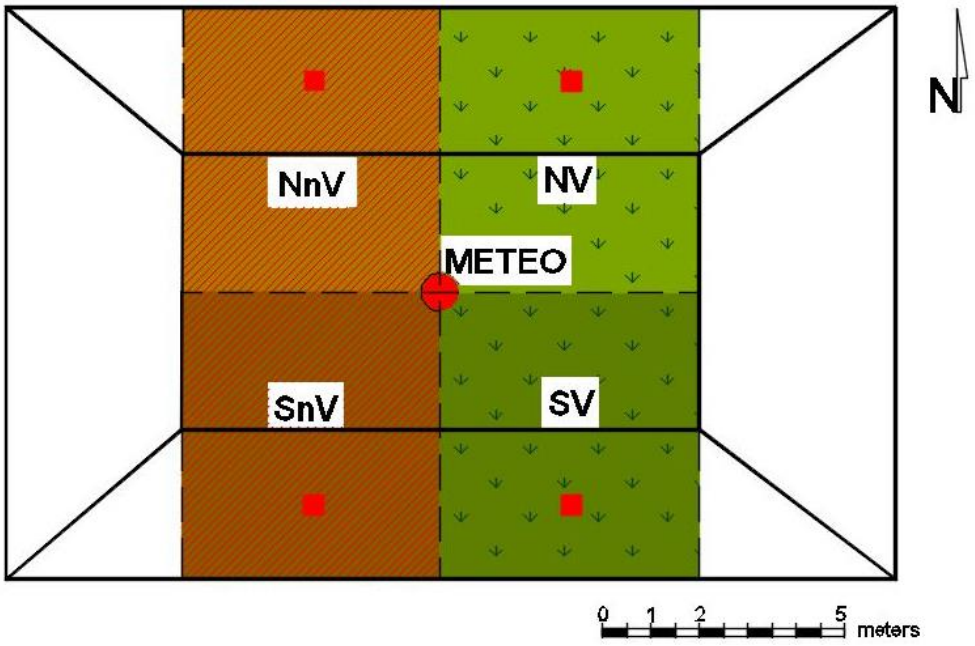

Figure 2.2: Schematic overview of the full-scale experiment divided into four partitions: SV, SnV, NV, and NnV (see text for explanations). The position of the four vertical sensor profiles (red squares) and the meteorological station (red dot) is illustrated.

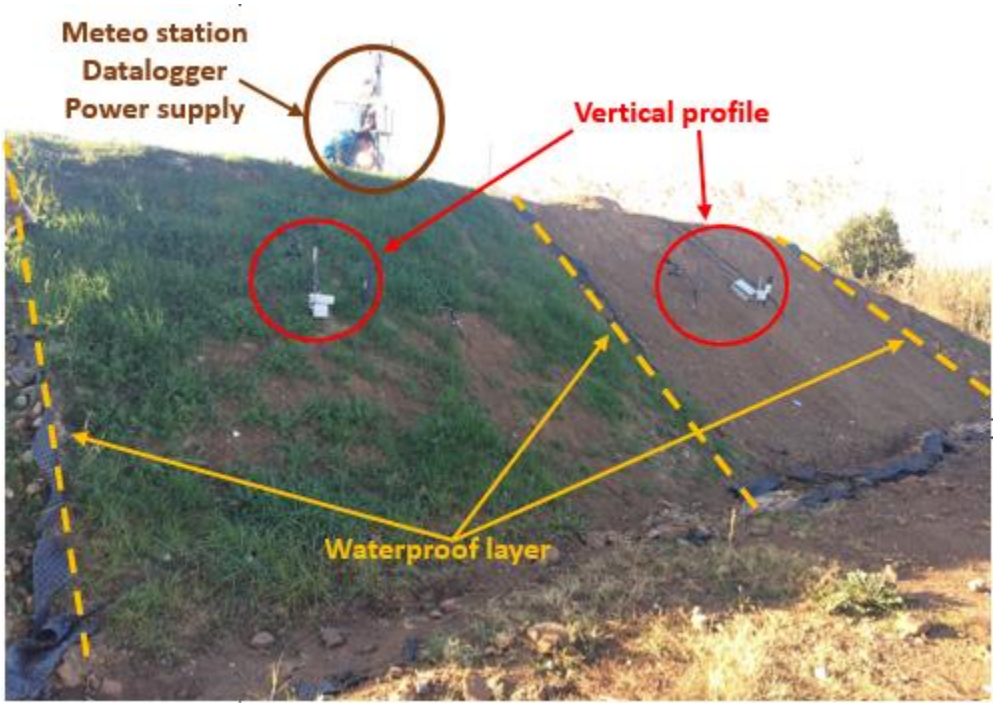

Figure 2.3: Photograph of the embankment after installation of the sensors looking towards the North slope.

2.2.3.1. Vertical sensor profiles

Each vertical profile measures air and soil temperature, relative humidity, barometric pressure, heat flux, pore water pressure (PWP), and volumetric water content (VWC) at different positions. A complete list of all the sensors and the recorded parameters is given in Table 2.1. Net solar radiation devices were installed at each of the orientations (North and South). The general distribution of the different devices is shown by the example of vertical profile NnV (Figure 2.4a). In addition, photographs of the soil texture format profiles NnV and NV during the sensors installation are shown in Figure 2.4b,c respectively. They show the sandy loamy soil with isolated gravel particles at both trenches, while the presence of organic material in the form of plant roots is visible in the vegetated North (NV) profile.

Not each vertical profile has the distribution of sensors as shown in Figure 2.4a and the final number of devices installed in each profile ranges from 13 to 14 (Table 2.2). The parameter that is measured at most positions is temperature, which is monitored at least at 7 positions along each vertical profile, while PWP and VWC are registered at a minimum of 3 and 4 positions, respectively. The total number of records measured at all sensors for each of

the non-vegetated slopes (SnV and NnV) and for each of the vegetated slopes (SV and NV) is 27 and 29, respectively. Some sensors had technical problems during the first year or were installed in the second phase. That is why the time series of specific sensors are not complete when presented in the results section.

Table 2.1: Characteristics of the sensors installed in the vertical slope profiles.

Parameter Measured	***Model***	***Measuring Range***
Soil temperature	Campbell 107	35 to +50 °C
Volumetric water content	Decagon 5TE	0 to 1 m^3/m^3
Soil temperature		−40 to +50 °C
Electric conductivity		0 to 23 dS/m
Pore water pressure	Decagon MPS-6	−9 to −100000 kPa
Soil temperature		−40 to +60 °C
Pore water pressure	UMS T4	−85 to +100 kPa
Air temperature	Decagon VP-4	−40 to +80 °C
Relative air humidity		0 to 100%
Atmospheric pressure		49 to 109 kPa
Wind speed	Davis Cup Anemometer	0.9 to 78 m/s
Wind direction		0 to 360°
Heat flux	Hukseflux HFP01	±2000 W/m^2
Net solar radiation	Kipp & Zonnen NR Lite2	±2000 W/m^2

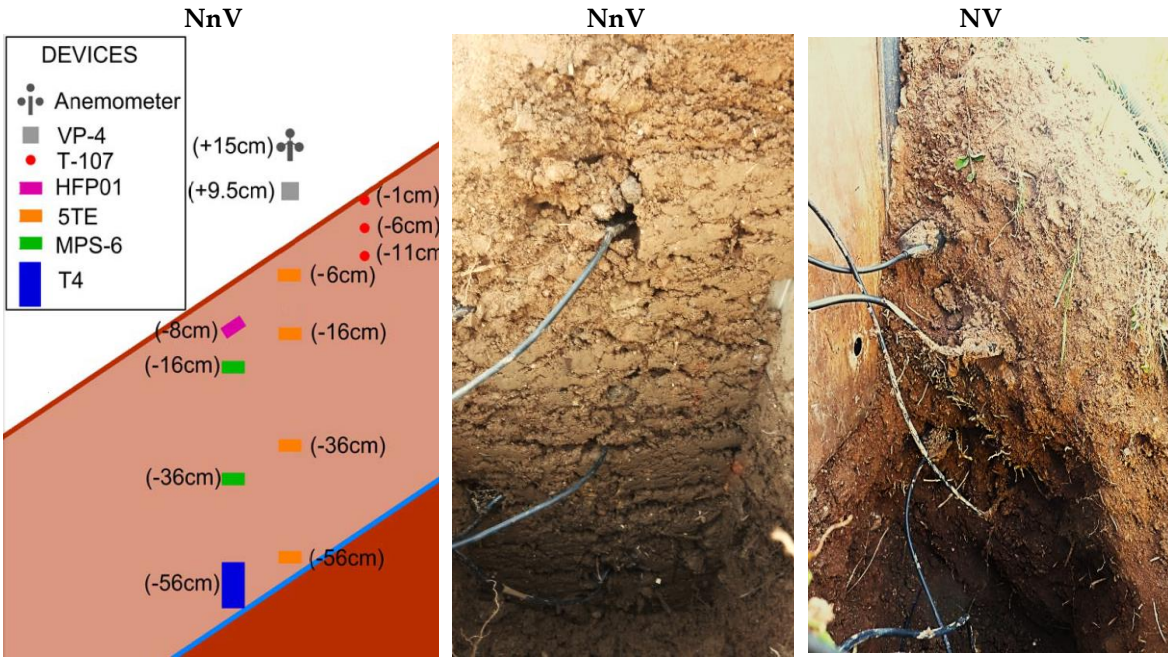

(a) (b) (c)

Figure 2.4: (a) Schematic design of the vertical profile of NnV indicating the location of the sensors; (b) photograph taken during installation of sensors at the NnV profile; (c) photograph taken during installation of sensors at the NV profile.

Table 2.2: Location of selected sensor in the four vertical profiles. Only devices focusing on temperature, volumetric water content, and pore water pressure are listed.

Sensor	***Depth of Installation (cm)***			
	SV	***SnV***	***NV***	***NnV***
Air/soil temperature	+9.5, −1, −6, −11, −16, −36, −43	+9.5, −1, −6, −11, −16, −32, −36, −57	+9.5, −1, −6, −11, −16, −36, −56	+9.5, −1, −6, −11, −16, −36, −56
Volumetric water content	−6, −16, −36, −43	−6,−16, −36, −57	−6, −16, −36, −56	−6, −16, −36, −56
Pore water pressure	−16, −36, −40, −43	−11, −32, −72	−16, −36, −56, −59	−16, −36, −56

In the following, the different types of devices will be described and some characteristics discussed. In this study, two types of sensors are considered: (1) devices measuring temperature changes and heat flux along the atmosphere–soil interface, and (2) devices focusing on the infiltration of rainfall into the soil layer.

Air and soil temperature is measured at different positions close to the surface. In the most superficial part of the soil layer, three thermistors encapsulated in an aluminum housing (107, Campbell Scientific, Logan, UT, USA) were buried. The rest of the soil temperature is monitored by the thermistors incorporated in other sensors (MPS-6, Decagon Devices, Pullman, WA, USA, and 5TE, Decagon Devices, Pullman, WA, USA). Another sensor (VP-4, Decagon Devices, Pullman, WA, USA) measures the air temperature at 9.5 cm above the terrain surface.

The heat flux across a soil section is measured close and parallel to the surface, where most of the heat transfer is expected. For this reason, a thermopile (HFP01, Hukseflux, Delft, The Netherlands) is installed at 8 cm depth and transforms the measured voltage into heat flux. Finally, wind speed and direction is also registered at each vertical profile by a cup and vane anemometer installed 15 cm above the terrain surface.

Water content and pore water pressure are fundamental parameters to understand the atmosphere–vegetation–soil interactions related to rainfall infiltration into the soil. In the experiment, multiple devices register these processes in the vertical profiles, principally tensiometers and soil moisture sensors.

Two different types of tensiometers were installed for measuring pore water pressure: (i) porous ceramic disc tensiometers (MPS-6, Decagon Devices, Pullman, WA, USA), and (ii) porous ceramic cup tensiometer (T4, UMS , München, Germany). The MPS-6 dielectric water potential sensors are designed to measure suction values up to 100 MPa and are located close to the surface (Table 2.2), where high suction values are expected. In contrast, the UMS T4 is a tensiometer that measures PWP in a negative and positive range. Thus, its installation is at the lower part of the monitored soil layer, where low suction or positive PWP values are expected. The UMS T4 device is a rather delicate sensor in comparison with the robust MPS-6. The UMS T4 tensiometers were refilled and calibrated in the laboratory before their installation. The refilling was made with de-aired water, ensuring no air bubbles remained inside the ceramic cup, which would lead to an incorrect pressure reading. In addition, the pressure measured by the transducer has to be corrected twice: (i) due to the elevation difference between the pressure transducer and the ceramic cup, and (ii) because of the different power excitation (our system supplies 12 V, while the manufacturer calibration is

performed at 10.6 V). The installation of the UMS T4 tensiometers has to be carried out very carefully. To prevent surface runoff running down into the borehole along the tensiometer, a rubber water-retaining disk was slipped around the sensor at the soil surface and a perfect fit between the previously drilled hole and the device was performed.

The volumetric water content (VWC) is measured by Decagon 5TE sensors (Decagon Devices, Pullman, WA, USA), which are installed at different depths in the soil layer (Table 2.2). The 5TE uses an electromagnetic field to measure the dielectric permittivity of the surrounding medium. Prior to field installation, a calibration of the sensor was performed in the laboratory using soil samples with a similar bulk density as the embankment slope. The VWC that was recorded by the sensor was compared with the one determined by the standard procedure incorporating the void ratio, the gravimetric water content, and the specific gravity of the soil samples. The calibration results showed that there was no significance difference with the equation given by the manufacturer, therefore this equation was finally used for the transformation of the sensor reading into VWC.

2.2.3.2. Meteorological station

The meteorological station consists of a standard tipping-bucket rain gauge with a resolution of 0.2 mm (ECRN-100, Decagon Devices, Pullman, WA, USA), a sensor which measures relative humidity, air temperature, vapor, and atmospheric pressure (VP-4, Decagon Devices, Pullman, WA, USA), a solar radiation sensor (Davis Vantage Pro2, Davis Instruments, Hayward, CA, USA), and a cup anemometer/wind vane, which measures wind direction and wind speed (Davis Cup Anemometer, Davis Instruments, Hayward, CA, USA). Details of the sensors installed at the meteorological station are listed in Table 2.3. In total, 8 different parameters are measured.

Table 2.3: Sensors installed at the meteorological station. * Minimum resolution of sensor.

Parameter measured	*Model*	*Measurement range*
Rainfall	Decagon ECRN-100	0.2 mm *
Air temperature	Decagon VP-4	−40 to +80 °C
Relative air humidity		0 to 100%
Atmospheric pressure		49 to 109 kPa
Solar radiation	Davis Vantage Pro2	0 to 1800 W/m^2
Wind speed	Davis Cup Anemometer	0.9 to 78 m/s
Wind direction		0 to 360°

2.3. Results

2.3.1. Laboratory results

The laboratory results from different soil samples of the material used for the construction of the embankment from the Llobregat river delta are summarized in Table 2.4.

Table 2.4: Soil properties of the material used for the construction of the embankment.

Soil Property	*Value*
Gravel content (%)	34–42
Sand content (%)	30–43
Silt content (%)	20–25
Clay content (%)	4–6
Fines (%)	25–31
Liquid limit (%)	29.5–34.4
Plastic limit (%)	19.9–21.2
Plasticity index (%)	9.7–13.5
Specific gravity (Mg/m^3)	2.65–2.70
Cohesion (kPa)	0
Friction angle (º)	58
Hydraulic conductivity (m/s)	7.7×10^{-8}–1.8×10^{-7}

Table 2.5 lists a summary of the most important parameters determined from undisturbed soil samples. Differences in density between the North and South slopes may be due to the compaction process during the construction.

Table 2.5: Soil properties of materials sampled after construction of the embankment at the two monitored slopes (South and North).

Soil Property	***South Slope***	***North Slope***
Bulk density (Mg/m^3)	1.72–1.78	1.85–1.93
Dry density (Mg/m^3)	1.52–1.57	1.55–1.61
Water content (%)	13.23–15.11	19.08–19.84
Void ratio (-)	0.70–0.76	0.66–0.72
Porosity (-)	0.41–0.43	0.40–0.42

2.3.1.1. Basic soil characterization

First, the grain-size distribution was determined for two samples. The resulting curves show some minor differences (Figure 2.5) and the values are listed in Table 2.4. According to the Unified Soil Classification System (USCS) the soils can be classified as SC (clayey sand) including a large part of coarse-grained particles. The Atterberg limits indicate that the fine-grained part has a low plasticity behavior (Table 2.4). This low plasticity index indicates that small changes in soil humidity involve important changes of its consistency.

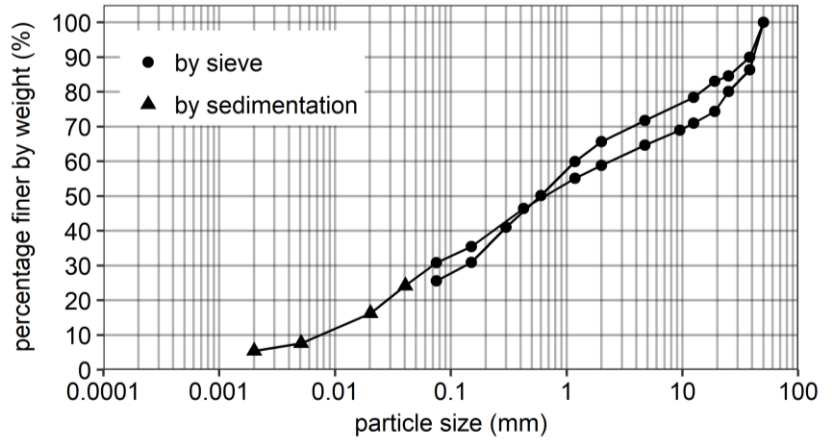

Figure 2.5: Particle-size distribution of the material used for the construction of the monitored embankment.

2.3.1.2. Strength parameters

Figure 2.6 shows the results of three soil samples sheared with a normal stress of 21 kPa under partially and saturated conditions. Samples under partially saturated conditions presented a clear peak shear strength and a dilatant behavior. This is a typical behavior of over-consolidated soils [Skempton, 1964]. In contrast, saturated samples showed a contractive behavior with no clear peak. This behavior indicates that the saturation process induces a reduction in the apparent preconsolidation pressure of soil [Alonso et al., 1990].

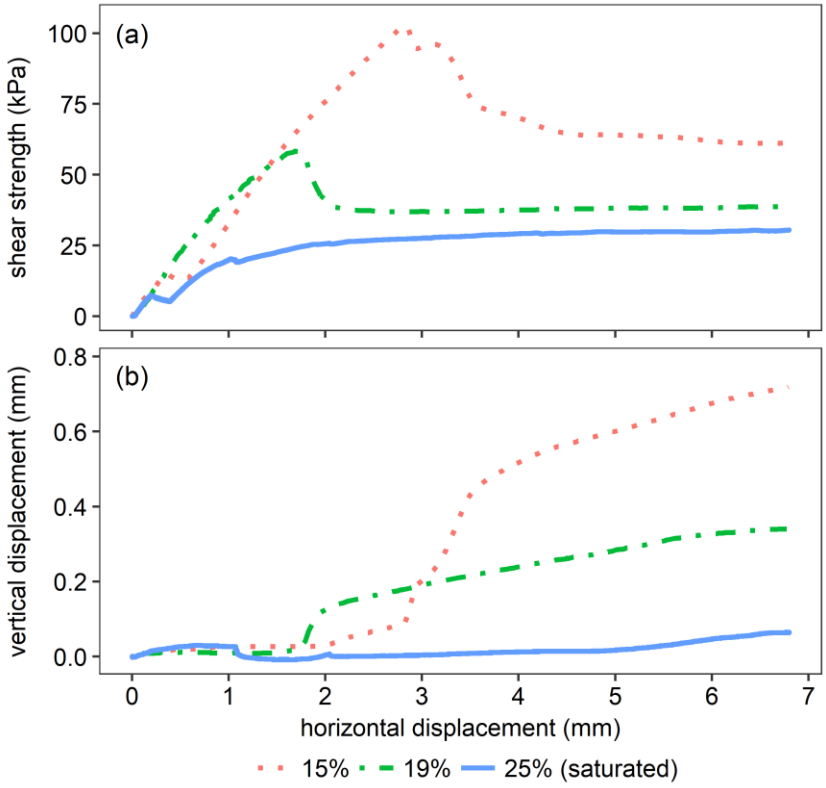

Figure 2.6: Results of three direct shear tests performed on partially and completely saturated samples applying a normal stress of 21 kPa. (a) Shear strength versus horizontal displacement; (b) Vertical displacement versus horizontal displacement.

The normal versus shear stress relation of all tests are plotted in Figure 2.7. Results confirm the importance of water content in the soil, when strength parameters are analyzed. In particular, the great contribution of suction to the shear strength must be taken into account. The data of the direct shear test also shows that peak shear stress decreases and gets closer to constant volume shear stress when the sample is closer to saturated conditions. For unsaturated soils, the intergranular stress may be defined as [Bishop, 1959]:

$$\sigma_n' = \sigma_n + \chi \cdot s = \sigma_n + S_r \cdot s \qquad (1),$$

where σ_n' is the Bishop's generalized normal effective stress for unsaturated soils, σ_n is the normal stress, χ is the Bishop's parameter and *s* is suction. Bishop's parameter χ is a function of the saturation degree S_r and is imposed to vary between 0 for dry soils to 1 for saturated soils which can be roughly assumed to have the value of the saturation degree [Schrefler, 1984].

In addition, the shear strength of unsaturated soils can be defined in terms of two independent stress variables, the normal stress and suction [Fredlund et al., 1978]:

$$\tau = c' + \sigma_n \tan\phi' + s \tan\phi^b \qquad (2),$$

where τ is the shear strength, c' the effective cohesion, σ_n the normal stress, *s* is suction, ϕ' the effective friction angle and ϕ^b represents the frictional contribution by suction to shear strength. Replacing Bishop's generalized effective stress for unsaturated soils in Equation (*1*) with Fredlund's unsaturated shear strength of Equation (*2*) and considering $\chi = S_r$, the following expression is obtained:

$$\tau = c' + \sigma_n \tan\phi' + s\, S_r \tan\phi' = c' + \sigma_n \tan\phi' + s \tan\phi^b \qquad (3),$$

from which can be deduced that:

$$\tan\phi^b = S_r \tan\phi' \qquad (4).$$

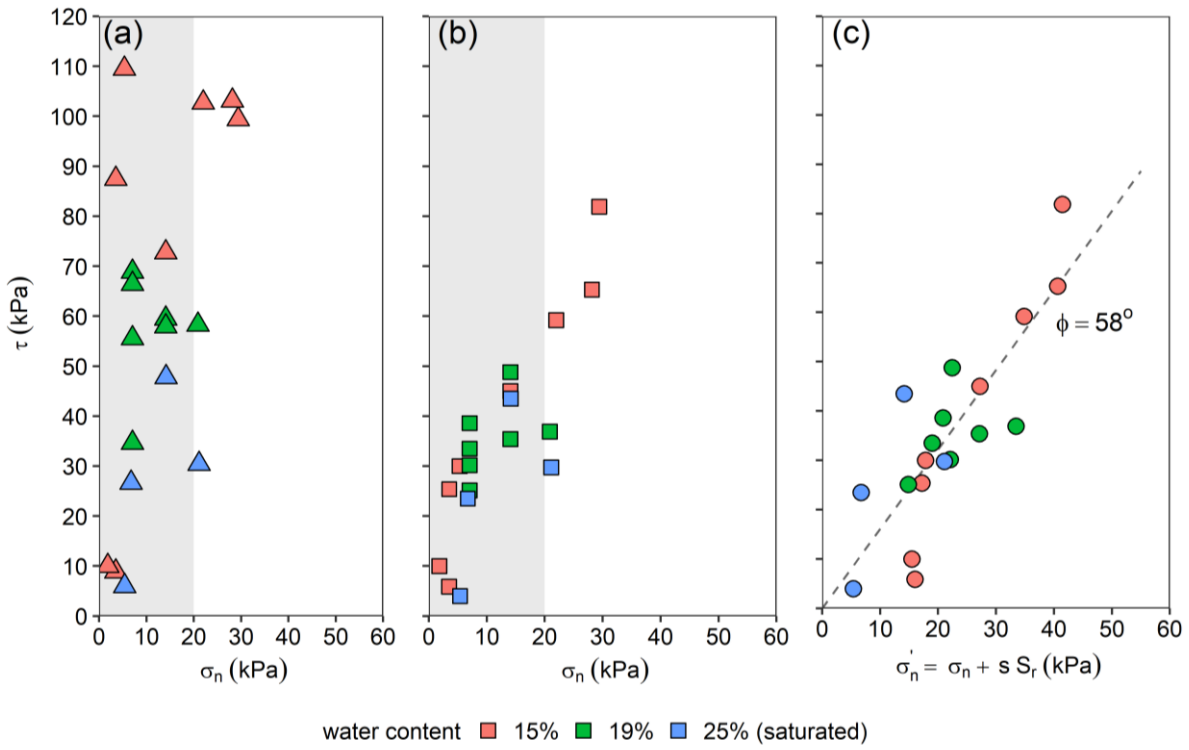

Figure 2.7: Results of direct shear tests performed on partially and completely saturated samples. (a) Normal stress versus peak shear stress; (b) normal stress versus constant volume shear stress; (c) Bishop's generalized effective normal stress versus constant volume shear stress. Shaded grey area represents the range of normal stresses expected on the monitored soil layer.

The resulting failure envelope using Bishop's generalized effective stress for partially saturated soils at constant volume shear strength is defined by a friction angle of 58° and zero cohesion (Figure 2.7c). This high friction angle is the result of the low normal stress up to 30 kPa applied to the samples. For higher normal stress values, a lower friction angle and a non-linear failure envelope are expected [Maksimovic, 1989].

2.3.1.3. Hydraulic behavior

The permeability ranges over almost four orders of magnitude (Figure 2.8), while values are between 7.7×10^{-8} and 1.8×10^{-7} m/s regarding void ratios observed in the embankment (0.66–0.76). However, in situ infiltration tests must be performed to finally determine the permeability, since field hydraulic conductivity may be much higher than the one achieved in the laboratory [Day & Daniel, 1985].

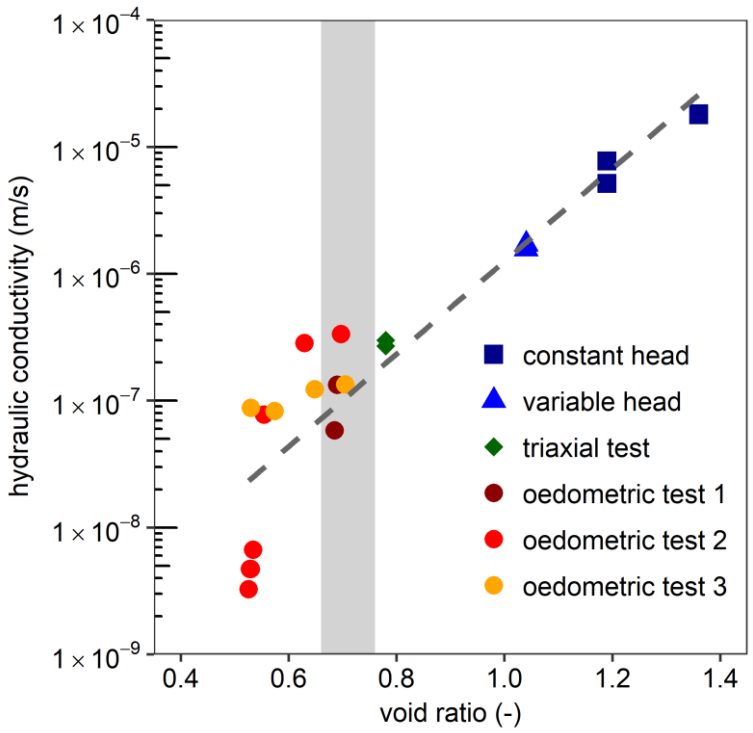

Figure 2.8: Saturated hydraulic conductivity for different void ratios obtained by different laboratory tests. Dashed line shows the best-fit relation. Grey shaded area represents the expected void ratio in the embankment.

In addition, an experiment was performed using a column with a diameter of 14.3 cm and a height of 35 cm, filled with a soil dry density of 1.52 Mg/m^3. A laboratory and field ceramic cup tensiometer (UMS T5x and UMS T4) and a dielectric water potential sensor (Decagon MPS-6) were installed in the column in order to measure suction and a capacitance moisture probe (Decagon 5TE) was used to measure volumetric water content. This soil column experiment provided supplementary data using a slightly smaller dry density sample. Initially, the sample was fully saturated, and it dried out progressively with time.

An extra experiment was performed on samples with a dry density of 1.39 Mg/m^3, using a dielectric water potential sensor (Decagon MPS-6) to measure suction and a capacitance moisture probe (Decagon 5TE) to measure volumetric water content. This experiment was performed without following a specific drying-wetting path, measuring the suction on statically compacted samples with different water contents. An important aspect is that all these experiments helped to check the handling and accuracy of the sensors that later were placed at the embankment.

The data measured by the different methods allowed defining the wetting and drying SWRCs (Figure 2.9). The suction readings obtained by T5x sensor during the soil column experiment were not represented, since they were identical to those measured by sensor T4. A modified van Genuchten model that is more suitable for high suction values was applied. It can be expressed as [Sánchez Castilla, 2004]:

$$S_e = \frac{S_r - S_{rl}}{S_{ls} - S_{rl}} = \left(1 + \left(\frac{s}{P}\right)^{\frac{1}{1-\lambda}}\right)^{-\lambda} \left(1 - \frac{s}{P_s}\right)^{\lambda_s} \quad (5),$$

where S_e is the effective degree of saturation, S_r is the current saturation degree, S_{ls} and S_{rl} are the maximum and residual degree of saturation respectively, s is suction, and P and λ are the van Genuchten material parameters. λ_s and P_s are the modified van Genuchten material parameters, which reduce high suction values, P_s is the maximum suction at the minimum degree of saturation. The resulting modified van Genuchten fitted parameters for both drying and wetting paths are summarized in Table 2.6.

Table 2.6: Modified van Genuchten soil–water retention curve (SWRC) fitting parameters for drying-wetting paths.

Fitted Parameters	***Drying***	***Wetting***
P (kPa)	66.7	9.5
λ (-)	0.28	0.20
P_s (kPa)	2.5×10^5	2.5×10^5
λ_s (-)	1.30	2.80
S_{ls}	1	1
S_{rl}	0	0

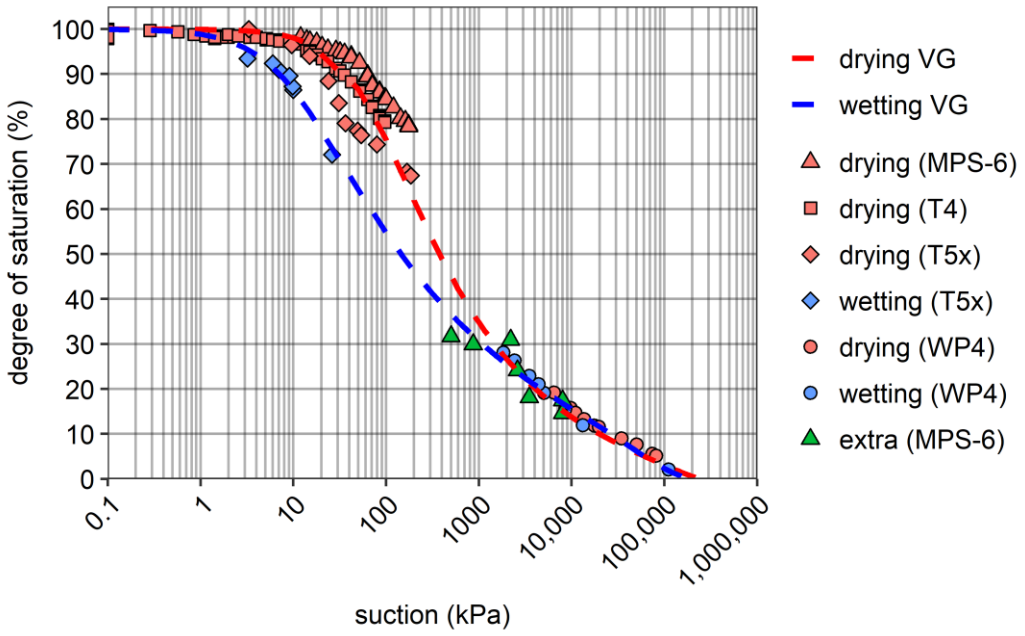

Figure 2.9: SWRC obtained by laboratory tests using different sensors. The resulting curves were calculated for drying-wetting conditions applying the modified van Genuchten (VG) model.

2.3.2. Monitoring results

In this section, the data measured during the first year are presented and discussed. Emphasis has been given on the complete time series registered by the sensors installed at the bare slopes (NnV and SnV). The time series cover the period of almost one year between April 2017 and the end of March 2018. Data measured at the two vegetated slopes are not presented, because on one side, there is no complete time series and on the other side, the vegetation is not fully developed. Data loss between the 7th and the 22th of September occurred due to technical problems.

2.3.2.1. Temperature data

Time series of temperature measurements at different depths from the North bare slope are compared with the ones of the South bare slope together with daily rainfall (Figure 2.10). A clear difference is appreciated between the North and South slopes and a generally higher temperature is recorded on the South slope. In addition, the sensors, which are installed close to the ground surface, indicate larger daily fluctuations at the South slope. These daily fluctuations decrease with depth and no prominent variations can be observed at

−56 cm between the two slopes. During spring and summer, temperature measurements at the deepest sensors (at −56 and −57 cm) are closer to the lower bound of the daily fluctuations of the most surficial sensors (at −1 and −16 cm), while in autumn and especially in winter, these measurements are closer to the upper bound. This characteristic is more noticeable on the North-facing slope, where soil temperatures at −56 cm sometimes are higher than the temperature at ground surface (−1 cm). This effect is due to the minor atmosphere interaction on the deepest soil layer, at −56 cm, and due the high thermal capacity of the soil to retain the heat transferred by radiation during spring and summer by the shallower layers. Soil temperature is mostly affected by climate interaction determined by air temperature, solar radiation, air humidity, rainfall, and wind, but also due to the ground surface cover (bare ground, vegetated slopes, etc.) and soil structure and physical properties [Florides & Kalogirou, 2004].

The effect of rainfall on the soil temperature is of minor influence when looking at the complete time series, but some individual temporal decreases of temperature close to the surface can be observed. An example of these specific rainfall episodes, which affect the temperature measurements, is illustrated in continuation.

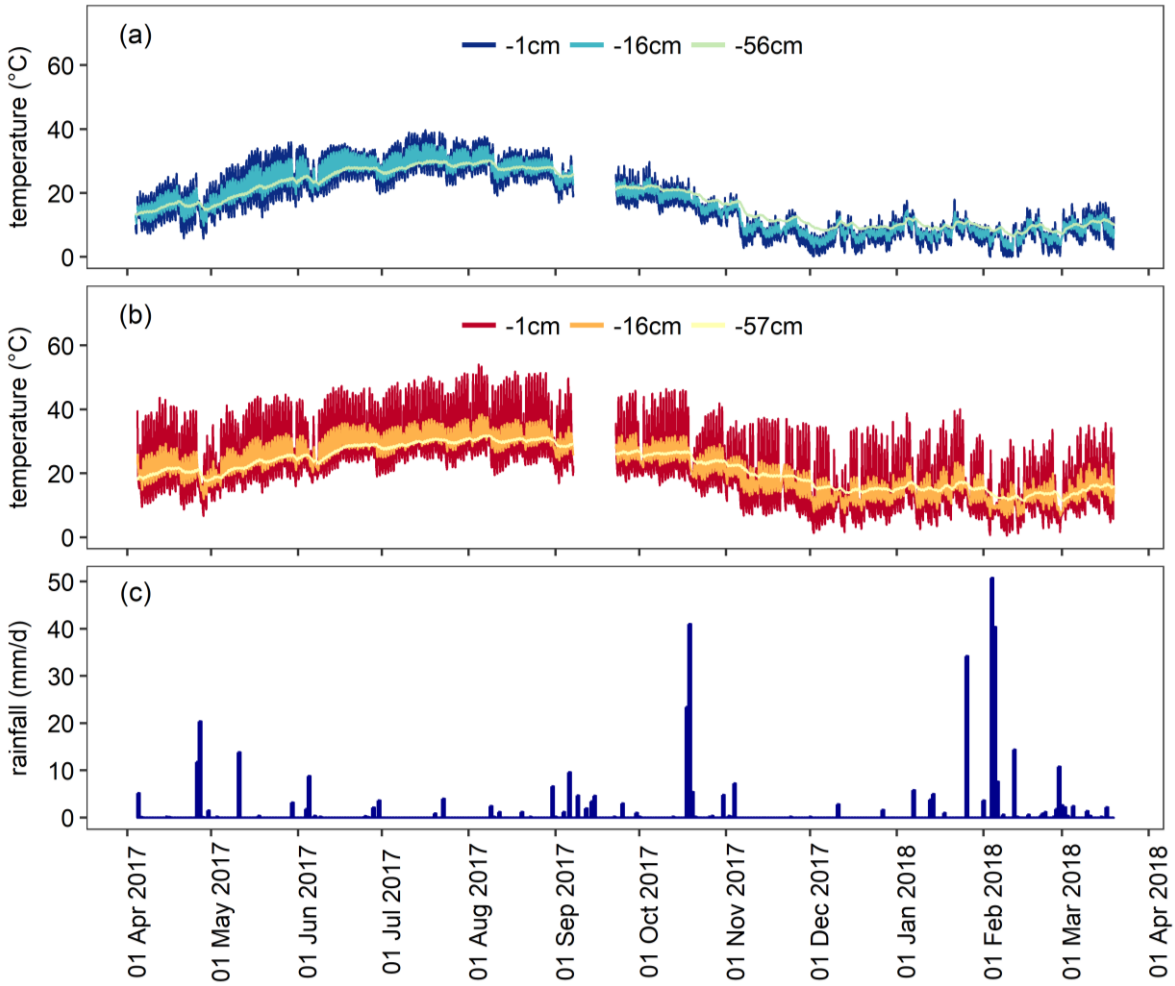

Figure 2.10: Soil temperature of the complete time series registered at the full-scale experiment. (a) North slope without vegetation; (b) South slope without vegetation; (c) daily rainfall.

The effects of an individual rainfall episode that occurred at the end of April 2017 are shown in Figure 2.11. The measured data indicate a strong relation between the rainfall and both the air and soil temperatures. While the daily temperature fluctuations are clearly visible before and after the rainfall episode at most sensors, temperature records contain a smoothening and slight general decrease during the rainfall, probably due to solar radiation reduction during rainy periods. Another interesting fact is that at the south slope the soil temperature at shallow depths are due to solar radiation much higher than the air temperature during sunny days. It can also be observed that the maximum or minimum peaks of the soil temperature occur later than the air temperature peak values, with an increasing of the lag effect with depth. This effect is detected at both slopes, but is much more intense in the South

profile. In addition, soil temperature during the event is slightly higher than air temperature measured at 9.5 cm over the soil surface.

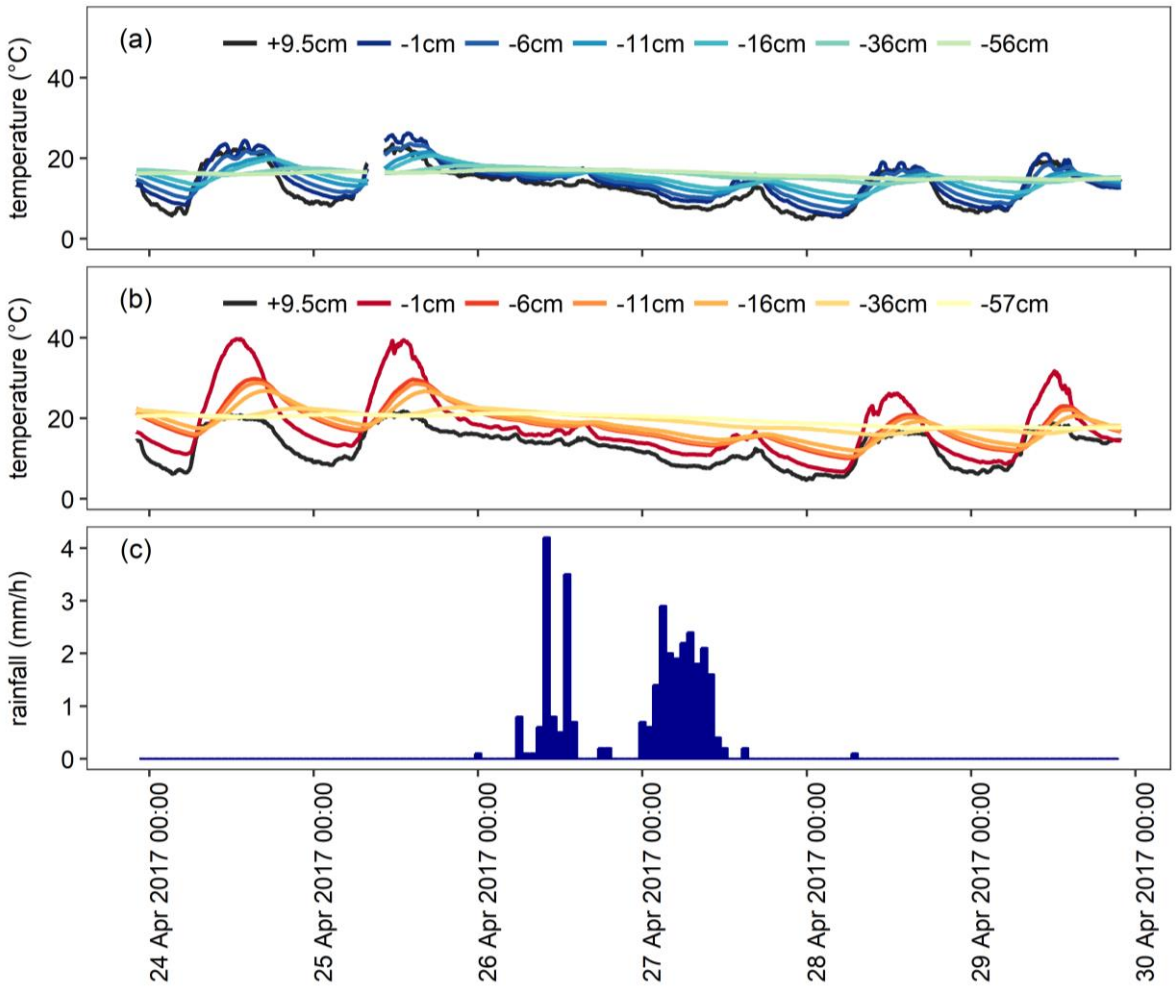

Figure 2.11: Air and soil temperature registered at the North (N) and South (S) slopes without vegetation during a rainstorm in April 2017. (a) Temperature data at the North slope; (b) temperature data at the South slope; (c) hourly rainfall.

2.3.2.2. Hydrologic slope response

Slope response to rainfall infiltration and its interaction with the atmosphere was evaluated through the changes in PWP and VWC. Time series of VWC and PWP measurements at three different depths at the North and South bare slopes are compared with the corresponding daily rainfall (Figure 2.12). Two well-known trends can be observed: (i) infiltration due to rainfall increases VWC and PWP and therefore reduces suction in partially saturated conditions, and, (ii) time intervals with less rainfall decreases VWC and PWP and

thus increase suction. In addition, the measurements show that the soil close to the surface is strongly influenced by rainfall and evaporation, while this effect decreases with depth. The relation between rainfall and both VWC and PWP is confirmed by sharp increases at the shallow sensors (at −16 cm and with minor magnitude at −36 cm) and at both slopes. The rainfall episodes with clearest VWC and PWP response occurred on 26–27 April 2017, 18–19 October 2017, 26 January 2018, and 4–5 February 2018. A comparison of the two slopes shows that the North slope is generally characterized by slightly higher soil moisture than the South slope.

Regarding the entire time series, the highest VWC values and reduced suction were recorded just after the installation of the sensors for approximately two months (April and May 2017). Following this period, the most important drying phase occurred, which took place during the month of June with a suction increase of ~36–60 kPa/day for the shallower sensors (−11 and −16 cm respectively), ~31–48 kPa/day for the middle sensors (−32 and −36 cm respectively), and ~3–4 kPa/day for the deepest sensors (−72 and −62 cm respectively). In the following months (July–mid October), a smooth decrease in both VWC and PWP was recorded. This trend breaks with an extreme rainfall episode recorded on the 18th and 19th of October 2017, when 64 mm rainfall over 24 h were measured. This rainfall provoked a sharp and important increase at the shallow sensors of both slopes. The increase in VWC and PWP is less important with soil depth and has no prominent variation at the deepest soil moisture sensors (located at −56 and −57 cm respectively). After this heavy and long duration rainfall, the shallow soil layer down to 16 cm depth was near to saturation for both slopes, since the suction measurements were close to 0 kPa. The VWC registered very high values at the south slope, while the same sensor at −16 cm at the North slope exhibited technical problems with some data lost. Nevertheless, it can be deduced from the readings recorded during the month of November that the VWC increase was also important. Two rainfall events at the beginning of 2018 triggered an important increase in water content and pore water pressure. One on the 26th of January with 34 mm rain in 24 h, and the highest rainfall recorded during the entire study, which occurred on the 4th and 5th of February 2018 and included 90 mm rain in 30 h. After these two rainfall episodes, VWC and PWP values strongly increased and continued at high values with only a slight decreasing trend.

In the following, special attention is given to the pore water pressure measurements gathered by the T4 ceramic cup tensiometers (Figure 2.12c). These tensiometers are the most delicate devices in the monitoring set-up, because the water-filled cup starts to de-saturate when the soil gets dryer than ~90 kPa suction. In this case, it needs to be uninstalled in the field and saturated again in the laboratory with de-aired water. The initial T4-readings show a similar behavior as the ones recorded by the MPS-6 dielectric water potential sensors (Figure 2.12b): very low suction values close to saturation during the first 2 months. After the high drying rate of June, the North tensiometer, at 62 cm depth, reached its maximum suction value of about 85 kPa and remained constant for several days. Then, the measures changed abruptly to 0 kPa. The interpretation of this sharp change is that the soil at that depth got even dryer at that moment, reaching the ceramic bubble point of 1500 kPa. Consequently, the cup, which is filled with de-aired water, quickly ran out and was fully filled with air. Therefore, the tensiometer was extracted on the 20th of September and saturated with de-aired water in the laboratory, reinstalling it on the 5th of October. The measurements after reinstalling the North tensiometer reached its maximum suction value of 85 kPa in 36 h, indicating suction at that depth was higher than 85 kPa, partially de-saturating the ceramic cup. This reading remained almost constant for two weeks until a heavy and long duration rainfall on the 18th and 19th of October saturated the ceramic cup and its readings reached the value of 4 kPa suction over 24 h. In contrast, the South T4 tensiometer did not reach its maximum suction value of 85 kPa during the month of June and suction values were slightly decreasing from August 2017 (~30 kPa) until February 2018 (~17 kPa). Then, the very important rainfall event on the 4th and 5th of February 2018 produced a sharp change. After this heavy rainfall, readings at the North and South tensiometers indicate a complete saturation at that depth (0.85 kPa and 1.13 kPa). These PWP values represent a water column of 8.7 cm and 11.6 cm above the sensors at the North and South slope, respectively.

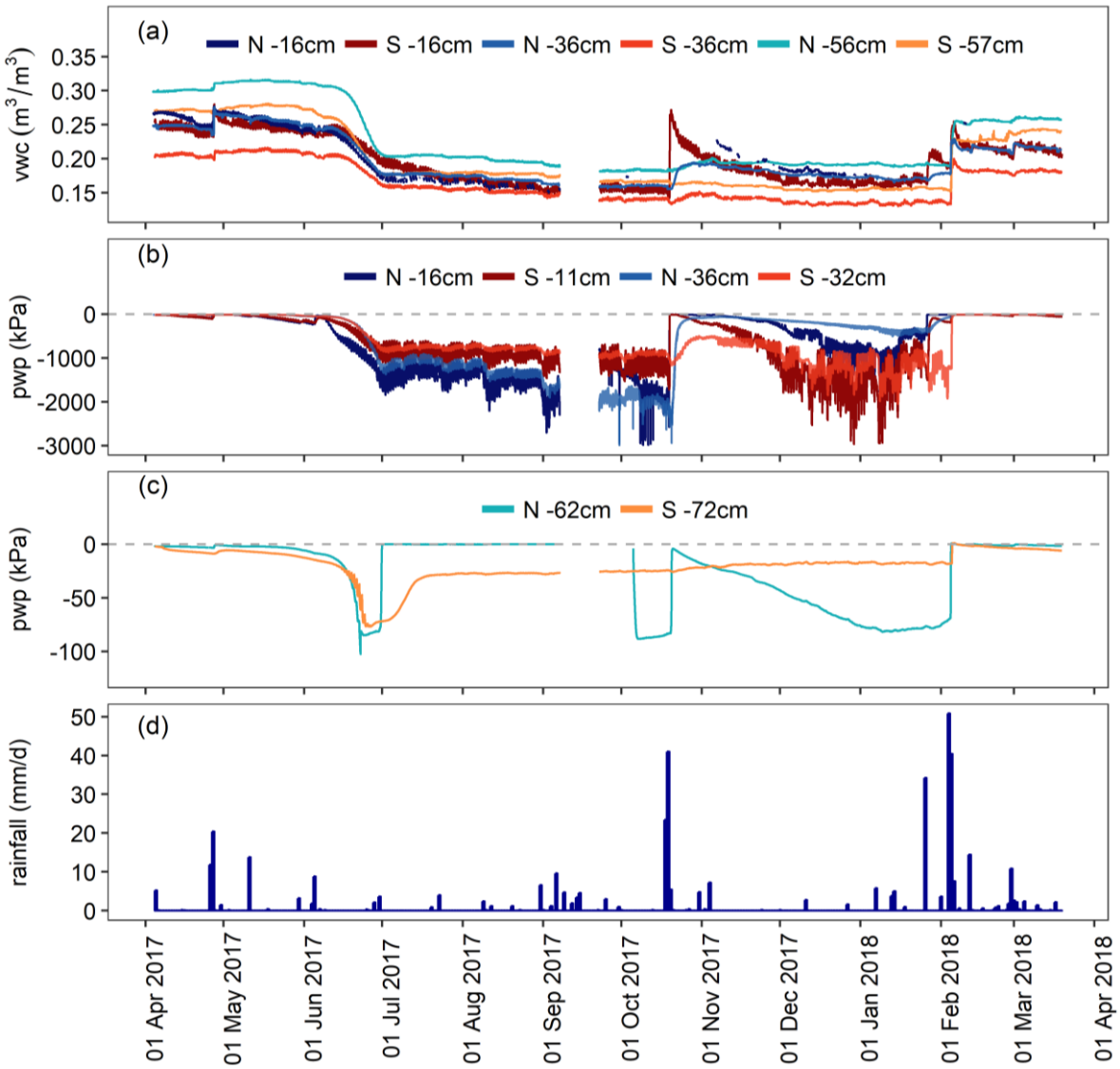

Figure 2.12: Rainfall infiltration at the North (N) and South (S) slope without vegetation. (a) Volumetric water content data measured by 5TE; (b) pore water pressure recorded by MPS-6 tensiometers; (c) pore water pressure measured by T4 tensiometers; (d) daily rainfall.

Many rainfalls have been recorded throughout the recorded period, but most of them did not trigger a significant change in moisture and pore water pressure. These results suggest that part of the rainfall did not infiltrate, but transformed into surface runoff. That's why the ratio between infiltration and surface runoff is closely related to the duration and intensity of rainfall, as well as the initial conditions of soil moisture and the slope angles, amongst others [Horton, 1940]. In the following, two examples of the time series are selected: (i) a "long duration" rainfall that generated important changes in terms of moisture and pore water

pressure (Figure 2.13), and, (ii) a “short duration” rainfall that lasted 3 h and did not trigger significant variations (Figure 2.14).

The “long duration” rainfall episode lasted ~35 h, accumulated a total amount of 32 mm, and therefore had an average rainfall rate of 0.9 mm/h. The effect of rainfall on moisture and pore water pressure shows a direct relation between the rainfall timing and the infiltration process (Figure 2.13). There is a clear time lag that increases with depth, indicating a vertical flow trajectory. The magnitude of moisture and pore water pressure changes decreases with depth and has negligible variations at the deepest soil moisture sensors (at −56 and −57 cm, respectively). Both MPS-6 and T4 tensiometers finally reached values close to 0 kPa (9 kPa is the minimum suction range for MPS-6 device), which indicated that the soil was close to saturation after this rainfall episode.

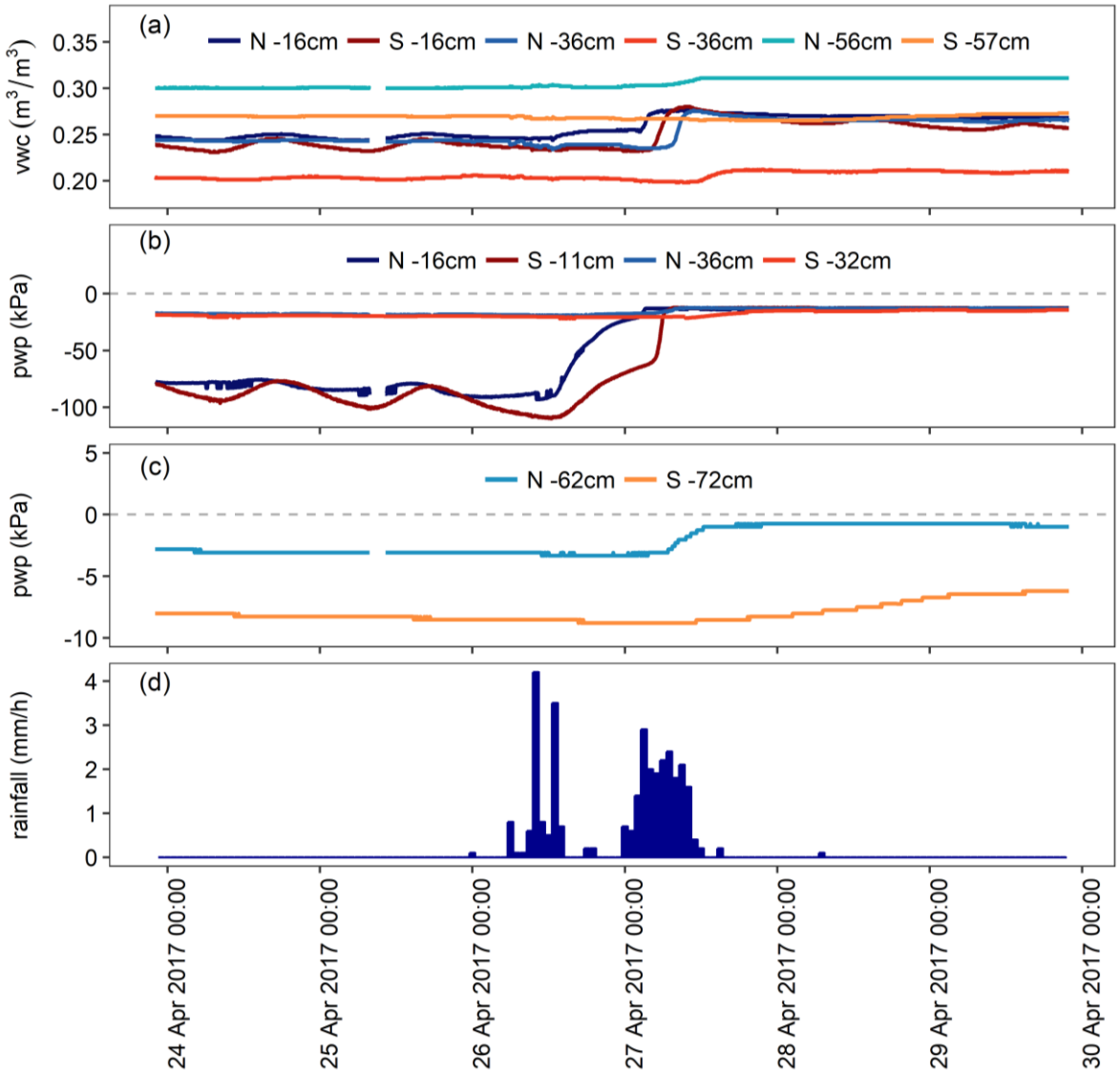

Figure 2.13: Soil moisture and pore water pressure registered during a rainstorm in April 2017 at the North (N) and South (S) slopes without vegetation. (a) Volumetric water content data measured by 5TE; (b) pore water pressure recorded by MPS-6 tensiometers; (c) pore water pressure measured by T4 tensiometers; (d) hourly rainfall.

The "short duration" rainfall lasted only three hours, accumulated a total amount of 13.8 mm, and had a clear hourly peak with an intensity of 12.7 mm/h. There is no response on the volumetric water content sensors at all depths, while pore water pressure slightly increase on the most superficial sensors located at 16 cm depth (Figure 2.14). This suggests a clear relationship between rainfall duration and intensity and the subsequent infiltration process. Therefore, a runoff measurement system will be installed in 2018 at each of the four

monitored slopes in order to understand better the rainfall infiltration and runoff process and to corroborate the infiltration rate.

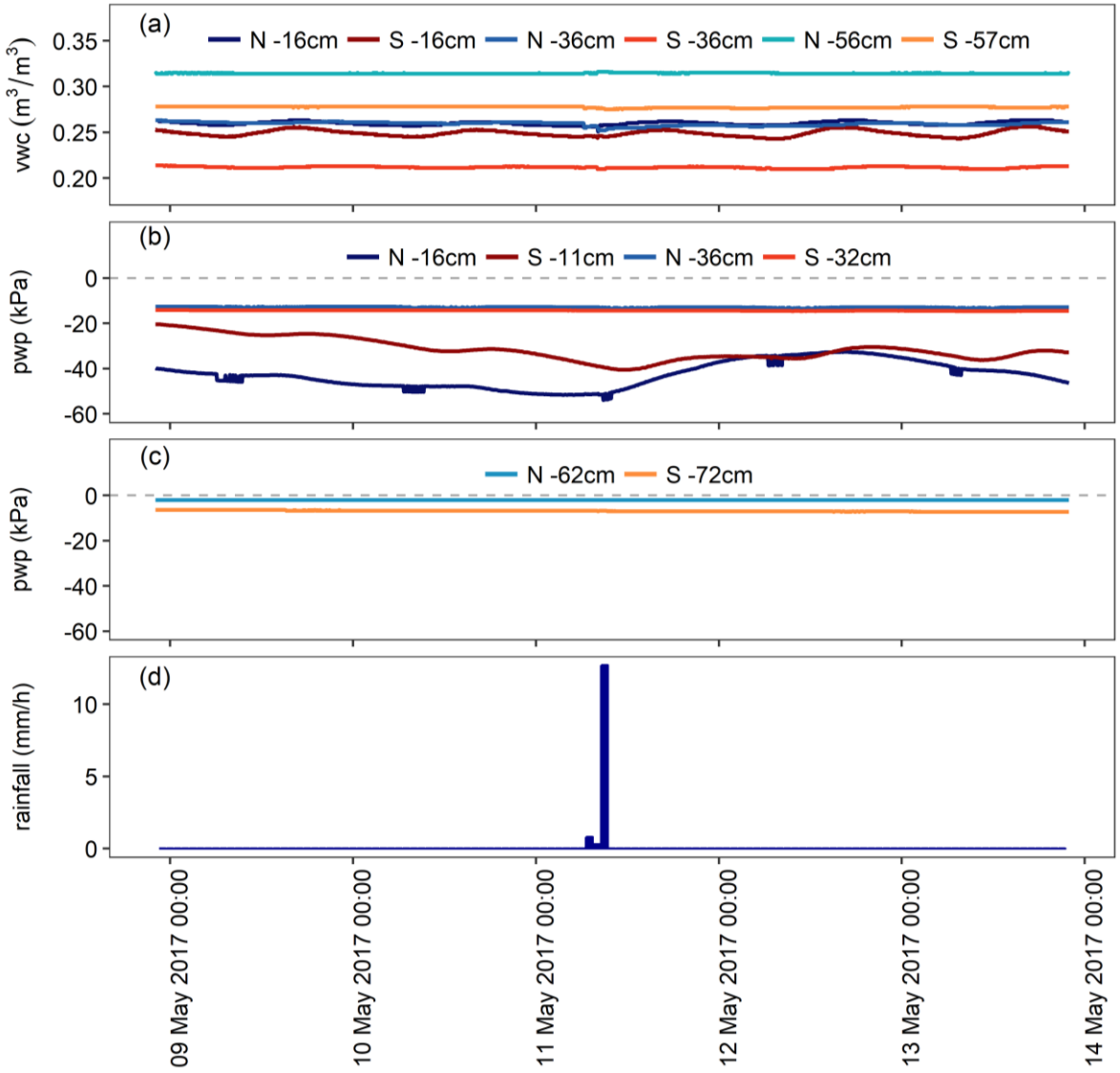

Figure 2.14: Soil moisture and pore water pressure registered during a rainstorm in May 2017 at the North (N) and South (S) slopes without vegetation. (a) Volumetric water content data measured by 5TE; (b) pore water pressure recorded by MPS-6 tensiometers; (c) pore water pressure measured by T4 tensiometers; (d) hourly rainfall.

Finally, the temporal variation of VWC, PWP, and soil–air temperature with depth is illustrated for both North and South bare slopes during the first year of monitoring in two-month intervals (Figure 2.15). The data show that the South slope is somewhat dryer in terms of VWC, with the lowest VWC values at 36 cm depth for almost all the recorded period. Changes in PWP are more important on the shallower devices while there are no important

variations on the deepest ones. There are no PWP readings at −62 cm during the months of August and October 2017 because of the desaturation of the North T4 tensiometer. In terms of soil temperature, a clear difference is appreciated between the North and South slopes with higher values on the South-facing slope. This difference in temperature is much more noticeable at the most surficial sensor, at 1 cm depth, with temperatures up to 40 °C due to solar radiation. In contrast, the radiation effect is not appreciated on the North-facing slope. This radiation effect strongly decreases with depth and only a minor influence is observed at 6 cm depth. On the South-facing slope, temperature differences of about 10 °C between the sensors at −1 cm and −6 cm are observed for most months.

The higher VWC values measured at intermediate depth could be explained by taking into account differences in the porosity of the soil surrounding the sensors.

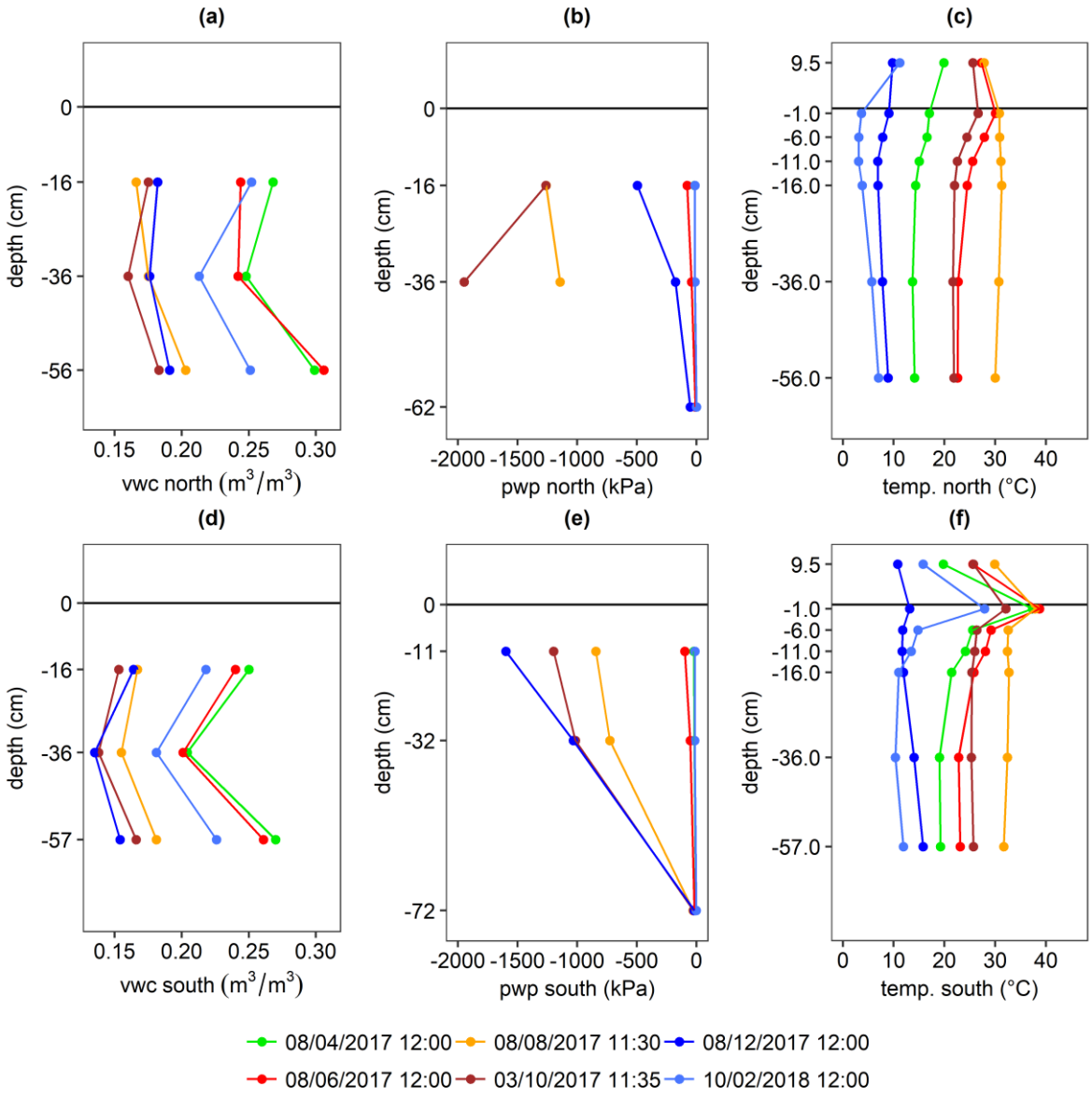

Figure 2.15: Temporal variation of the variations in volumetric water content (VWC), pore water pressure (PWP), and temperature (temp.) with depth at the North and South bare profiles. The data are represented in two-month intervals from April 2017–February 2018. (a) Volumetric water content at North slope; (b) pore water pressure at North slope; (c) air and soil temperature at North slope; (d) volumetric water content at South slope; (e) pore water pressure at South slope; (f) air and soil temperature at South slope.

2.4. Conclusions

The monitoring of soil–vegetation–atmosphere interactions is a necessary but difficult task. The experience of installing and verifying the correct sensing of all devices confirms that the monitoring of so many different processes is complex in an outdoor

experiment and strongly differs from laboratory tests, which are performed under controlled conditions. The correct calibration, adequate installation and permanent maintenance of the sensors is time-consuming, but fundamental. In our set-up, the most critical devices are the water-filled ceramic cup tensiometers, which de-saturated sometimes.

A good laboratory characterization of strength and hydrologic parameters is essential to understand correctly the infiltration process and to model the slope failure mechanisms. In this case, the laboratory tests indicate that there is a great contribution of suction to the shear strength. However, laboratory results may diverge from field observations, since heterogeneities are much more common in large experiments like this embankment. For example, in the trenches which were excavated at the four slope partitions, we observed cracks, fissures, and macropores that may have developed due to small displacements in the soil or due to root growing. All these features create preferential flow paths of the water and increase soil permeability and reduce suction and consequently also its strength. Therefore, permeability in the embankment is certainly much higher than the one measured in the laboratory (in the order of 10^{-8} and 10^{-7} m/s), which was obtained from a small homogeneous soil sample.

Preliminary analysis of the recorded data during the first year revealed the following outcomes regarding temperature and heat flux: (i) soil temperature strongly differs from North to South. (ii) At the terrain surface (sensors installed at −1 cm) of the South-facing slope, the temperatures are much higher (up to 55 °C) than the air temperature due to the solar radiation. This effect was not observed at the North-facing slope. (iii) A clear daily temperature fluctuation is visible at the most surficial sensors, while this effect is negligible at about −50 cm.

Regarding the rainfall infiltration, the results show: (i) high soil moisture during winter/spring and a dry period during summer and autumn. Only the most important rainfall, recorded on the 4th and 5th of February 2018 (90 mm rain in 30 h), saturated the deepest soil layer at both North and South bare slopes. The highest drying rate took place during the month of June. (ii) There is a clear relationship between rainfall duration and intensity and the subsequent infiltration process. Most of the short duration rainfalls did not trigger significant variations in terms of VWC and PWP at all depths. In contrast, long duration

rainfalls triggered a sharp increase on both VWC and PWP, while this effect decreases with depth.

All the monitored data will improve the understanding of the soil–vegetation–atmosphere interactions. Furthermore, the records provide essential input data for numerical modelling of the coupled thermo-hydro-mechanical processes in geological media and will serve to validate the SVA models with the aim of applying them to natural slopes of the Pyrenees.

Chapter 3

SLOPE ORIENTATION AND VEGETATION EFFECTS ON SOIL THERMO-HYDRAULIC BEHAVIOR. AN EXPERIMENTAL STUDY.

This chapter reproduces the article published in the *Sustainability* journal on December 22, 2020. It focusses on slope thermo-hydraulic response to climatic actions considering different orientations (North and South) and slope covers (bare and vegetated).

Publication reference:

Oorthuis, R., Vaunat, J., Hürlimann, M., Lloret, A., Moya, J., Puig-Polo, C., & Fraccica, A. (2020). Slope Orientation and Vegetation Effects on Soil Thermo-Hydraulic Behavior. An Experimental Study. *Sustainability*, *13*(1), 14. https://doi.org/10.3390/su13010014.

Abstract

The stability and erosion of natural and man-made slopes is influenced by soil-vegetation-atmosphere interactions and the thermo-hydro-mechanical slope conditions. Understanding such interactions at the source of slope mass-wasting is important to develop land-use planning strategy and to promote environmentally adapted mitigation strategies, such as the use of vegetation to stabilize slopes and control erosion. Monitoring is essential for calibrating and validating models and for better comprehending the physical mechanisms of soil-vegetation-atmosphere interactions. We approached this complex problem by means of an experimental work in a full-scale monitored embankment, which is divided into four instrumented partitions. These partitions are North or South-faced and present a bare and vegetation cover at each orientation. Our main findings show that vegetation enhances rainfall infiltration and decreases runoff, which reduces slope stability and surficial erosion,

while plant transpiration induces higher suctions and hence slope stability. Concerning thermal aspects, vegetation reduces the incidence of net solar radiation and consequently heat flux. Thus, daily temperature fluctuations and evaporation decreases. However, the effect of vegetation in the development of dryer soil conditions is more significant than the orientation effect, presenting higher drying rates and states at the North-vegetated slope compared to the South-bare slope.

Keywords: embankment; rainfall; infiltration; temperature; vegetation cover; monitoring

3.1. Introduction

Slope mass-wasting induced by erosion and slope failures has become, in the past decade, one of the most important environmental problems in present and forthcoming semi-arid regions [Boardman & Poesen, 2006]. This geomorphological process has many direct and indirect socio-economic consequences such as loss of agricultural and forest lands, reduction of reservoir capacity by sedimentation, damage to infrastructures and hazard related fatalities [Spiker & Gori, 2003, Guzzetti et al., 2004; Petley, 2012; Sidle & Bogaard, 2016;]. All these impacts may be a limitation for the sustainable development of human society. Therefore, the understanding of the processes leading to slope mass-wasting is crucial. One of the main mechanisms pointed out as responsible of the triggering of slope failures is the reduction of soil shear strength due to increase in pore water pressure during heavy rainfall [Fredlund & Rahardjo, 1993; Rahardjo et al., 1995; Vanapalli et al., 1996; Fourie et al., 1999; Highland & Bobrowsky, 2008]. On the other hand, rainfall energy is known to be the principal cause of soil erosion on bare land, when the soil lacks a protective vegetation cover [Durán Zuazo & Rodríguez Pleguezuelo, 2008]. There is also a strong concern about the effect of the current climate change on slope mass-wasting, since recent studies have shown increases of extreme precipitation events after more intense droughts [Nearing et al., 2005; Durán Zuazo & Rodríguez Pleguezuelo, 2008; IPCC, 2014; Panagos et al., 2014].

The adoption of traditional engineering measures to prevent landslides and slope erosion can be costly, unsustainable and difficult to construct. Alternatively, solutions based on the use of vegetation on the surface of the slope, whether natural or man-made, provide

sustainable and environment-friendly measures at a relative low cost [Donald H. Gray, 1996; Jotisankasa et al., 2014]. Slope erosion is related to the characteristics of surface water flow, the hydrologic surface conditions, soil texture and the slope gradient and cover, among others [Igwe et al., 2017; Q. Zhao et al., 2019]. Vegetation cover reduces rainfall energy by protecting the soil surface from rainfall drops and intercepting runoff, which decreases soil erosion [Bochet et al., 2006]. In addition, plant roots can reinforce the soil due to root tensile strength, which increases the soil shear strength and consequently slope stability [Ali & Osman, 2008; Chok et al., 2015; Maffra et al., 2019]. Adequate design of such solutions requires accounting for multiple soil-vegetation-atmosphere interactions [Greenway, 1987; Gens, 2010; Rahardjo et al., 2012; Elia et al., 2017; Ni et al., 2018], such as rainfall canopy interception, protection from both raindrop impact and solar radiation, changes in infiltration/runoff mechanisms, evapotranspiration, and root soil reinforcement [Coppin & Richards, 1990; Simon & Collison, 2002; Ali & Osman, 2008; Preti & Giadrossich, 2009; Eab et al., 2015; Capilleri et al., 2016], among others. The balance between solar, atmospheric and heat fluxes at ground surface plays an important role as it controls the evaporation rates [Sauer & Horton, 2015] and thus the suction in the soil. This effect is patent on bare ground where soil heat inflow can be half of the net solar radiation [Idso et al., 1975] but is known to be reduced in vegetated ground [Oliver et al., 1987; Lozano-Parra et al., 2018]. There are, however, few quantitative experimental evidences of the effect of vegetation on ground temperature. Slope orientation is another factor controlling the net solar radiation entering in the soil.

On the other hand, water uptake by roots is responsible for suction increase at depth while root growth and penetration modify soil permeability. Gain in suction due to root water uptake enhances soil shear strength and consequently slope stability [Ng et al., 2013, 2016; Garg, Leung, et al., 2015; Zhu & Zhang, 2015; Gonzalez-Ollauri & Mickovski, 2017; Yildiz et al., 2019]. Results concerning the effect of plants on soil permeability are more diverging and depend on the type of vegetation, root architecture and ageing. Depending on the conditions, authors report lower [Rahardjo et al., 2014; Garg, Coo, et al., 2015; Leung et al., 2015] or higher [Le Bissonnais et al., 2004; Joshi & Tambe, 2010; J. Huang et al., 2013;

Vergani & Graf, 2016; Ni et al., 2017; Fraccica et al., 2019] water infiltration in vegetated soils.

Only a few studies are available on full-scale experiments that monitor the soil-vegetation-atmosphere interactions in a comprehensive way over a long time period [e.g., Y. J. Cui et al. 2010; Yoshioka et al. 2015; Bicalho et al. 2018]. Therefore, with the perspective to provide quantitative data on the relative effect of vegetation and atmosphere conditions, this work presents results from a large-scale experiment purposely built to monitor thermo-hydraulic variables over a long period of time and exposed to site climatic actions.

3.2. Methods

3.2.1. Site, embankment and monitoring description

The experimental embankment was built at the end of 2016 at the site of Parc UPC Agròpolis (41°17′18′’N 2°02′35′’E), located 20 km southwest from Barcelona, Spain.

The embankment is 18 m long, 12 m wide, 2.5 m high and has 3H:2V slopes (34 degrees); it consists of four instrumented partitions with different slope orientations and covers: North not Vegetated (NnV), North Vegetated (NV), South not Vegetated (SnV) and South Vegetated (SV). In each partition, thermo-hydraulic variables are monitored within a shallow soil layer of 50–70 cm thickness, wrapped into an impervious polyethylene geomembrane to avoid water transfer with other partitions. The soil used is a silty sand with a large part of coarse-grained particles. A complete description of the monitoring set-up, soil properties and laboratory tests can be found in Oorthuis et al. [2018]. Figure 3.1 shows details of the North-facing partitions.

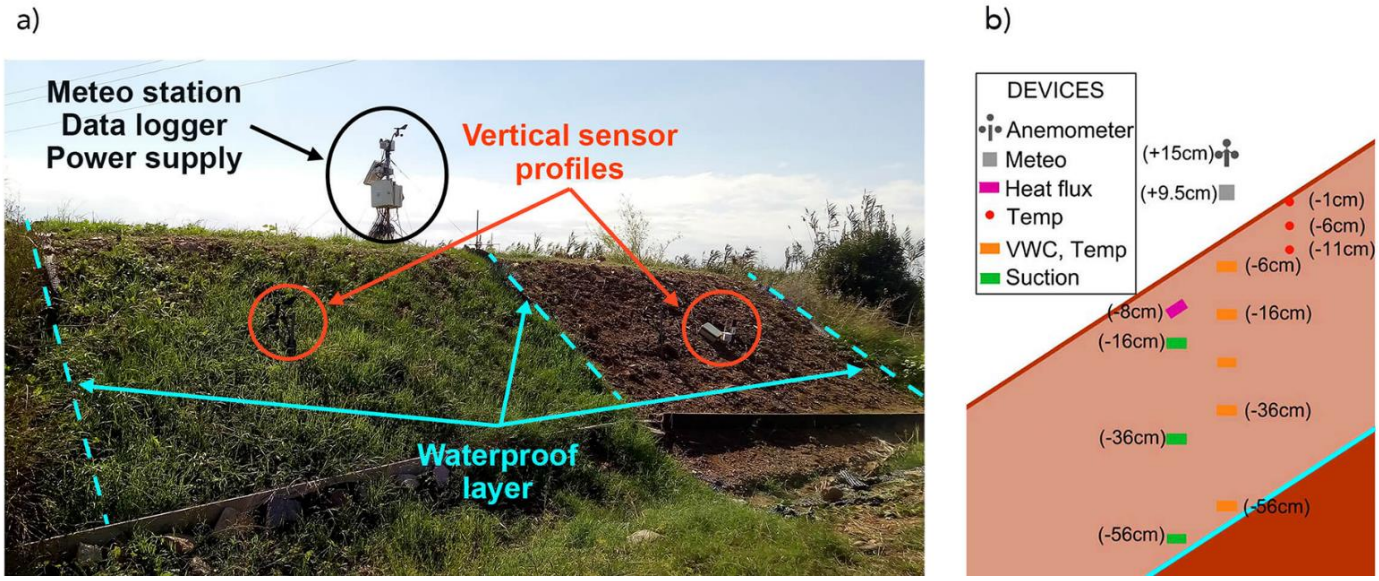

Figure 3.1: (a) Photograph of the embankment looking towards the North-faced slope and (b) schematic distribution of North vegetated (NV) sensor profile. Meteo stands for air temperature, relative humidity and barometric pressure, VWC for volumetric water content, Temp for temperature and Suction for matric suction.

The monitoring of the slopes includes 56 sensors installed at four vertical profiles. They record 114 variables at different depths each 5 min: volumetric water content (VWC), matric suction (S_m), pore water pressure, temperature, heat flux, and electrical conductivity. In addition, measurements of air temperature, relative humidity, and barometric pressure are recorded above each partition (at 9.5 cm height). Wind velocity and direction are measured at 15 cm height above the soil. The same variables are monitored on the top of the embankment by a standard meteorological station including a tipping bucket rain gauge of 0.2 mm resolution and a total solar radiation sensor located at 180 cm above soil surface. Finally, sensors to measure net solar radiation have been installed at 55 cm above ground level in the direction parallel to the slope at both North and South bare slopes.

3.2.2. Characterization of the vegetation species

The growth of vegetation at the bare slopes was prevented by periodic application of herbicide. A seed mix 80% Cynodon dactylon and 20% Festuca arundinacea was hand sowed with a seeding density of 34 g/m^2 and an average plant spacing of 30 ± 5 mm. Seed sowing density and distance are factors affecting the hydraulic behavior of soils [Ni et al., 2017; Ng et al., 2019]. These perennial species were chosen because they have a high drought

tolerance, increase soil strength due to their roots and are commonly used in bioengineering for slope revegetation in warm climates [Bacon, 1993; Elmi & West, 1995; Wilman et al., 1998; M. Zhang et al., 2013; F. Chen et al., 2015; Garg, Coo, et al., 2015]. A mix of the hand sown vegetation species and native plants from the Llobregat river delta coexist and grow under natural conditions with no irrigation.

The specific vegetation cover (SVC) was defined as the relation between vegetated covered area and the total slope area and determined by means of the image processing freeware software ImageJ 1.52a [https://imagej.nih.gov/ij/]. The evolution of the SVC was assessed by converting color images taken from the vegetated slopes to 8-bit black and white images and by applying a threshold color tool to recognize vegetation from soil.

3.3. Results and discussion

3.3.1. Hydraulic aspects

Figure 3.2 presents almost 2.5 years of VWC and S_m time series monitored at three and four different depths, respectively, within the vegetated and bare slopes. For comparison purposes, daily rainfall and time variation of the SVC are also indicated. Discussion of Figure 3.2 is further supported by Figure 3.3, which presents a comparison of changes in water contents measured in the different slopes at the same depth and for the same event, distinguishing between rainfall infiltration events (Figure 3.3a,b) and drying periods (Figure 3.3c–e). For drying periods (time windows between rainfall events), the decrease in water content is divided by the drying period duration in order to provide an averaged drying rate. For wetting or infiltration events, the increment in water content is assessed by the difference between the initial VWC prior to the rainfall event, and the maximum VWC observed during or after the rainfall event. The interval of analysis considered in Figure 3.3 lasts over the period of full vegetation cover (SVC = 1) and only events causing perceptible variations in VWC, at least at the most surficial sensor, have been reported.

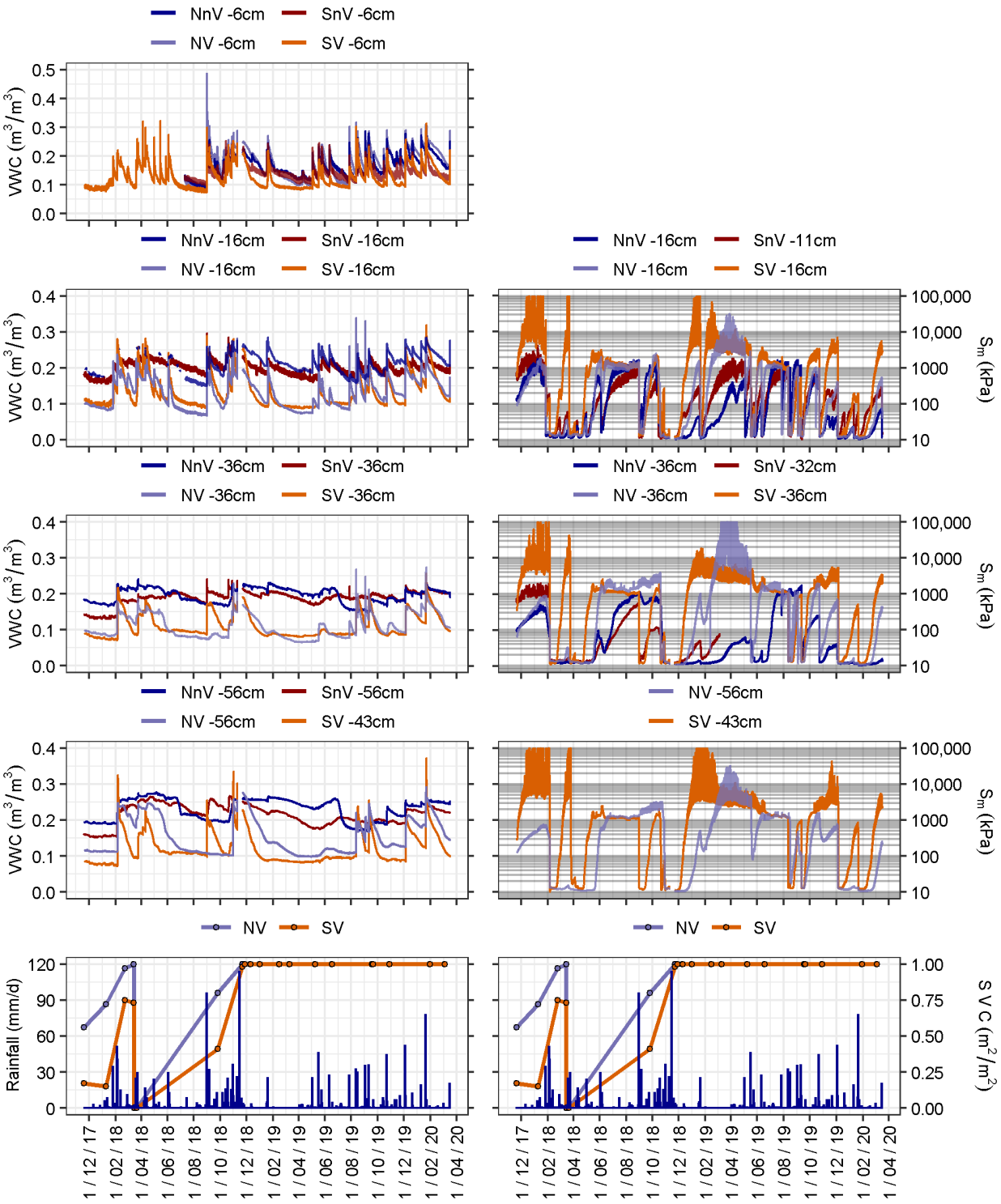

Figure 3.2: Time series of hydraulic variables at all embankment slopes. Left column; volumetric water content (VWC) at several depths. Right column; suction (S_m) at different depths. Last row of each column: daily rainfall and Specific Vegetation Cover (SVC) at North and South vegetated slopes. Labels NV, NnV and SnV indicate: North vegetated, North non-vegetated, South vegetated and South non-vegetated slopes, respectively.

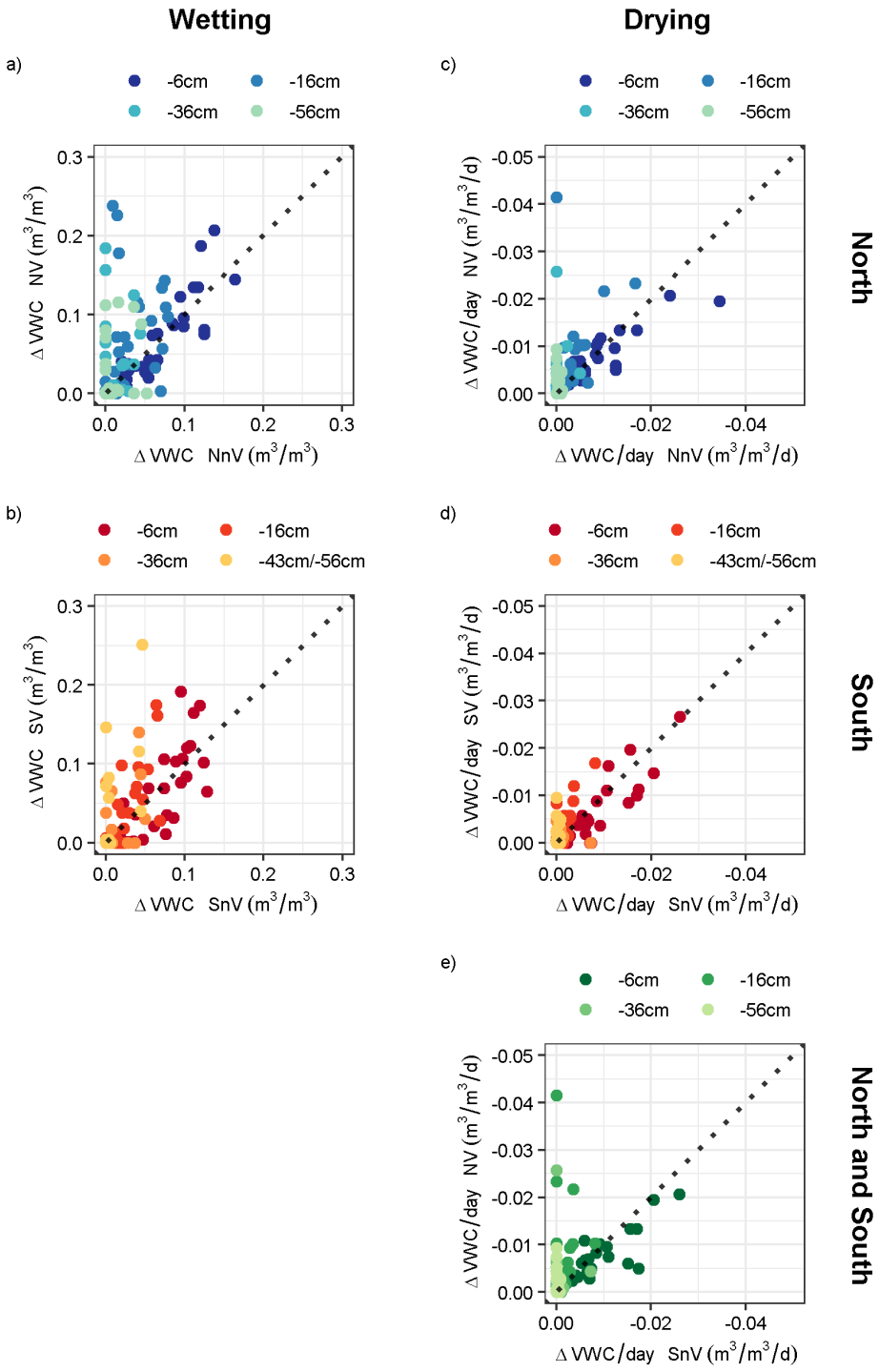

Figure 3.3: Comparison between changes of water contents (ΔVWC) at the same depth and for the same event in the four embankment slopes: (a) and (b) ΔVWC during infiltration in the North and South slopes; (c) and (d) ΔVWC (divided by drying period duration) during drying in the North and South slopes; (e) ΔVWC (divided by drying period duration) in the North vegetated and South non-vegetated slopes. Note: vegetated data correspond to the period when slopes were fully covered by vegetation (SVC = 1, from December 2018 to March 2020).

From a general point of view, VWCs exhibit lower values in the vegetated than in the non-vegetated slopes, independently of the orientation. They also experiment higher and quicker increments during rainfall events. This applies to all sensors, with the exception of the shallowest one (−6 cm depth), where all VWC series present similar variations over the whole period (see comment below). These results highlight, on the one hand, higher infiltration rates at the vegetated slopes and, thus, lower runoff. On the other hand, they point out that, whatever the slope orientation, drying is higher in the vegetated than in the non-vegetated slopes for depths below 6 cm, evidencing the in-depth effect of evapotranspiration due to root penetration pointed out by Guswa [2010]. The latter result is also portrayed in Figure 3.3c,d where data at depths greater than 6cm are located above the line of equal changes of VWC in vegetated and non-vegetated slopes.

Analysis of water content variation is further supported by the monitoring of S_m (negative water potential), which is the driving variable for water flow within the soil and is related to VWC by the soil-water retention curve. S_m ranges between 10 kPa and 1 MPa in the non-vegetated slopes and between 10 kPa and 100 MPa in the vegetated ones. 10 kPa is the air entry potential of the largest pores in the ceramic discs of the sensor and corresponds to the lower limit of sensor measurement range, it can be reasonably interpreted as indicating soil quasi-saturation. In the upper range, measurements present large oscillations, particularly for values higher than 3 MPa. This is a consequence of the moisture characteristic curve of sensor porous ceramic, characterized by large variations of matric suction under small changes in water content for suctions higher than 3 MPa [Decagon Devices, 2016]. In any case, suction measurements exhibit higher values and variations in the vegetated than in the non-vegetated slopes, which corroborates the measurements of water content and consistently support the in-depth effect of plants transpiration.

Regarding infiltration, both suction and water content measurements present faster recovery after rainfall events in the vegetated slope, whatever the slope orientation is. VWC and S_m records show that the instrumented soil layer gets saturated at all depths during the most intense rainfalls, while water only percolates into the shallowest layer during the low intensity ones. Comparison of time series monitored at sensors located along the same

vertical profile indicates moreover an attenuation of VWC changes and suction drops with depth, which is consistent with the process of water transport in the layer.

These results can be favorably contrasted with other works on vegetation effect, which highlight the importance of root content and morphology. Since the shallow layer is quickly dried to low water content during periods without rainfall, plants are forced to develop roots at higher depths [Schenk & Jackson, 2002; Guswa, 2010]. As root growth generates in-depth fissures and preferential paths, the hydraulic conductivity is enhanced in the corresponding layer [Gray & Norum, 1967; Schenk & Jackson, 2002; Guswa, 2010; Vergani & Graf, 2016; Song et al., 2017], which causes a faster hydraulic response [Song et al., 2017]. The latter is clearly illustrated in Figure 3.3a,b where the points corresponding to depths greater than 6 cm are located above the line of equal changes of water contents in vegetated and non-vegetated slopes.

A striking result concerns the similarity existing between VWC measurements at 6cm depth, whatever the slope is vegetated or not (see Figure 3.2 and Figure 3.3a,b). Suction has not been measured at this depth, but, since water content is related to suction by the retention curve of the soil, it is also expected that suction values, and thus hydraulic gradients between soil surface and 6 cm depth, are similar in the two types of slope covers. This reasoning supports the existence of higher soil permeability in the vegetated slopes. In fact, the higher infiltration evidenced by the quicker saturation of the vegetated layer during rainfall cannot be explained by an increase of hydraulic gradients at slope surface. This is consistent with the existence of preferential water paths through macropores created by root growth mentioned before.

A cross-comparison between vegetation and orientation effect is finally provided by Figure 3.3e. It depicts the correlation between changes in water content in the North vegetated and the South non-vegetated slopes. Data are mostly above the bisecting line, indicating that drying is higher in the North slope despite of its orientation. This result states the prominent effect of vegetation transpiration on slope orientation.

In conclusion, the study quantitatively confirms that vegetation globally increases the amount of water transfer between the soil and the atmosphere, regardless of the slope

orientation and the period of the year. Insights provided by measurements of water content and suction variations at different depths allow moreover to forward mechanisms for the increase in water transfer: evapotranspiration in periods of drying, and enhanced permeability by in-depth root penetration in periods of infiltration. It is worth noting that the study covers a wide range of solar radiation values, as data were collected during different seasons.

3.3.2. Thermal aspects

Five minute period time series of soil temperatures monitored at the SnV, SV, NnV and NV slopes are shown in Figure 3.4 (December 2017–April 2020), together with the maximum and minimum daily temperature measured at 9.5 cm above the surface. SVC evolution is also plotted for the vegetated slopes Figure 3.4b,d). Figure 3.4e,f show smoothed time series at the shallower (−1 cm) and deeper (−43/56 cm) sensors in order to compare daily variations. They have been obtained using the Locally Estimated Scatterplot Smoothing (LOESS) [Cleveland, 1979] with smoothing parameter equal to 0.3.

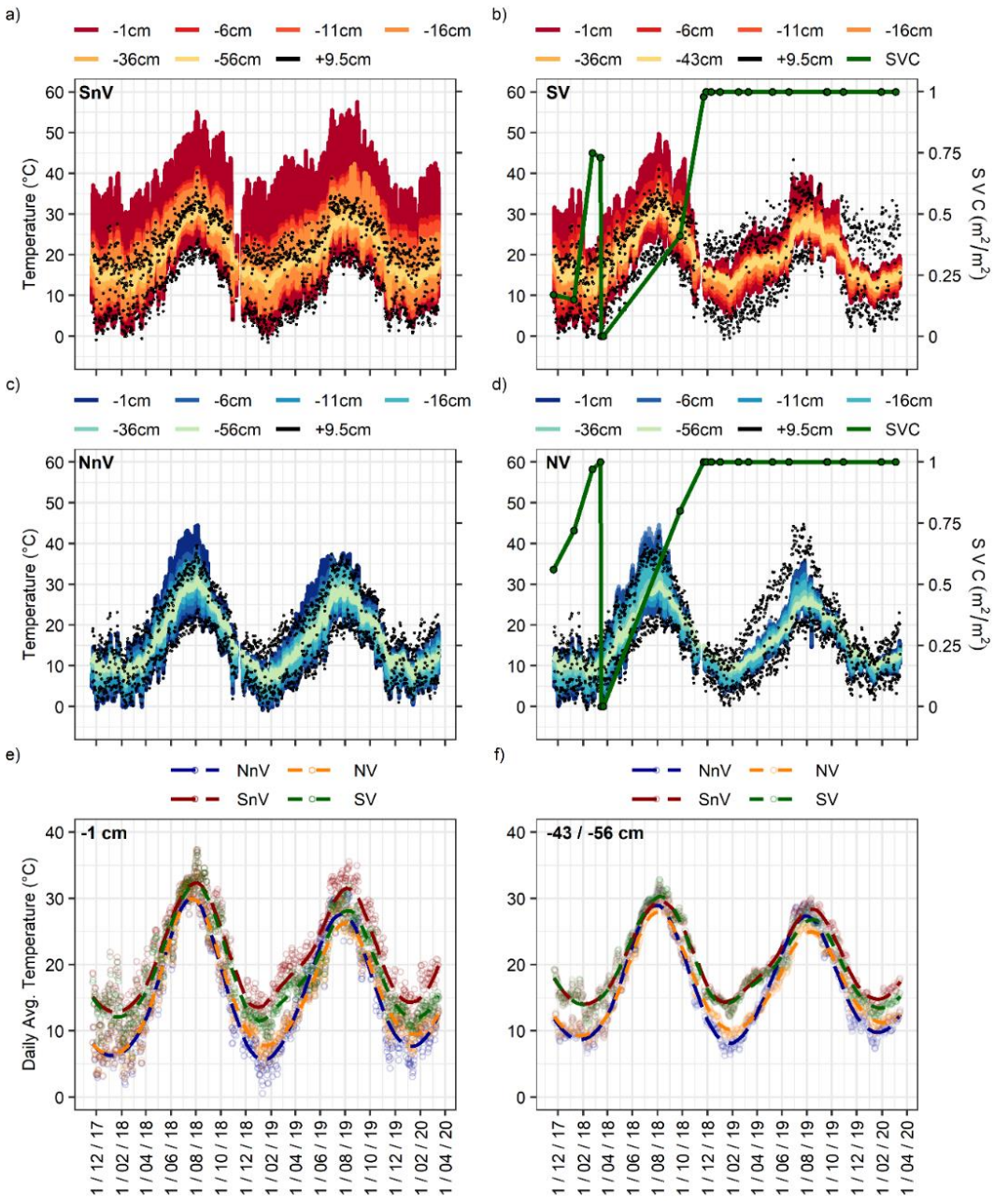

Figure 3.4: Time series of temperature at all slopes partitions: (a) South non-vegetated (SnV); (b) South vegetated (SV); (c) North non-vegetated (NnV); (d) North vegetated (SV); (e,f) daily average temperature at depth 1 cm and 43/56 cm, respectively. In figures (a–d), minimum and maximum daily air temperatures measured at 9.5 cm above soil surface are plotted by black dots. Time series of daily average temperatures plotted in figures (e,f) have been obtained by LOESS local regression with smoothing parameter a = 0.3.

Curves evidence a clear superimposition of daily and seasonal variation of temperature at almost all depths. They highlight a decrease with depth of the amplitude of temperature variations. Daily variations reduce and vanish at −50 cm while seasonal

variations globally decrease (Figure 3.4e,f). This is consistent with theoretical results on heat diffusion into a medium with periodic heat input prescribed at its upper boundary.

Another general aspect concerns the respective effect of orientation and vegetation. As shown in Figure 3.4e,f, highest mean daily temperatures have been measured in the SnV slope, then in the SV, NnV and NV slopes. Maximum daily average temperature at −1 cm is 15.3 °C and 6.9 °C higher in SnV and SV partitions than in NnV and NV respectively. Minimum daily temperature is only 1.3 °C higher at SnV slope and 1.5 °C higher at SV slopes, compared to the North-facing slopes. Similar conclusion about the effect of vegetation and slope orientation can be drawn in depth, but differences are less pronounced. It also applies to temperature daily variations shown in Figure 3.4a to Figure 3.4d.

It is interesting to note that the highest differences between South and North slopes occurs in winter, which evidences the effect of the incidence of solar radiation on slope temperature. Heat input into the ground is due to the component of solar radiation normal to the surface. Due to the nonlinearity of the projection, the decrease of solar incidence angle in autumn and winter results in a higher relative drop of its normal component on surface experiencing low incidence angle (North). In fact, in the present experiment, the normal component totally cancels in the North slopes from November to March and heat inflow by radiation is due only to atmosphere diffraction. The variations of temperature measured in the North slopes during the winter period evidence the importance to account for the latter component in the total heat exchange balance.

Curves presented in Figure 3.4b,d evidence the clear effect of vegetation on ground temperature: while temperatures range between 0 and 55 °C in SnV and SV slope before vegetation growth, their variations drop between 4 and 40 °C in SV slope with SVC = 1. For the North slopes, maximum temperatures decrease from 45 °C in the non-vegetated partitions to 35 °C in the vegetated one, while minimum temperatures increase from 0 to 3 °C. Maximum daily temperatures at 1 cm depth are higher than air temperatures in non-vegetated partitions, while close to or less than them in the vegetated ones. This indicates a loss of heat input by radiation in the vegetated slopes because of cover protection effect. On the other hand, minimum daily temperatures in vegetated slopes are above or close to air temperature, indicating that vegetation also limits outflow of heat during periods of inversion of the air-

soil thermal gradients (mainly during the night). This fact highlights the additional effect of vegetation to create an insulating thermal layer made of bio matter and air. Finally, Figure 3.4e,f evidence the low effect of vegetation on temperature variations at the seasonal scale.

Figure 3.5 illustrates the previous conclusions by contrasting the increments of maximum, minimum and daily average temperature in the different partitions. Maximum, minimum and average temperatures are higher in the South than in the North slopes and decrease with depth (Figure 3.5a,b). Maximum temperatures are the most sensitive to slope orientation. Since it limits solar radiation, the presence of vegetation has a significant effect on temperatures and lowers the effect of orientation. The presence of vegetation has an effect on both maximum and minimum temperatures, but does not modify average daily temperatures (Figure 3.5c,d). According to the figures, minimum temperatures are higher in the vegetated slopes than in the bare slopes, while maximum temperatures are lower.

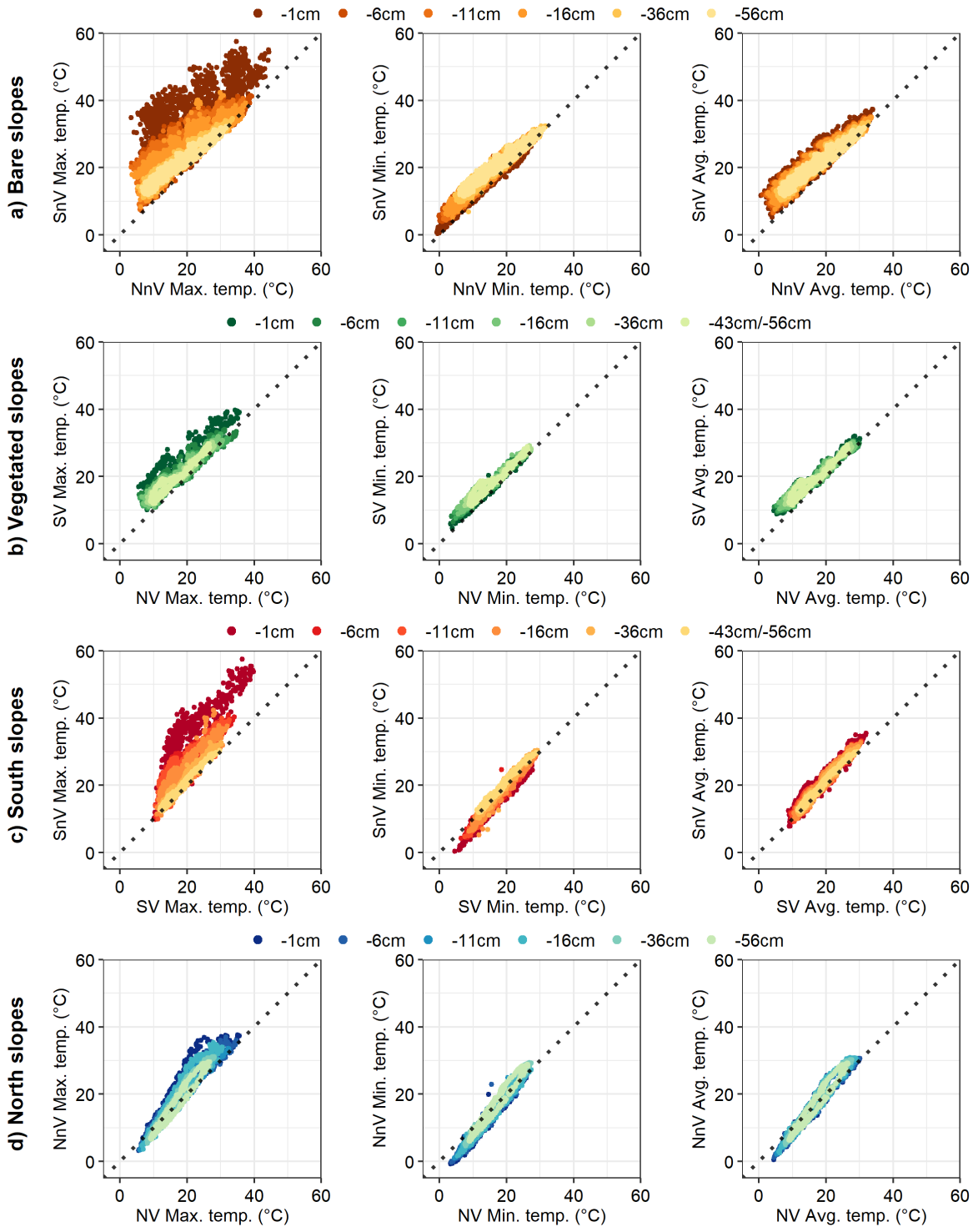

Figure 3.5: Daily maximum, minimum and average temperatures comparing orientations and slope cover. Comparison of bare (a) and vegetated (b) slope cover, and South (c) and North (d) slope orientations. Note: vegetated data correspond to the period when vegetation was fully-covering the vegetated slopes, with SVC = 1 (December 2018–March 2020).

Figure 3.6 provides an insight into daily heat flux (Figure 3.6a) and temperature variations (Figure 3.6b) during a five days period with and without rainfall. Solar radiation is measured at 55 cm above the surface and heat flux at 8 cm depth in the slope. Temperatures are measured above and below the heat flux sensor, at 1 and 11 cm depth. During the selected period, SVC at SV and NV slopes was 0.75 and 0.90, respectively. By convention, heat flux is considered positive when entering in the soil.

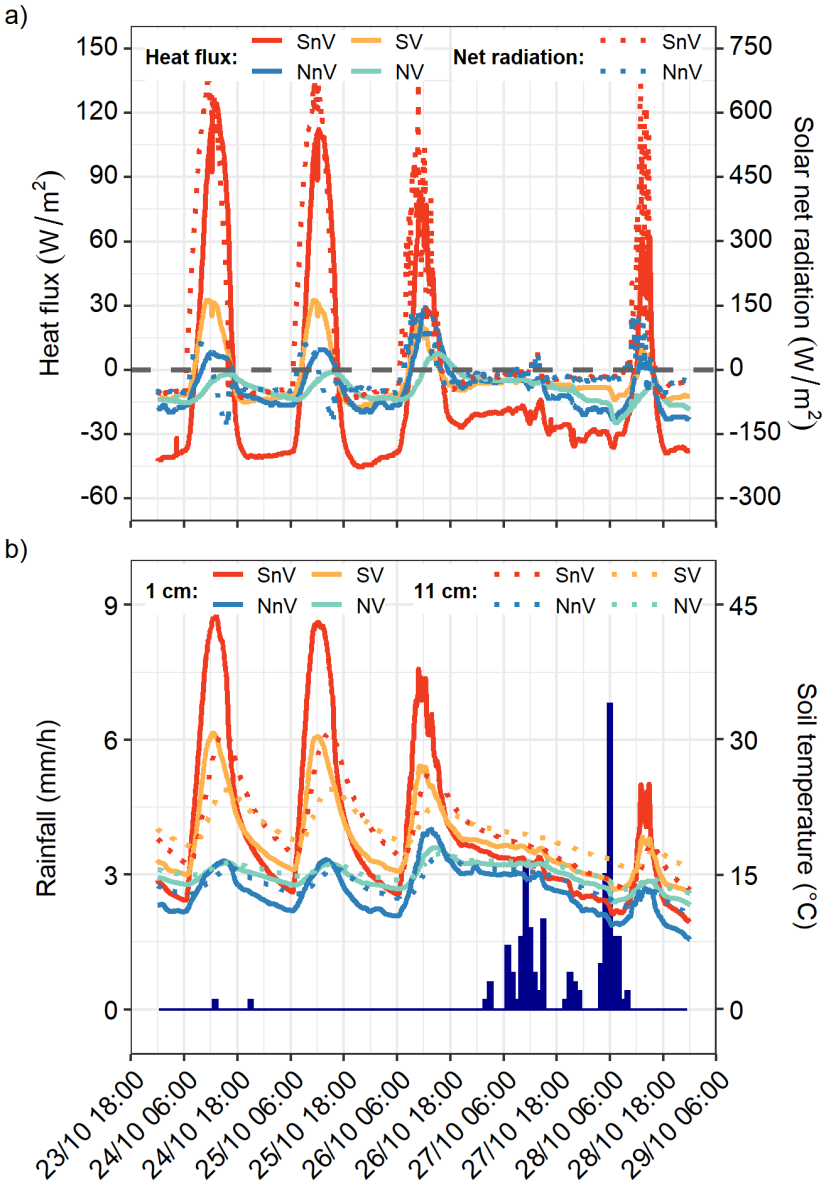

Figure 3.6: Time series of solar net radiation, heat flux, soil temperature and hourly rainfall during a 5 days period in October 2018. (a) Heat flux and net solar radiation at 8 cm depth and 55 cm above soil surface, respectively. (b) Temperature at 1 cm and 11 cm depth. Hourly rainfall is also indicated. Time is given in UTC.

Daily variation of heat flux is consistent with solar radiation: heat inflows into the soil during the day with a maximum at 12:00 UTC and outflows during the night. In the North slopes, a slight delay is observed between the maxima of heat flux and solar radiation. Soil heat flux at the bare slopes represents around 20% of the incoming solar net radiation. Vegetation has a strong effect as it reduces this value by 75% at the South-facing slope. The ratio is less important for the North slopes because of lower incoming solar radiation. As shown in Figure 3.6b, amplitudes of temperatures consequently decrease in the vegetated slopes (by 15 °C in the South and less than 5 °C in the North slopes).

Figure 3.6 finally shows the effect of rainfall on soil-atmosphere heat exchange. Net solar radiation decreases almost to 0 W/m^2 during the rain, which prevents soil temperature increase at soil surface and enhance outflow of heat from the soil to the atmosphere.

3.4. Conclusions

The paper describes results of a large-scale experiment that provides quantitative insights into the thermo-hydraulic response of slopes with two different orientations (North and South) and two vegetation covers (bare and vegetated). In addition to the hydraulic variables measured in other studies, this research combines thermal data such as soil heat flux and soil temperature at different depths, and atmospheric variables like solar radiation, air temperature and rainfall. Experiments measuring such a wide range of variables and combining soil-vegetation-atmosphere interactions over a long time-period are scarce.

For the conditions considered in the experiment, vegetation has a strong effect on all thermo-hydraulic variables: it increases suction by in-depth transpiration, enhances infiltration (and thus lowers run-off) and reduces soil-atmosphere heat exchange. On the other hand, orientation plays a fundamental role in bare slopes as a result of solar angle incidence: temperatures, and thus evaporation, are higher in the South- than in North-facing slopes. The orientation effect is however significantly diminished, when vegetation is present. Vegetation reduces by 75% the incoming heat flux in South-facing slopes, but the resulting reduction of evaporation is largely compensated by transpiration. Therefore, our results suggest that vegetation effect is more important than orientation and maintains slopes in drier states in absence of rainfall, which enhance soil strength and slope stability.

The effect of vegetation on slope-mass wasting during rainfall events is more controversial. Results from the experiment indicate a quicker saturation in the vegetated layers, which is in principle more prejudicial for slope stability and mass-wasting in general. Nevertheless, this effect should be contrasted with others not studied in this work and often cited in the literature: increase of soil strength by roots, protection against raindrop impact, sediments trap or decrease of runoff. Other studies have shown that vegetation can significantly reduce slope runoff and surficial erosion. Thus, the use of vegetation to prevent soil losses, a correct maintenance of vegetated slopes or reforestation, especially in areas with sparse or no vegetation, are highly recommended.

Due to the high number of involved variables, more research is needed to better understand all these slope-vegetation-atmosphere interactions and to promote vegetation in sustainable engineering designs. Therefore, our next research steps will focus on the determination of runoff and slope erosion rates comparing both hydrological and thermal slope response under different orientations and slope covers (bare and vegetated).

Chapter 4

MONITORING RAINFALL AND SOIL MOISTURE AT THE REBAIXADER CATCHMENT (CENTRAL PYRENEES)

This chapter reproduces the article published in the *Environmental and Engineering Geoscience* journal on March 15, 2021, on the results of rainfall characteristics and soil moisture for the triggering of torrential flows in the Rebaixader catchment.

Publication reference:

Oorthuis, R., Hürlimann, M., Abancó, C., Moya, J., & Carleo, L. (2021). Monitoring of Rainfall and Soil Moisture at the Rebaixader Catchment (Central Pyrenees). *Environmental and Engineering Geoscience*, *27*(2), 221–229. https://doi.org/10.2113/EEG-D-20-00012.

Abstract

The instrumental monitoring of torrential catchments is a fundamental research task that provides necessary information to improve our understanding on the mechanisms of debris flows. While most monitoring sites include meteorological sensors and analyze the critical rainfall conditions, very few contain soil moisture measurements. In our monitoring site, the Rebaixader catchment (Central Pyrenees), 11 debris flows and 24 debris floods were detected during the last nine years. Herein, the initiation mechanisms of these torrential flows are analyzed focusing on the critical rainfall conditions and the soil water dynamics. Comparing the temporal distribution of both rainfall episodes and torrential flows, kernel density plots show maximum values for rainfall at the beginning of June, while the peak for torrential flows is on July 20th. Thus, the antecedent rainfall, and especially the soil moisture conditions, may influence the triggering of torrential flows (as infiltration capacity is strongly

dependent on soil moisture). In a second step, an updated rainfall threshold was proposed including total rainfall duration and mean intensity. The analysis of soil moisture data was more complicated and showed no clear trends. Therefore, additional data has to be recorded in order to quantitatively analyze the role of soil moisture on the triggering of flows and to define thresholds. Some preliminary results show that the soil moisture at the beginning of a rainfall event affects the maximum increase of soil moisture, while a slight trend was visible comparing the initial soil moisture with the necessary rainfall amount to trigger a torrential flow.

Keywords: monitoring, rainfall infiltration, torrential flows, soil moisture, threshold, Pyrenees

4.1. Introduction

Torrential flows like debris flows and debris floods are an important natural hazard for society and infrastructures in mountainous regions due to their high velocities, long runout distances and great impact forces [Hilker et al., 2009]. Detailed data recorded in catchments with monitoring systems are necessary to improve our knowledge about the triggering mechanisms of debris flows and other torrential processes. Understanding the triggering mechanisms is a complex task since it depends on several variables, where the slope angle, sediment availability and water input play the most important role [Takahashi, 1981, 2014; Iverson, 1997; Jakob & Hungr, 2005; Brayshaw & Hassan, 2009]. Herein, we present data recorded at the Rebaixader torrent, where torrential flow activity is high and a comprehensive time series on the initiation of debris flows and debris floods is available. In this study, we distinguish between the torrential flows using the classification of Hungr et al. [2001, 2014].

There are three principal approaches to monitor and analyze debris-flow triggering [Hürlimann, Coviello, et al., 2019]. The most common approach focuses on rainfall measurements, the main triggering factor of torrential flows [Wieczorek & Glade, 2005], and generally defines thresholds of some rainfall characteristics for debris-flow triggering [Deganutti et al., 2000; Gregoretti & Fontana, 2007; Coe et al., 2008; Abancó et al., 2016; Bel et al., 2017]. Debris flows are commonly triggered by intense convective rainfalls

[Hürlimann, Corominas, et al., 2003; Underwood et al., 2016; Prenner et al., 2019], which are known to have strong spatial and temporal variations. Therefore, the location of the rain gauge should be as close as possible to the initiation area to better asses the triggering rainfalls. The second approach analyzes the soil water dynamics by recording soil moisture and/or pore water pressure in natural slopes of the catchment [Comiti et al., 2014; Hürlimann et al., 2014] or in the channel bed [McArdell et al., 2007; Gregoretti, 2012; McCoy et al., 2012]. Soil moisture and pore water pressure are strongly related to soil infiltration capacity and consequently runoff generation, which is known to trigger debris flows or other torrential flows. The third approach investigates the channel discharge and the mobilization of sediments in the channel [Coe et al., 2003; Gregoretti & Fontana, 2008; Gregoretti et al., 2016]. However, initiation mechanisms are still not totally resolved due to the complexity of debris flow phenomenon and the harsh mountainous conditions where torrential flows develop (steep slopes, possible rockfalls, difficult accessibility, etc.), which complicate the task of installing and maintaining the monitoring system [Imaizumi et al., 2005].

The present investigation focuses on rainfall and soil moisture measured at the Rebaixader catchment. The rainfall time-series covers the last 10 debris flow seasons (2009 to 2018), while the soil moisture records started in 2012. The main objective of the study is to improve our understanding on the initiation mechanisms of debris flows and debris floods. A secondary goal includes the definition of critical values or thresholds that are necessary information for the launch of early warning or alarm systems.

4.2. The Rebaixader monitoring site

4.2.1 Setting

The Rebaixader monitoring site is located in a small first order basin at the Southern Central Pyrenees, which shows a typical morphology of a torrential catchment (Figure 4.1) developed in an ancient glacial valley. The catchment drains an area of 0.53 km^2; the altitude ranges from 1350 m a.s.l. at the fan apex up to 2475 m a.s.l. at the highest peak. The debris flows and debris floods initiate in a steep bare scarp of about 32º with a badland-like morphology, and progress to the channel zone. This latter is 150 m long, 8-10 m wide and

has a mean slope of 21º. At the bottom of the slope, the fan or deposition zone has an area of 8.4 Ha and an average slope of 18º.

The bedrock consists of Paleozoic slates and phyllites formed during Hercyanian orogeny [Muñoz, 1992], while the soils include colluvium and glacial deposits. The main scarp is located in a thick lateral moraine till, which consists of sandy gravels, and provides significant sediment availability. The main reasons to locate a monitoring system in this catchment is the steep gradient and fact that the catchment has almost no restriction in sediment supply, which promotes torrential activity. Therefore, water input due to rainfall events is the main factor triggering torrential flows in the Rebaixader catchment. Since the installation of the monitoring network, more than 30 torrential flows have been detected, with one debris flow and two debris flood events per year on average.

The climate conditions are affected by three principal factors: i) the west winds from the North-Atlantic; ii) the vicinity of the Mediterranean Sea; and, iii) the orographic effects of the Pyrenean mountain range. The mean annual precipitation ranges from 800 to 1,200 mm [Abancó et al., 2016]. In the Pyrenees, the most common triggering rainfalls are typically either short duration and high intensity convective summer storms, or long-lasting rainfalls with moderate intensity during autumn [Hürlimann, Corominas, et al., 2003].

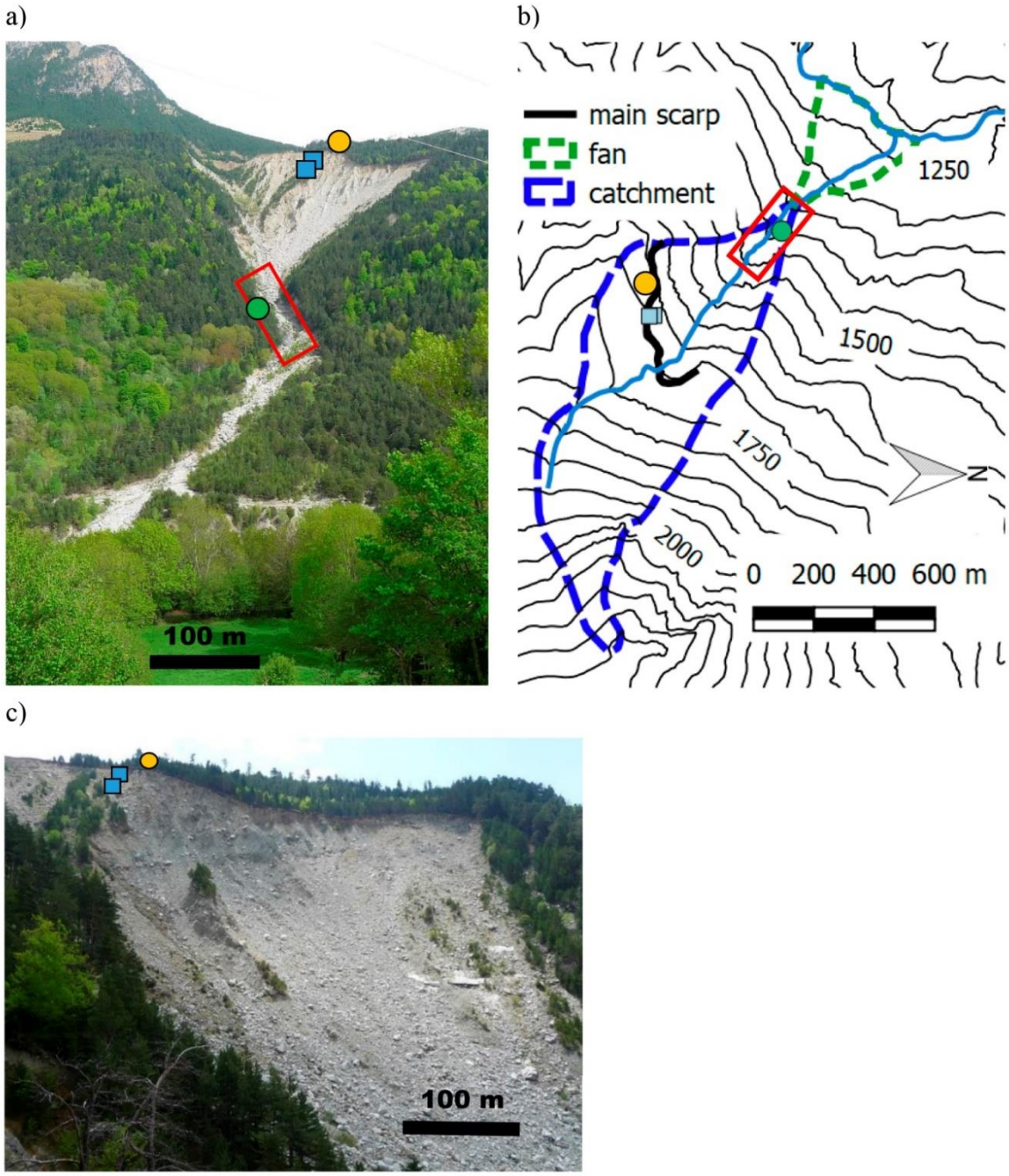

Figure 4.1: The Rebaixader monitoring site. (a) General view of the catchment with the open scarp where the debris flows and debris floods initiate, the channel zone where the torrential flows develop and the fan or deposition zone. The red rectangle specifies the channel reach, where the sensors of the flow detection station are installed (FLOW-WR), the green dot indicates the principal rain gauge (METEO-CHA), yellow dot designates the secondary rain gauge (METEO-TOP) and the light blue squares represent the infiltration stations (INF-SCARP1 and INF-SCARP2). (b) Topographic map showing the location of the monitoring stations and principal geomorphological features. (c) Close-up of the open scarp, which provides significant sediment availability.

4.2.2 Monitoring description

Monitoring in the Rebaixader torrent began in summer 2009, with the aim to detect debris flows and other torrential processes. Since that time, the monitoring system has been improved and includes five different stations at the moment. Four stations monitor the initiation mechanisms, including two meteorological stations (METEO-CHA and METEO-TOP, installed in 2009 and 2012, respectively), two infiltration stations (INF-SCARP1 and INF-SCARP2, 2012 and 2015, respectively), and the FLOW-WR station (2009) which detects and identifies the different torrential flows (Figure 4.1). In this study, records at the INF-SCARP2 station are not included, as the time series are shorter compared to INF-SCARP1.

The principal rain gauge is METEO-CHA, which is installed in the lower part of the catchment. It is a standard tipping bucket rain gauge with a resolution of 0.2 mm (until 2015, the resolution was 0.1 mm). The rain gauge METEO-TOP was temporarily installed just above the main scarp and was removed in November 2016. The infiltration stations are built in a steep (30-40º) bare slope at the highest part of the open scarp, which is actually stable but very close to the most active portion of the initiation zone. They consist of eight Decagon 10HS moisture sensors, which measure volumetric water content (VWC) at different depths between 5 and 50 cm, and two Decagon MPS-2 water potential sensors, recording matric suction at 15 and 50 cm depth. This set-up is totally different than other sites in the literature, where soil moisture and pore water pressure are measured in the channel bed [McCoy et al., 2012]. All of the meteorological and infiltration stations have a sampling rate of 5 minutes.

The FLOW-WR station, which detects and allows classifying the torrential flows, is the most important part of the monitoring system. The sensors in this station include five geophones, which trigger a radar device and an ultrasonic sensor to measure the depth of the flow, and a video camera, if a certain ground-vibration threshold is exceeded [Abancó et al., 2012, 2014; Hürlimann et al., 2014]. All these devices are located in the channel reach or at the highest part of the fan (Figure 4.1) and record the data at 1 Hz when the ground-vibration threshold is exceeded (otherwise the recording rate is every 2 hours). More detailed information on the monitoring system is available in Hürlimann et al. [2014, 2019]. Figure

4.2 shows a video frame of a debris flow of about 10,500 m^3 passing through the channel zone on 17th July 2013 (13:18h UTC) detected at FLOW-WR station.

Figure 4.2: Video frame of a debris flow passing the channel zone and detected at FLOW-WR station (17th July 2013, 13:18h UTC). Flow is moving from top right to bottom left.

4.3. Analysis of the rainfall data

Between July 2009 and September 2018, a total of 11 debris flows and 24 debris floods were observed. Rainfall data from METEO-CHA are available for all torrential events except one debris flow, which was measured by METEO-TOP. Moreover, 446 rainfall episodes that did not trigger any important torrential flow were selected. Rainfall parameters like duration (D), total rainfall (P_{tot}), mean intensity (I) and maximum intensity for different durations (e.g. I_{max_5min} for 5 minutes), were evaluated. An important and critical task during the rainfall analysis is the definition of the total rainfall duration. Herein, this parameter was determined by the condition that no rainfall was observed one hour before and after the episode [Abancó et al., 2016].

In the first step, the rainfall events were analyzed searching for seasonal or cyclic patterns using kernel density plots. The kernel density is a method to estimate the density of a sample smoothly by removing the dependence of the end points of histogram bins centering the blocks at each data point [Duong, 2001]. The temporal distribution of all 481 rainfall

episodes (both triggering torrential flows or not) is plotted in Figure 4.3a. The results show that the highest density for the rainfall episodes is at 14:00 UTC and between April and July, with a maximum on June 5. When comparing this density plot with a plot of debris flows and debris floods occurrence (Figure 4.3b), some interesting facts can be observed. First of all, the maximum kernel density for the triggering of torrential flows is shifted 45 days to July 20 and the range of high density values is between June and August. In terms of time of the day, the maximum density of triggering is approximately at the same hour as for the rainfall episodes (13:00 UTC). The difference of the temporal occurrence between rainfall and triggering of torrential flows (about 1.5 months) likely is associated with the effects of antecedent rainfall and the soil moisture evolution during late spring and early summer. Similar results were observed by other authors, which found that antecedent rainfall, up to 45 days, increased the soil moisture conditions and debris flow occurrence [Eyles, 1979; Govi & Sorzana, 1980; Wieczorek & Glade, 2005]. The importance of antecedent rainfall and the corresponding increase of soil moisture has been reported many times in debris-flow and landslide research [Wieczorek & Glade, 2005; Gregoretti & Fontana, 2007], but until now, no clear relation between antecedent rainfall and debris-flow triggering was observed at Rebaixader [Abancó et al., 2016]. Nevertheless, a possible effect of snowmelt cannot be neglected for debris flows that occur in late spring or early summer [Hürlimann et al., 2010; Abancó et al., 2016]. It must be stated that additional information of rainfall (intensity, duration or total rainfall) was not incorporated in the density plot. However, the measurements gathered at Rebaixader confirm the hypothesis that debris flows are generally triggered in summer by convective rainstorms of short duration and high intensity, while long-lasting rainfalls during spring normally do not provoke events [Hürlimann et al., 2014].

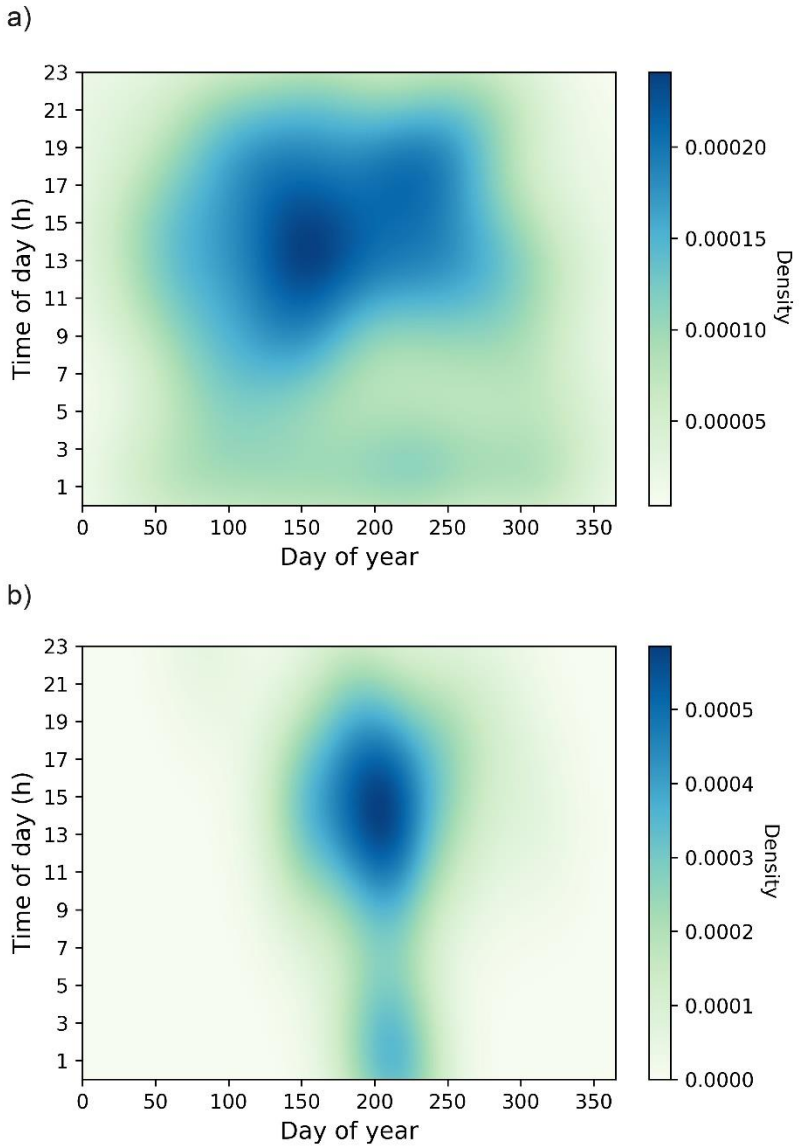

Figure 4.3: Temporal distribution of rainfall and torrential activity. Kernel density plots of 481 rainfall episodes (a) and 35 debris flow or debris flood events (b). Note that: days 357-78: winter; 79-172: spring; 173-265: summer; 266-356: autumn.

In the second step, the rainfall threshold for the triggering of torrential flows was assessed. Abancó et al. [2016] already proposed two thresholds for the data registered during 2009-2014. The present dataset includes additional records of the last four years (the new dataset spans from 2009 to 2018). Therefore, the threshold for the relation between total duration and the mean intensity was reconsidered and updated (Figure 4.4). The new threshold line was defined applying the following procedure: first, a power-law trend line was fitted using the data of the 11 debris-flow triggering rainfalls. Then, the scale parameter

defined in the previous step was reduced, keeping constant the exponent, until all the debris flows were located above the threshold line. The new updated threshold can be expressed by

$$I = 11D^{-0.74} \quad (6),$$

where I is the mean intensity (in mm/hours) and D is the duration (in hours) of the rainfall events. Although the rainfall events that triggered debris floods were not used to define the threshold, it is noteworthy that most of them are located above the threshold. Indeed, only four debris floods (usually of small volume) did not fulfill the threshold condition.

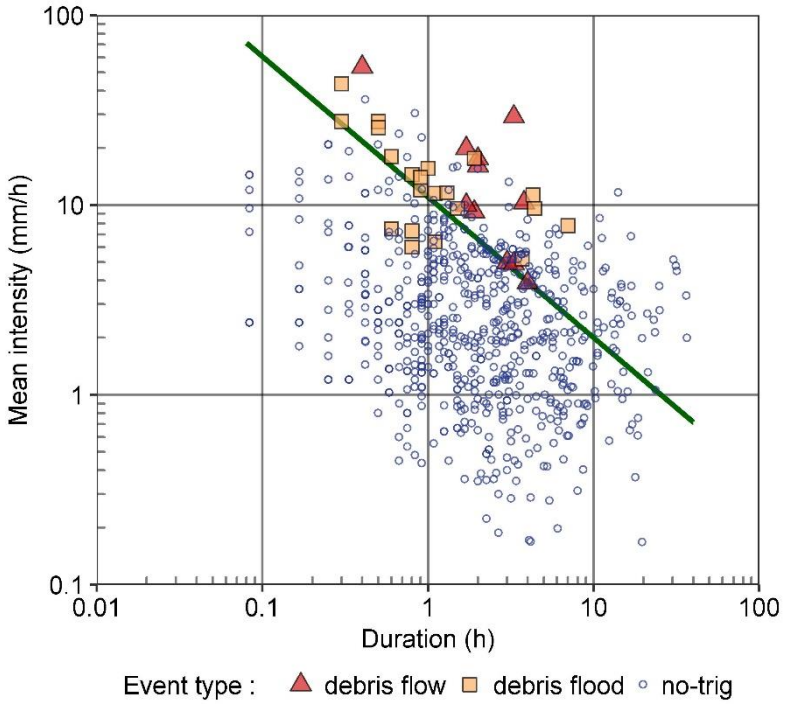

Figure 4.4: Relation between total rainfall duration and mean intensity for debris flows/debris floods triggering and non-triggering (no-trig) events. The resulting threshold is illustrated by the green line and expressed in Eq. (*6*).

4.4. Analysis of the soil moisture data

The analysis of the soil moisture due to rainfall infiltration focuses on station INF-SCARP1, which has the longest time series (2012-2019) and is installed in the upper part of the debris flow initiation area. In the first step, time series of VWC (ratio of water volume to soil volume) measurements at three different depths are compared with the corresponding

daily rainfall from March until October 2013 (Figure 4.5). This period covers all the torrential flows detected during 2013: one debris flow in mid-July and five debris floods between June and September. Vertical dashed lines indicate the moment of their peak discharge at the FLOW-WR station. The main meteorological station METEO-CHA was clogged during July 2013 and the corresponding missing data was completed with recordings of METEO-TOP station. The VWC time series at 15 and 30 cm depth present some missing data due to technical problems. Despite this temporal lack of data, all the torrential flows detected at the FLOW-WR station, except the last debris flood in September 2013, present VWC measurements at all depths. Note that the 17th of June event corresponds to a small debris flood of about 100m^3 which was triggered by a short and low-intensity rainfall (P_{tot} = 4.4 mm, D = 0.6 h, I_{max_5min} = 12 mm/h). The rest of the listed torrential flows mobilized volume was in the range of 600 – 10,500 m^3.

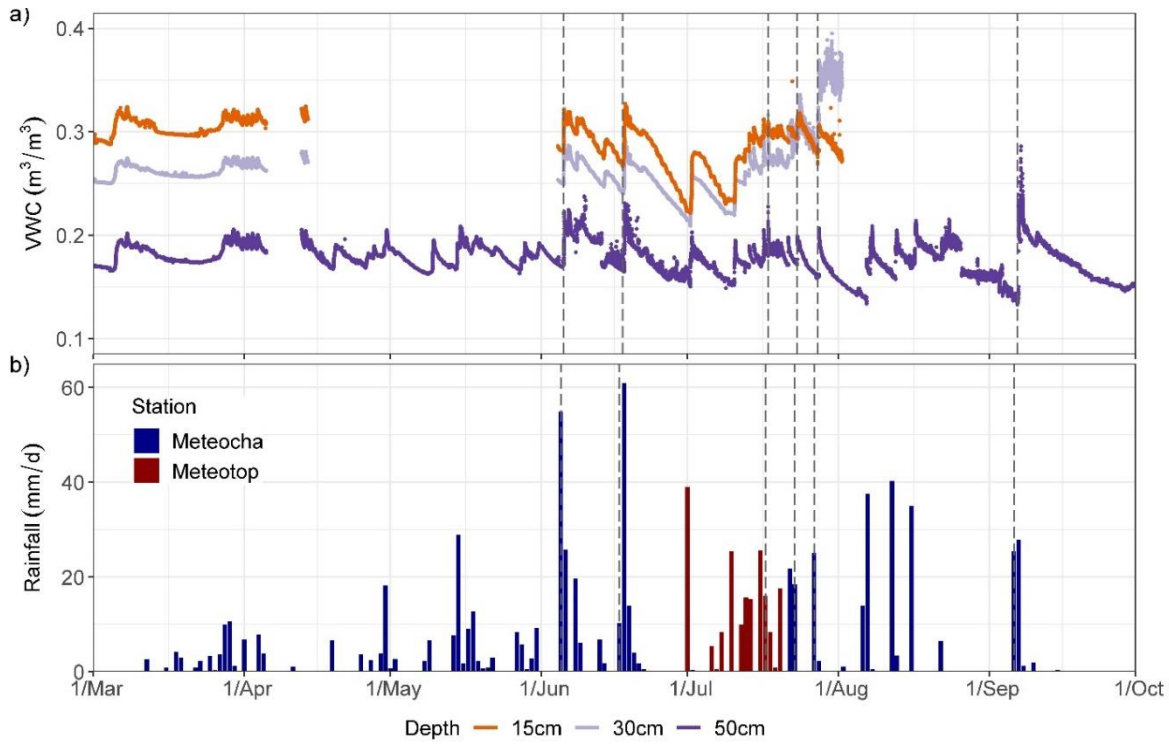

Figure 4.5: Volumetric water content (VWC) and daily rainfall time series from March until October 2013. (a) VWC measured at three different depths at infiltration station INF-SCARP1. (b) Daily rainfall of METEO-CHA and METEO-TOP meteorological stations. Vertical dashed lines indicate the moment of torrential flows peak discharge observed at the FLOW-WR station.

Results show that torrential flows at the Rebaixader catchment are mainly triggered during summer and not necessary due to the heaviest rainfalls in terms of total rainfall amount, as observed during months of July and early September in Figure 4.5. Regarding VWC measurements, results point out that higher rainfall amounts are necessary to trigger torrential flows when the soil is initially drier before the rainfall event, while if the initial water content at 15 and 30 cm depth is higher (close to the highest VWC values), less rainfall is needed. This can be noted when comparing the event that occurred on June 5th, where the soil at 15 and 30 cm depth was initially drier and the necessary rainfall amount to trigger a torrential flow was high, or during July, which had an initial wetter soil condition and lower triggering rainfalls. This suggests that as soil saturates, higher runoff rates are developed, which implies a higher erosion and transport energy that may trigger torrential flows. As a result of this link between soil moisture, runoff and transport energy, the hypothesis is proposed that torrential flows at Rebaixader may develop from continuous erosion due to intensive runoff. In conclusion, it can be stated that the initial soil moisture content affects the values of the necessary triggering rainfalls.

Figure 4.6 shows two examples of the soil moisture response during rainfalls that triggered torrential flows. The soil moisture is given by the volumetric water content (VWC) and is measured at three different depths (15, 30 and 50 cm). The first case shows the fast response and sharp increase of the VWC at the three depths due to a short and intense rainstorm (P_{tot} = 15.8 mm, D = 3.25 h, I_{max_5min} = 96 mm/h) that triggered a large debris flow of about 10,000 m^3. The second example illustrates the soil moisture response during a rainfall with a longer duration and smaller maximum intensity (P_{tot} = 54.5 mm, D = 7 h, I_{max_5min} = 49.2 mm/h), which triggered two debris floods with a total volume of about 2,000 m^3. In the second case, the VWC slowly increased during about 2 – 3 h, and maximum values were generally lower than in the first example, although the total rainfall is more than three times higher. A significant time lag occurred between the start of the rainfall and the increase of VWC.

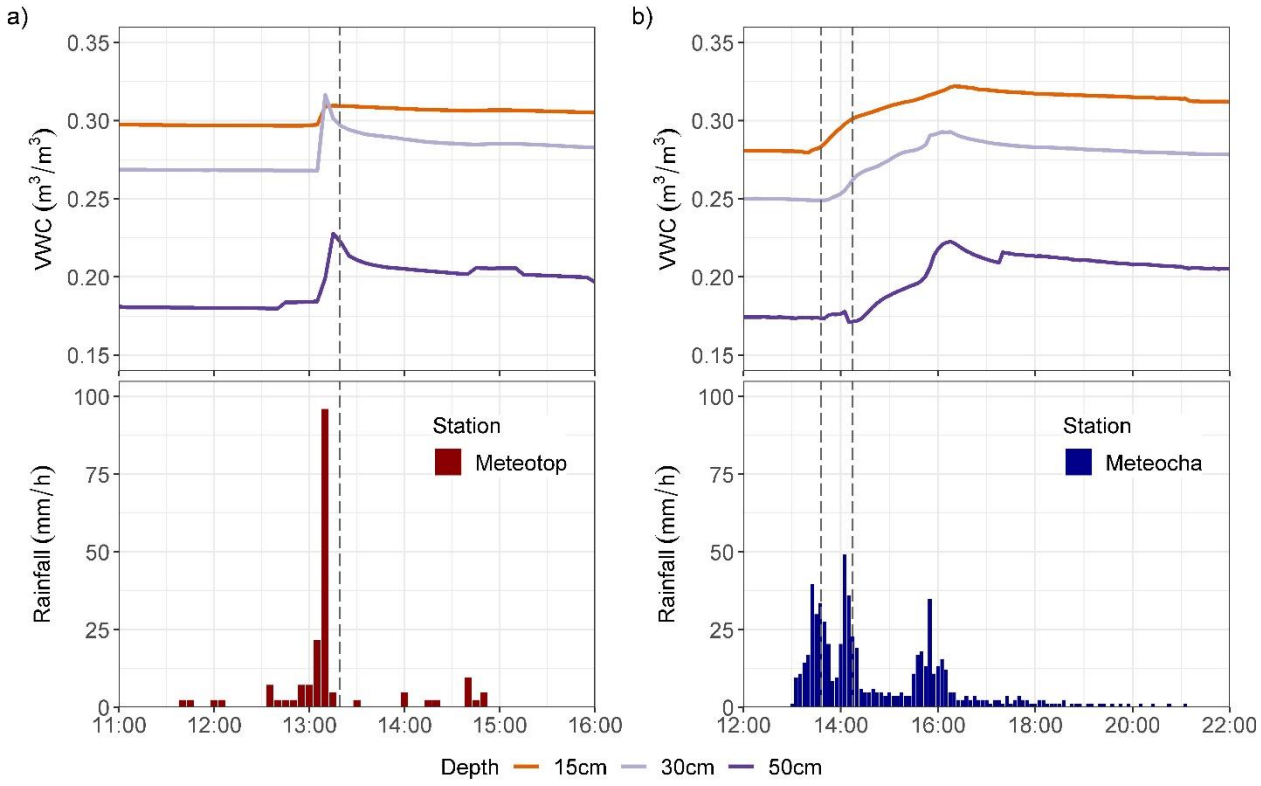

Figure 4.6: Relation between hourly rainfall and soil volumetric water content (VWC) during the triggering of torrential flows. Examples of 2013 July 17th debris flow (a) and 2013 June 5th debris floods (b). VWC is measured at the three different depths of station INF-SCARP1. Vertical dashed lines indicate the moment of peak discharge observed at the FLOW-WR monitoring station.

Unfortunately, soil moisture measurements are not available for all the debris flows and debris floods that occurred in the site. Technical problems have occurred many times, since maintenance is complicated in such a remote high-mountain environment, and because processes like soil thawing and freezing, rock falls and other slope instabilities are very common. Nevertheless, a complete record of rainfall and soil moisture is available for ten of the torrential events (four debris flows and six debris floods). Figure 4.7 shows the soil moisture values measured at 30 cm depth at INF-SCARP1. The ten torrential events are compared with soil moisture data from non-triggering rainfalls, which were selected for I_{max_5min}-values larger than 12 mm/h.

The relation between the initial VWC before the rainfall and the increment of VWC due to the rainfall is presented in Figure 4.7a. A tentative trend is observed for the rainfalls that triggered torrential flows: a larger increase of soil moisture was measured when the soil was drier at the beginning of the rainfall. In addition, maximum rainfall intensity recorded in

5 minute time step were compared with the initial VWC (Figure 4.7b). A slight trend might be identified, which show that smaller rainfall is needed to trigger debris flows when the initial VWC is higher, although much more data would be needed to verify this correlation. Such a pattern has been observed during a rainfall analysis in Italy [Gregoretti & Fontana, 2007]. Note that the debris flood triggered by the low intensity rainfall of 12 mm/h mobilized a small volume of about 100 m^3.

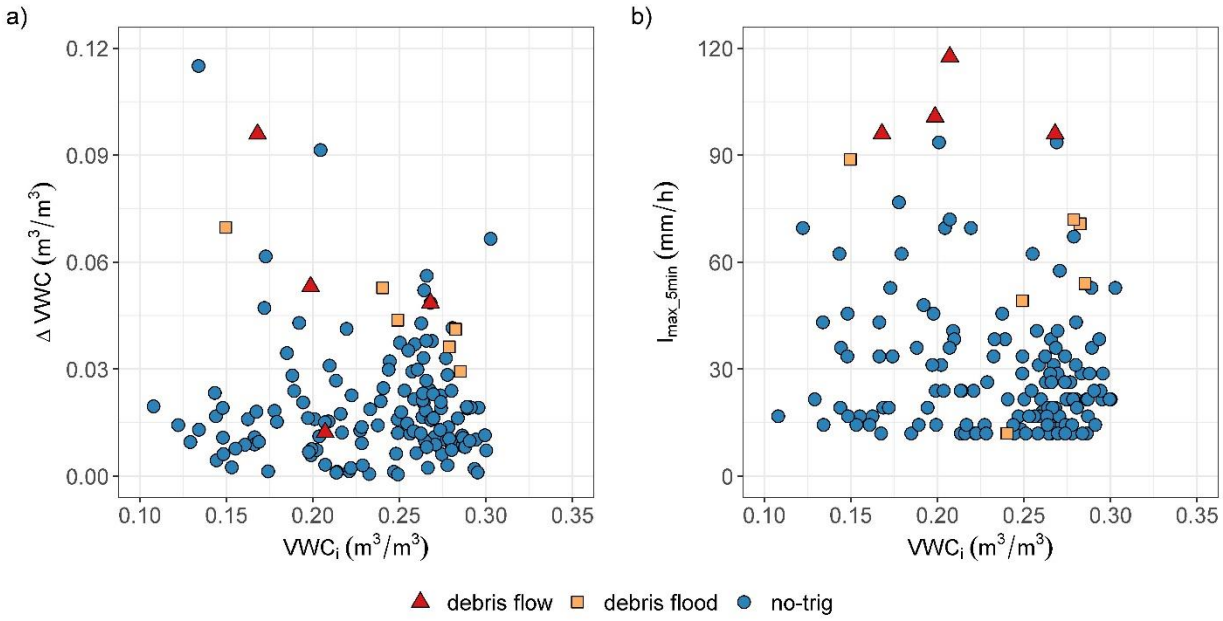

Figure 4.7: Comparison between rainfall and soil moisture corresponding to debris flows/debris floods triggering and non-triggering (no-trig). (a) Relation between initial volumetric water content (VWC_i) and the increment in volumetric water content (ΔVWC). (b) Relation between initial VWC and maximum rainfall intensity for 5 min duration (I_{max_5min}). VWC values correspond to the sensor installed at 30 cm depth at INF-SCARP1 monitoring station.

4.5. Conclusions

Monitoring data on debris-flow triggering has been recorded at the Rebaixader catchment since 2009. A total of 11 debris flows and 24 debris floods were detected during this period. In this work, we focused on the initiation mechanisms of these torrential flows by analyzing the critical rainfall conditions and the soil moisture related to water infiltration into the soil.

The results show that most of the torrential flows in the test site occurred in summer (between June and August) around 13:00 UTC. In contrast, the highest probability of

rainstorms is about 1.5 months earlier (between April and July), which supports the hypothesis that antecedent rainfall, snowmelt and/or soil moisture conditions are important for debris-flow triggering. The intensity and duration of rainfall is not included in this analysis, but previous studies at Rebaixader showed that most debris flows are provoked by short and intense rainstorms in summer, while spring rainfalls of lower intensity and longer duration normally do not trigger debris flows. In addition, an updated threshold was defined including total duration and mean intensity of the rainfalls.

Regarding the soil water dynamics, the VWC changes during rainstorms were analyzed. Results show that a higher soil moisture increment is produced when the soil is drier at the beginning of a rainstorm. Comparing rainfall and soil moisture measurements, the data indicate that the maximum 5 minute rainfall intensities required for the triggering of torrential flows are generally larger than the non-triggering rainfalls, as it could be expected. Moreover, it seems that the initial soil moisture content affects the values of the triggering rainfalls, and smaller 5 minute rainfall intensities are necessary to trigger a torrential flow when soil moisture content is higher at the beginning of the rainstorm. However, a complete data set is available only for a small number of events. Therefore, additional data are necessary to confirm the former hypothesis and to define threshold values of soil moisture causing torrential flows.

Chapter 5

MONITORING THE ROLE OF SOIL HYDROLOGIC CONDITIONS AND RAINFALL FOR THE TRIGGERING OF TORRENTIAL FLOWS IN THE REBAIXADER CATCHMENT (CENTRAL PYRENEES, SPAIN)

This chapter is pending of publication. This work focusses on the characterization of the necessary rainfall and the effects of soil hydrology in torrential flows triggering. To this end, rainfall and hydrometeorological thresholds for torrential flows initiation are defined and compared.

Publication details pending of publication:

Oorthuis, R., Hürlimann, M., Vaunat, J., Moya, J., & Lloret, T. Monitoring the role of soil hydrologic conditions and rainfall for the triggering of torrential flows in the Rebaixader catchment (Central Pyrenees, Spain).

Abstract

Torrential flows (debris flows and debris floods) are mainly triggered by precipitation and soil hydrological processes. Most early warning systems in torrential catchments are rainfall-based. However, this approach can result in frequent false positives, due to its pure black-box nature, in which soil water conditions are neglected. We aim to contribute to the understanding of the conditions required for triggering torrential flows by considering also the soil water content. Herein, monitoring data of 12 years of rainfall and torrential flow occurrence (2009-2020), and 8 years of soil hydrologic conditions (2013-2020) in the

Rebaixader catchment (Central Pyrenees, Spain) are analyzed. The dataset includes more than 1000 rainfall events, of which 37 triggered torrential flows. First, rainfall thresholds using maximum rainfall intensity (I_{max}) and mean intensity (I_{mean}) are defined. For the 2013-2020 dataset, which includes 15 torrential events, the I_{mean} threshold predicted 2 false negatives and 73 false positives (a positive predictive value, PPV, of 15.1%) and the best I_{max} threshold predicted also 2 false negatives but only 11 false positives (PPV of 54.2%). However, our observations confirmed quantitatively that the lower is the soil moisture the higher is the rainfall intensity to trigger torrential flows. Then, we combined I_{max} and volumetric water content at 15 and 30 cm depth to define an hydro-meteorological threshold. This latter threshold reduced false negatives to 1, false positives to 8 and increased the PPV to 63.6%. These results confirm that soil hydrological conditions are key factors for torrential flow triggering and may improve early-warning predictions.

Keywords: monitoring, torrential flows, rainfall, soil moisture, rainfall threshold, hydrometeorological threshold

5.1. Introduction

Torrential flows, like debris flows and debris floods, are mixed masses of debris and water that move at high velocities in steep channels in mountainous regions [Godt & Coe, 2007; Hungr et al., 2014]. The properties of these flows range between those of water floods and dry rock avalanches, depending on how solid and fluid forces interact in the flow dynamics [Iverson, 1997]. In addition to their relative high velocities, torrential flows are characterized by long runout distances and great impact forces [Jakob & Hungr, 2005]. The flow characteristics, paired with the fact that human settlements and activities have increased in mountainous regions, turn torrential flows into one of the most important hazards [e.g. Takahashi 2014]. Therefore, understanding the triggering and initiation mechanisms of these flows is crucial to mitigate theirs socio-economical losses [Jakob & Hungr, 2005; J. Chen et al., 2019].

The initiation and triggering mechanisms of debris flows and debris floods involve many factors like sediment availability, slope angle, groundwater conditions [Iverson et al., 1997; Brayshaw & Hassan, 2009; Takahashi, 2014] and rainfall [Wieczorek & Glade, 2005].

Moreover, snowmelt can combine with rainfall to trigger torrential flows in late spring and early summer [Church & Miles, 1987; Abancó et al., 2016; Mostbauer et al., 2018]. Initiation mechanisms, or how debris sediments are transformed into flowing debris, are generally complex and not fully understood. Debris flow or floods can result from the occurrence of slope mass failure that later evolves into torrential flow, or from progressive channel bed and bank erosion due to intense runoff [Pastorello et al., 2020]. In the first case, debris flow occurrence is mainly related to rainfall-induced instability of slope superficial debris layers [Iverson et al., 1997; Imaizumi & Sidle, 2007; Takahashi, 2007; Berger et al., 2011], whereas it is more likely associated to the reach of critical runoff rate (or critical surface discharge) [Berti & Simoni, 2005; Coe et al., 2008; Gregoretti & Fontana, 2008; Simoni et al., 2020] in the second case.

Whatever is the initiation mechanism, flowing mass mobilization is controlled by slope hydrological response to rainfall. The latter is usually characterized by discriminating between predisposing (e.g. soil moisture, topography, thickness of sediments) and triggering (e.g. rainfall) factors [Bogaard & Greco, 2016]. Hydrological data can be directly monitored in the field [Walker et al., 2004; Ochsner et al., 2013] or using remote sensing technologies [S. Zhao et al., 2010]. Alternatively, in absence of measurements, hydrological conditions can be estimated from current and antecedent rainfall records by using simple infiltration [Chleborad et al., 2008] or hydrological regional models [B. Zhao et al., 2020]. This last approach suffers however the limitations that the relationship between antecedent rainfall and antecedent soil moisture is indirect, as the result of the coupled interactions between several processes like infiltration, evapotranspiration, snowmelt, drainage, etc. [Brocca et al., 2008].

As a consequence, monitoring of rainfall and groundwater hydraulic variables (soil moisture, pore water pressure) appears to be a fundamental task for a better understanding and prediction of slope hydrological response in the initiation zone of torrential flow. This task is however often made difficult by the field conditions prevailing in mountain areas prone to torrential flows: harsh climatic conditions, difficult access, steep slopes covered by unconsolidated debris, rockfalls and other hazardous phenomena, etc. [Berti et al., 2000; Comiti et al., 2014]. In addition, full understanding of torrential mechanisms requires

monitoring debris mass flow dynamics in the run-out zone [Abancó et al., 2014; Bel et al., 2017; Hürlimann, Oorthuis, et al., 2019]. When feasible despite of these difficulties, field monitoring provides data of high interest, susceptible to be used for the definition of initiation thresholds in Landslide Early Warning Systems (LEWSs), an essential tool for debris flow detection and prediction.

Current prediction tools rely mostly on rainfall thresholds in terms of rainfall intensity and duration (ID) (or other similar rainfall characteristics) [Caine, 1980; Crosta & Frattini, 2001; Gregoretti & Fontana, 2007; Guzzetti et al., 2008], although it is well-known that the hydrological conditions previous to the triggering rainfall play a crucial role in debris flow initiation. Some recent studies have included subsurface hydrological variables, such as pore water pressure or soil moisture, in the definition of the thresholds [Glade et al., 2000; Godt et al., 2006; Ponziani et al., 2012; Bogaard & Greco, 2018; Mirus, Morphew, et al., 2018; Marino et al., 2020;]. For example, Mirus, Becker, et al. [2018] improved the rainfall threshold defined by Scheevel et al. [2017] by replacing the antecedent rainfall with the average saturation obtained from direct volumetric water content (VWC) measurements over the same timeframe.

This work analyzes the effect of both rainfall and hydrological slope conditions on the triggering of debris flows and debris floods in the Rebaixader catchment (South Central Pyrenees, Spain). For this purpose, we analyze VWC and suction measurements in the initiation area of Rebaixader torrential flows together with rainfalls and mass movements occurrences. In a first part, the relevance of using specific rainfall characteristic values (mean and peak values of different durations) for the computation of triggering thresholds is investigated by statistical analysis of flow events over the period 2009-2020. In a second part, we study the improvement in prediction provided by the use of hydro-meteorological thresholds, which consider both rainfall maximum intensity and current value of VWC at an appropriate location within the slope.

5.2. Materials and methods

5.2.1. The Rebaixader catchment

5.2.1.1. General settings

The Rebaixader catchment is a small first-order basin tributary of the Noguera Ribagorzana River, located in Southern Central Pyrenees (42º32'57.02" N 0º45'12.57" E), which shows a typical torrential morphology (Figure 5.1). The source area is a concave scarp draining 0.53 km^2 with a slope of 35º in average and 70º in maximum; where the debris flows and debris floods initiate. The channel below the initiation zone is not very long (150 m and 8-10 m wide) with an average slope of 21º. At the lower part of the basin there is a small deposition fan (0.09 km^2 extent) with a mean slope of 8º. The elevation ranges from 2475 m a.s.l. to 1345 m a.s.l., at the fan apex.

The source material is a glacial till deposited during the Last Glacial Maximum, and 15 to 20 m thick, thus providing almost unlimited material for torrential flows [Hürlimann et al., 2014]. The bedrock consist of Paleozoic slates and phyllites [Muñoz, 1992].

The till is mainly composed by sandy gravels and large boulders. The fraction of fines (silt and clay) is minor but variable. Two layers are distinguished in the deposit. The lower one is a subglacial till overlying the bedrock; which has a higher proportion of fines and a lower porosity than the upper one, that is a supraglacial till. Geotechnical properties of the two soils are indicated in Table 5.1 and Figure 5.2.

The climate in the area is mainly affected by the orographic effects of the Pyrenees, the westerly winds from the Atlantic, and the closeness to the Mediterranean Sea. The mean annual precipitation in the site fluctuates between 800 and 1200 mm [Abancó et al., 2016].

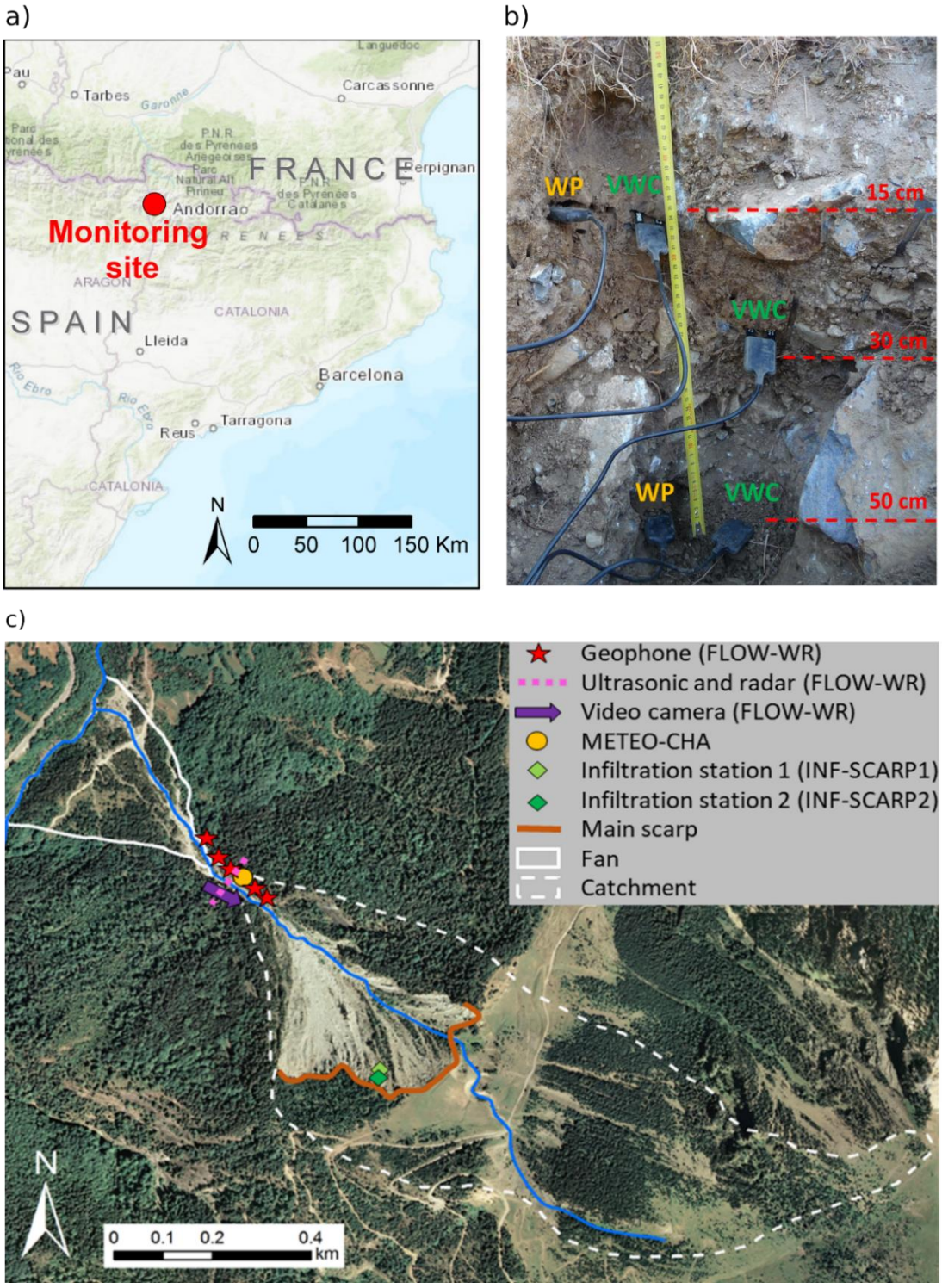

Figure 5.1: The Rebaixader catchment and monitoring site. (a) Location of the Rebaixader catchment in the Pyrenees. (b) Detail of the supraglacial till at infiltration station INF-SCARP1 indicating the volumetric water content (VWC) and water potential (WP) sensors (see (c) for location). c) Orthophoto and location of the infiltration stations (INF-SCARP1 and INF-SCARP2), meteorological station (METEO-CHA) and the specific sensors at the flow dynamics station (FLOW-WR).

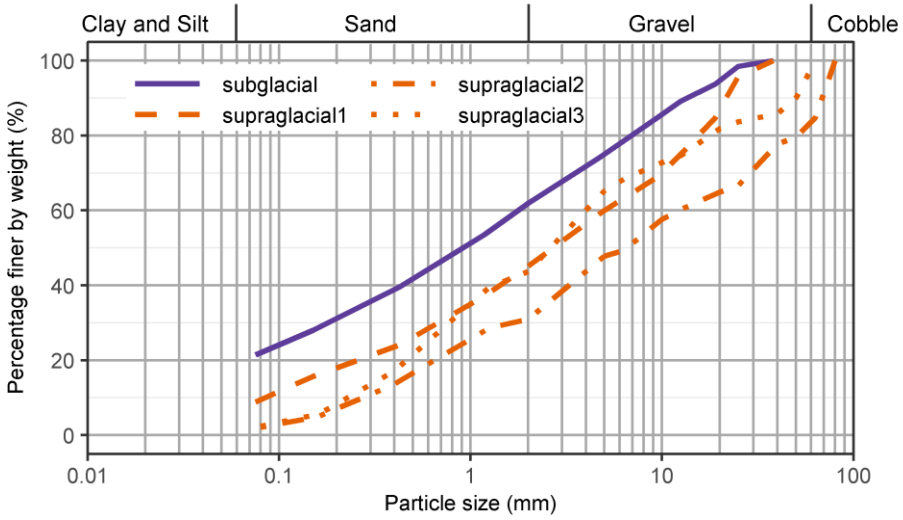

Figure 5.2: Grain-size distribution of materials taken at the source area of torrential flows (one sample of subglacial till and three samples of supraglacial till).

Table 5.1: Soil properties obtained from field and laboratory tests.

Soil property	***Material type***	
	Supraglacial	***Subglacial***
Gravel content (%)	54.9 – 56.3	38.1*
Sand content (%)	28.8 – 41.2	40.5*
Fine content (%)	2.1 – 8.8	21.4*
Dry density (ρ_d) (Mg/m^3)	1.82*	1.66 – 1.92
Density of solid particles (ρ_s) (Mg/m^3)	2.57 – 2.62	2.56 – 2.7
Soil moisture (ω)(%)	6.1 – 16.5	6.7 – 22.2
Porosity (n) (-)	0.29*	0.25 – 0.39
Saturated hydraulic conductivity (K_{sat}) (m/s)	4.06 x 10^{-6} – 2.53 x 10^{-4}	ND
Soil friction angle (φ') (º)	40 – 45	ND
Effective cohesion (c') (kPa)	0 – 4	ND

*: only one test performed; ND: no data.

Availability of granular sediment and steep slopes predispose the basin to torrential flows while amount of water input by rainfall provides the main triggering factor in the Rebaixader catchment. Previous analyses of rainfall in the catchment showed that most of the debris flows and debris floods were triggered by short-duration and high-intensity

rainfalls, mainly associated with summer convective rainstorms from June to September [Abancó et al., 2016; Oorthuis et al., 2021]. Other torrential flow events, as well as rockfalls, has been observed during spring and were affected by snowmelt [Hürlimann et al., 2010, 2012]. In addition, some minor torrential activity has been observed during autumn, which is generally triggered by long-duration and medium intensity rainfall events. The frequency of torrential events is close to one debris flow and two debris floods per year. The estimated volumes range from 100 m^3 to 16,000 m^3, corresponding to the smallest debris flood and the largest debris flow, respectively.

5.2.1.2. Monitoring description

The Rebaixader site presents a high torrential activity, which, in addition to the limited size of the catchment and the lack of protective measures, makes this catchment an ideal location for hosting a monitoring system. The monitoring in the catchment started in 2009 with the aim of detecting torrential flows such as debris flows and debris floods. For this purpose, two monitoring stations were installed in the channel area and lower part of the catchment: the meteorological station METEO-CHA, and the FLOW-WR station, which focuses on the detection and analysis of the flow dynamics. Since then, the monitoring system has been maintained and further improved. It includes today four active stations (Figure 5.1c).

The METEO-CHA station is located next to the channel. It consists of a tipping bucket rain gauge with a resolution of 0.2 mm, an air temperature sensor and a relative humidity sensor. The FLOW-WR station consists of five geophones distributed along the channel, two flow depth sensors and a video camera. This is the most important station as it detects the passing torrential flows and allows characterizing its main properties (flow type, velocity, flow depth and volume). Two infiltration stations were installed within the supraglacial till layer at the highest part of the open scarp on a steep (30 – 40º) and bare slope, and close to the most active part of the initiation area: INF-SCARP1 station (installed in 2012) and INF-SCARP2 station (installed at the end of 2015). These infiltration stations are recording a total of eight soil volumetric contents (VWC) at depths between 5 and 50 cm, and measures soil matric suction and soil temperature at 15 and 50 cm depth. Figure 5.1b

shows the installation of the soil VWC and matric suction sensors at the infiltration station INF-SCARP1.

The FLOW-WR station has a low-frequency sampling rate of 2 hours due to power and data management limitations. Under non-event conditions, it takes daily images of the channel cross section. Under event conditions, if a given ground vibration threshold is exceeded, FLOW-WR station samples sensors at 1 Hz and turns on the video camera [Abancó et al. 2012; Hürlimann et al. 2014]. Conversely, the meteorological and infiltration stations have a constant sampling rate of 5 minutes. In addition, all the stations installed in the initiation area are connected to a common wireless sensor network (WSN), which use a long-range wireless technique to transmit the data. All the monitored data are sent to the university server by GSM/GPRS communication, while multiple solar panels and batteries supply power to the monitoring stations. Table 5.2 summarizes the sensors that are actually installed at the Rebaixader monitoring site; for further details see Hürlimann et al. [2014] and Hürlimann, Coviello, et al. [2019].

Table 5.2: List of the sensors installed at Rebaixader monitoring site. Shaded grey area indicates the VWC sensors selected for the definition of hydro-meteorological thresholds.

Location	***Station***	***Process (predisposing / triggering/ dynamics)***	***Parameters***	***Sensor model (nº of sensors)***	***Installation depth (cm)***	***Installation year***
Open scarp (initiation area)	INF-SCARP 1	Predisposing mechanisms	Water potential & soil temperature	Decagon MPS-2 (2)	15	2012
					50	2012
			Volumetric water content	Decagon 10HS (4)	5	2018
					15	2012
					30	2012
					50	2012
	INF-SCARP 2 (left vertical profile)	Predisposing mechanisms	Volumetric water content	Decagon 10HS (2)	15	2018
					20	2015
	INF-SCARP 2 (right vertical profile)			Decagon 10HS (2)	10	2018
					30	2015
Channel	METEO-CHA	Predisposing and triggering mechanisms	Rainfall, air temperature and relative humidity	Decagon ECRN-100 (1)	-	2009
				Campbell Scientific CS215 (1)		2009
	FLOW-WR	Flow dynamics	Ground vibration	Geophones Geospace 20 DX (5)		2009
		Flow dynamics	Flow depth	Ultrasonic sensor Pepperl+Fuchs UC6000-30GM-IUR2-V15 (1)		2009
		Flow dynamics	Flow depth	Radar sensor VEGAPULS SR 68 (1)		2015
		Flow dynamics	Visual observation	Video camera Mobotix MX-M12D-Sec-DNight-D43N43 (1)		2011

5.2.2. Threshold types and definitions

Thresholds for debris flows and debris floods usually correspond to critical rainfall characteristics, which, when exceeded, are prone to trigger a torrential flow event [Guzzetti et al., 2007]. Such thresholds are defined by discriminating rainfalls that trigger an event from those that do not. In this study, we evaluate and compare two types of thresholds. The first and most common type relies only on rainfall characteristics and will be subsequently named as "rainfall threshold". The second type combines both hydrologic soil conditions (predisposing factors) and triggering rainfall characteristics and will be subsequently referred as "hydro-meteorological threshold".

5.2.2.1. Rainfall versus hydrometeorological thresholds

Rainfall thresholds can be based on several rainfall parameters. One threshold commonly used is expressed as a relationship between rainfall mean intensity (I_{mean}, mm/h) and duration (D, h). It is drawn as a line in the graph I_{mean}-D where the x and y-axes are plotted in logarithmic scale to capture rainfall data of multiple orders. I_{mean}-D thresholds are generally fitted by a power law equation:

$$I_{mean} = aD^b \qquad (7)$$

with *a* being the intensity of a rainfall event of unit duration, and *b* the slope of the log-plotted threshold line.

A second type of threshold is expressed by values of maximum rainfall intensity for selected rainfall durations ($I_{\max\_dur}$) and takes the form:

$$I_{\max\_dur} = c \qquad (8)$$

where *c* is a constant and I_{max_dur} is the value of maximum intensity necessary to trigger torrential flow for duration *dur*. In this work, six durations have been considered: 5, 10, 15, 20, 30 and 60 minutes. It results in a graph where maximum rainfall intensities are plotted in the y-axis.

Hydro-meteorological threshold is defined as a relationship between soil volumetric water content (VWC) at the start of the considered rainfall event, reported on the x-axis, and maximum rainfall intensity, plotted in the y-axis. In the present work, VWC monitored at

two depths (15 and 30 cm) in a profile located at the scarp of the slope (INF-SCARP1) will be used as they have the longest and most complete VWC time series. To determine the hydro-meteorological threshold, the maximum rainfall intensities given by Eq. (*8*) will then be plotted against VWC for the six different time durations previously mentioned. This results in six hydro-meteorological thresholds at each sensor depth, expressed by the following linear equation:

$$I_{\text{hydro}-\text{meteo}} = I_{\max\_durVWCdepth} = d\,VWC + e \qquad (9)$$

where $I_{max\_durVWCdepth}$ is the value of maximum intensity necessary to trigger torrential flow for duration *dur* when considering *VWC* at the start of the rainfall event at *depth* 15 or 30 cm, *d* is the slope and *e* is the y-intercept when VWC = 0.

The rainfall intensity used in these different concepts may represent an "instantaneous" measure of the rainfall rate, or an average value of precipitation, depending on the length of the observation period [in: Guzzetti et al., 2007]. Particularly, the mean rainfall intensity used in the I_{mean}-D approach does not consider intensity variations during rainfall event, which can lead to underestimate the rainfall intensity that actually triggered the torrential flows. I_{mean}-D thresholds ignore thus other information contained in the rainfall time series, such as peak intensities and antecedent rainfall conditions [Hirschberg et al., 2021]. Some studies show that the variability of the rainfall intensity, or the shape of the rainfall hyetographs, can strongly influence the triggering of landslides [D'Odorico, 2005; Peres & Cancelliere, 2014]. Furthermore, maximum rainfall intensities have been shown to have high predictive power at high temporal resolutions (≤ 10 min) [Abancó et al., 2016; Bel et al., 2017; Hirschberg et al., 2021]. This suggests that maximum rainfall intensity at time of landslide triggering would be a better characteristic than the I_{mean} value, which supports the definition of thresholds based on Eq. (*8*) or (*9*).

5.2.2.2. Available data

Before analyzing the performance of the different thresholds, it is necessary to standardize the way in which threshold variables are computed. Particularly, the computation of rainfall duration is not straightforward, as there could exist several overlapped rainfall events or long episodes of low rainfall before and after a high precipitation event. In this

work, according to Abancó et al. [2016], only the rainfall events delimited by a period of no rainfall for at least 1 h before and after the event are considered. Once defined the rainfall events, episodes with total precipitation of less than 0.4 mm were removed. As a result, 1037 events have been analyzed between 2009 and 2020: 1000 without triggers of torrential flows and 37 associated to occurrence of torrential events. In the following, this inventory will be referred as the rainfall dataset and includes all the monitored rainfall events and all the torrential flows detected in the catchment since the monitoring started. Each rainfall event was then characterized with the following parameters: total precipitation, P_{tot} (mm), total duration, D (h), mean rainfall intensity, I_{mean} (mm/h), and by six maximum rainfall intensities, I_{max_dur} (mm/h) for 5, 10, 15, 20, 30 and 60 minutes. The rainfall dataset (2009-2020) is further used in this work to assess and compare the performances of the I_{mean}-D vs I_{max_dur} rainfall thresholds over a longer period.

In parallel, a hydro-meteorological dataset has been set-up by adding VWC measurements to the rainfall dataset. VWC measurements include all data prior to the start of rainfall events (VWC_i) listed in the rainfall dataset and monitored at 15 and 30 cm depth at INF-SCARP1 station. Due to several technical problems of short duration, VWC recordings present some missing data. Because of that and the fact that the INF-SCARP1station was installed in the late 2012, the hydro-meteorological dataset has a shorter time period than the rainfall dataset and includes 15 triggering events and 470 non-triggering events with both VWC and rainfall data between 2013 and 2020. The hydro-meteorological dataset (2013-2020) is used to compare the performance of rainfall and hydro-meteorological thresholds.

Finally, in both the rainfall and hydro-meteorological dataset, a correction has been applied on rainfall data during the last torrential flows season (2020). Indeed, the rain gauge clogged twice during this period, leading to time intervals with no rainfall records. Missing data have been then completed by means of a correlation established between rainfalls observed in 2016 and 2017 at METEO-CHA station and at a rain gauge (https://altaribagorca.smartyplanet.com/ca/estacions/estacio/228/smartis/) located at a distance of 1800 m from our meteorological station.

5.2.2.3. Evaluation of threshold performance

The rainfall and hydro-meteorological thresholds equations (Eq. (*7*),(*8*) and (*9*)) were calibrated and evaluated by means of different scoring metrics from the receiver operating characteristics (ROC) and precision-recall curves (PRC) analysis [Fawcett, 2006]. First, the confusion matrix was obtained for any given threshold, thus, for any combination of *a* and *b* in Eq. (*7*), *c* in Eq. (*8*), and *d* and *e* in Eq. (*9*). The confusion matrix counts the four possible outcomes output by the threshold prediction: TP (true positive or true alarm), FP (false positive or false alarm), TN (true negative or true non-alarm) and FN (false negative or failed alarm). Second, the following evaluation/scoring metrics were computed for each threshold:

$$TPR = True\ positive\ rate\ or\ Sensitivity = Recall\ = \frac{TP}{TP+FN} \quad (10)$$

$$FPR = False\ positive\ rate\ or\ Specificity = \frac{FP}{FP+TN} \quad (11)$$

$$Precision\ or\ Positive\ predictive\ value\ = \frac{TP}{TP+FP} \quad (12)$$

$$F_1 - score = \frac{2}{\frac{1}{Precision}+\frac{1}{Recall}} = 2 \cdot \frac{Precision \cdot Recall}{Precision + Recall} \quad (13)$$

The most popular evaluation method for landslide thresholds is the ROC curve and the area under the curve (AUC), which relates the trade-off between the TPR and the FPR. This method is, however, not the most robust and easy to interpret when the negative class, or non-triggering events, is the majority class [Fawcett, 2006; Saito & Rehmsmeier, 2015]. In our case, both rainfall and hydro-meteorological datasets are highly imbalanced as they present a very low number of positive events, or events that triggered a torrential flow, compared to the high number of non-triggering events. When comparing thresholds with an elevated number of TN events, the FPR scores are low and the resulting ROC curves and AUC are more difficult to compare and to interpret. Hence, the precision-recall or precision-TPR curves (PRC) are more informative and appropriate for our evaluation, since the large number of TN events does not affect the precision, neither the recall metric.

Torrential flows thresholds aim at maximizing the prediction of TP events while minimizing the FP and FN events, which results in a higher F_1-score. The F_1-score weights precision and TPR equally and is the most often used variable when learning from

imbalanced datasets [Weiss, 2013]. Therefore, we select and optimize every threshold equation (I_{mean}-D, I_{max_dur} and hydro-meteorological) by maximizing the F_1-score and under the premise that the largest debris flows are predicted as TP events. Another consideration for threshold selection is that the number of torrential events correctly predicted is higher than 85% (TPR> 0.85).

In continuation, we will present an example for the rainfall I_{mean}-D thresholds and the ROC and PRC curves (Figure 5.3). A threshold with a perfect skill is represented as a point in the ROC space at TPR = 1 and FPR = 0, while it is defined in the PRC space at Precision = 1 and TPR = 1. First, the I_{mean}-D threshold with the best performance and highest F1-score is plotted (Figure 5.3a, Threshold 1). The best-fitting threshold is represented in the ROC and PRC space as a point (Threshold 1 in Figure 5.3b and Figure 5.3c, respectively). Second, the ROC and PRC curves are obtained by varying the y-intercept between the minimum (Figure 5.3a, Threshold 2) and the maximum (Figure 5.3a Threshold 3) y-range and while keeping the slope of the curve constant. This results in a point in the ROC and PRC space for every computed y-intercept and for a fixed threshold slope. The ROC and PRC curves are then plotted by joining the resulting points. Threshold 4 defines the minimum I_{mean}-D threshold for the triggering of torrential flows. The PRC and ROC curves are a valuable tool for the evaluation and interpretation of the thresholds performance. However, ROC curves (Figure 5.3b) can be misleading when compared to the PRC curves (Figure 5.3c): the elevated number of TN events diminish the FPR and do not truly reflect the high number of FPs or false alarms. This results in a quite optimistic ROC curve, even if the number of FPs are high related to the lower number of TPs, in comparison with the PRC curve. This is not the case of the PRC curve, which is more informative when dealing with imbalanced datasets, as it does not rely on the correctly predicted non-triggering events. Therefore, the PRC approach better represents the variability of the thresholds performance in torrential flow detection.

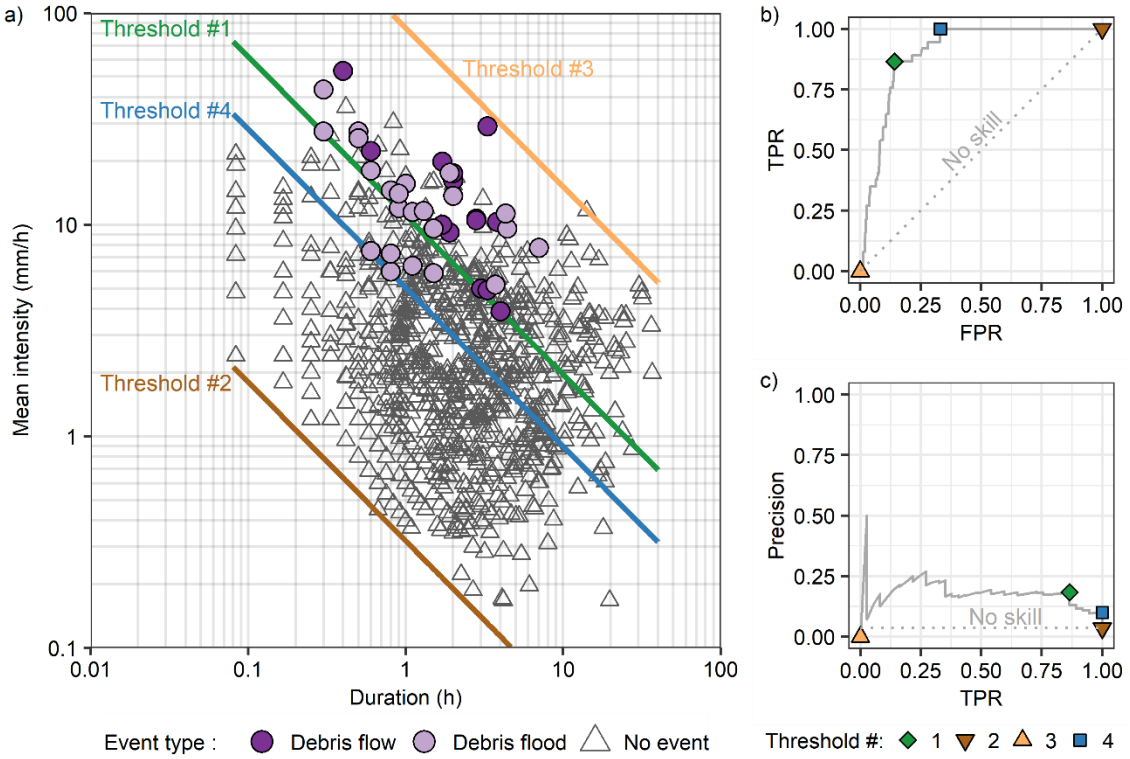

Figure 5.3: Methodology for the evaluation and interpretation of the threshold performance using the I_{mean}-D threshold for illustration. (a) Example of rainfall I_{mean}-D thresholds with the best performance (Threshold 1). The ROC (b) and precision-recall (c) curves are defined by varying the y-intercept while keeping the threshold slope constant. In all plots, Threshold 1 has the best performance; Threshold 2 defines the lower limit in the I_{mean}-D plot, while Threshold 3 defines the higher limit; Threshold 4 defines the minimum I_{mean}-D threshold for torrential flow detection.

5.3. Results

5.3.1. Monitoring data analysis

VWC, suction and daily rainfall time series from January 2016 to October 2020 are shown in Figure 5.4. This period covers the most complete and continuous recordings at the infiltration station INF-SCARP1, although some data are missing due to technical problems. Note that the VWC readings at 5 and 50 cm depth are only available since June 2018. In addition, vertical dashed lines indicate the timing of the peak discharge of torrential flows as they pass the radar and US sensors at the FLOW-WR station.

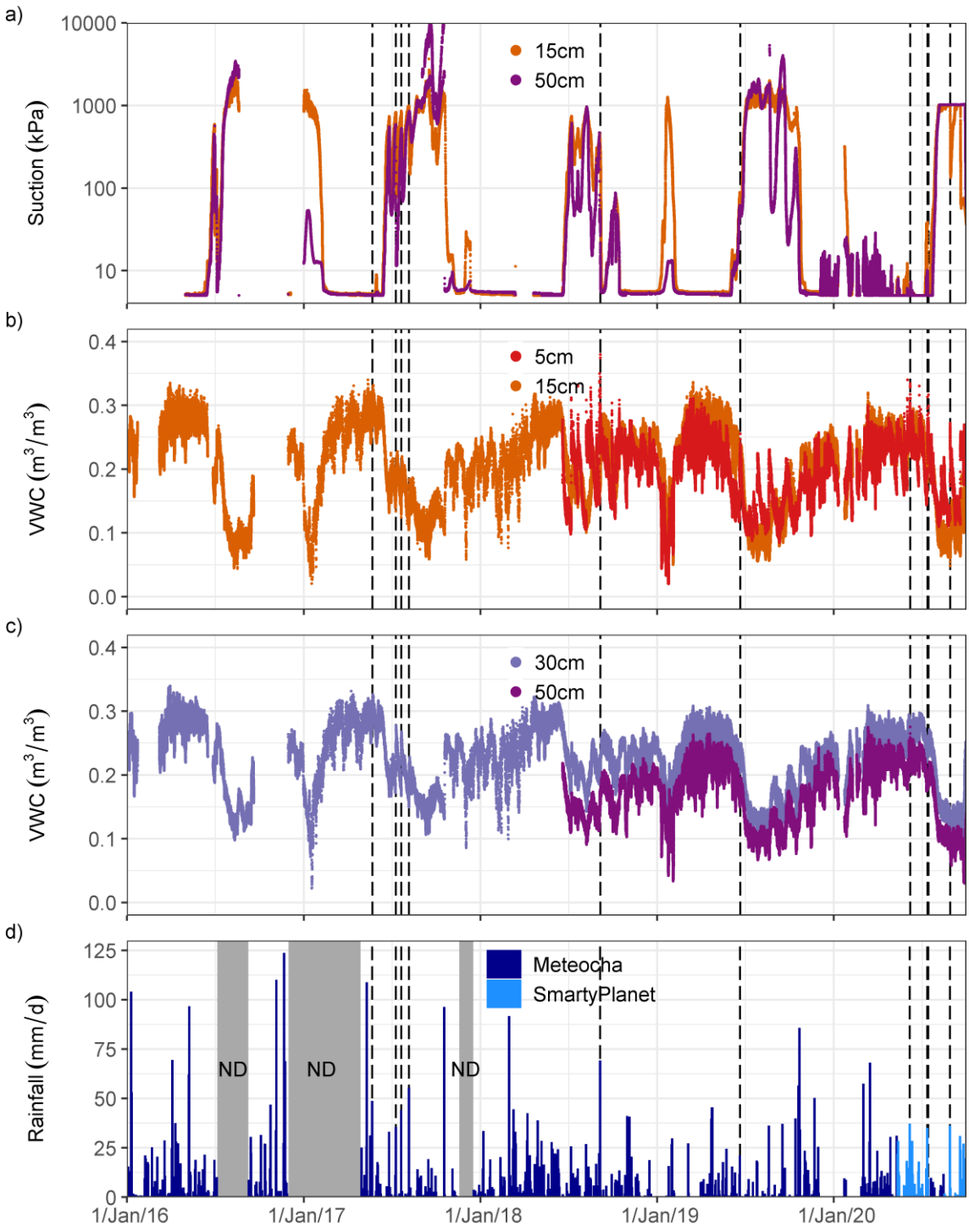

Figure 5.4: Volumetric water content (VWC), suction and daily rainfall time series from January 2016 to October 2020. The dashed vertical lines indicate the timing of the peak discharge of torrential flows at the FLOW-WR station. (a) Matric suction recorded at INF-SCARP1 station at 15 and 50 cm depth; (b) VWC recorded at 5-15 cm of INF-SCARP1 station; (c) VWC at 30-50 cm depth of INF-SCARP1; and (d) daily rainfall. ND stands for no data.

Time series evidence the seasonal fluctuation of soil water variables, driven by meteorological variations of precipitation, and also snowmelt and evapotranspiration. Generally, higher VWC and lower suctions are observed during spring and are related to heavy rainfalls and to possible water supply due to snowmelt [Hürlimann et al., 2010]. In contrast, high suctions values and low VWCs are mainly developed during the summer months. On top of the seasonal fluctuation, daily variations with magnitude of about 25% of the seasonal variations can be observed as the result of the daily cycle of evaporation and, when applicable, hourly rainfalls.

It can be seen from Figure 5.4 that torrential flows are triggered between late spring and early fall and not necessarily due to the heaviest rainfalls in terms of daily precipitation. Soil hydrologic state previous and during torrential flows appears also to vary from one event to other: suction and VWC can range from dry (VWC ≈ 0.10 m^3/m^3 and suction ≥ 1000 kPa) to wet (VWC ≈ 0.34 m^3/m^3 and suction ≈ 0 kPa) conditions. This demonstrates that the full-saturation of the sediment layer is not a required condition for the initiation of debris flows and debris floods, as can be stated by the three last torrential flow events of 2017 where both VWC and suction measurements indicated partial saturation.

Table 5.3 presents the torrential flow inventory since the installation of the infiltration station INF-SCARP1 (June 2013 to August 2020). Torrential flows of year 2014 and year 2015 were not added, as both the VWC at 15 and 30 cm depth were missing for these years. No torrential events were detected during 2016. As a result, the final inventory includes 7 debris flows and 8 debris floods. For each of them, VWC measurements at 5, 15, 30 and 50 cm depth and rainfall characteristics are indicated.

Data in Table 5.3 indicate that torrential flows in the Rebaixader catchment are mainly triggered by short duration and high intensity rainfalls between 12:00 and 18:00 h UTC. These rainfalls are strongly related to convective storms, which are generally shorter than 3 hours and have maximum rainfall intensities ranging from 48 to 120 mm/h regarding the 5 minutes recording rate (4 to 10 mm in 5 minutes). Data also indicate that long duration triggering rainfalls are characterized by lower mean intensity than short duration rainfalls.

This aspect has to be related to VWC measurements. The latter generally reveal that higher rainfall intensities are required to trigger torrential flows when the soil is in a rather dry initial condition (e.g. VWC between 0.07 and 0.18 for flow 7, 8, 9 and 15). Conversely, lower triggering rainfall intensities are observed when the soil is initially wetter (e.g. VWC between 0.22 and 0.30 for flow 1, 3, 4, 5, 12 and 14). In any case, largest debris flows (volume > 9000 m^3 for flow 3, 12 and 13), were preceded by medium to high VWCs (in the range of 0.18 to 0.30 at all depths) and were not triggered by the heaviest rainfalls in terms of rainfall intensity and total rainfall amount. All this suggests that the triggering of torrential flows depend on both the hydrologic soil conditions and the rainfall characteristics.

Table 5.3: Debris Flow (DFlow) and debris flood (DFlood) inventory combining both the rainfall characteristics and the volumetric water content previous to the triggering rainfall (VWC_i) at infiltration station INF-SCARP1. ND stands for no data.

Event ID #	*Event type*	*Date and triggering time (UTC)*	*Volume (m^3)*	*Total rainfall (mm)*	*Duration (h)*	*Mean rainfall intensity (mm/h)*	*I_{max_5min} (mm/h)*	*I_{max_10min} (mm/h)*	*I_{max_15min} (mm/h)*	*I_{max_20min} (mm/h)*	*I_{max_30min} (mm/h)*	*I_{max_60min} (mm/h)*	*VWC_i 5cm (m^3/m^3)*	*VWC_i 15cm (m^3/m^3)*	*VWC_i 30cm (m^3/m^3)*	*VWC_i 50cm (m^3/m^3)*
1	DFlood	05/06/2013 13:00	2100	54.5	7	7.8	49.2	42.6	36	32.7	28	26.4	ND	0.28	0.25	0.17
2	DFlood	17/06/2013 16:38	100	4.4	0.6	7.5	12	11.4	10.8	10.2	8.6	4.5	ND	0.27	0.24	0.16
3	DFlow	17/07/2013 13:05	10400	15.8	3.3	4.9	96	58.8	41.6	33	23.2	12.8	ND	0.30	0.27	0.18
4	DFlood	23/07/2013 12:03	600	12.8	0.5	25.6	54	45.6	38	37.8	25.6	12.8	ND	0.29	0.29	0.17
5	DFlood	27/07/2013 17:15	450	14.5	0.3	43.5	70.8	64.2	54.4	43.5	29	14.7	ND	0.27	0.28	0.16
6	DFlood	22/05/2017 15:22	800	48.2	4.3	11.3	72	61.2	48.8	42	37.2	31.2	ND	0.27	0.28	ND
7	DFlow	10/07/2017 02:55	2950	33.2	1.7	19.9	100.8	75.6	66.4	55.2	54	31	ND	0.13	0.20	ND
8	DFlow	21/07/2017 07:08	3100	38.6	3.8	10.3	96	72	52.8	42	32.4	25	ND	0.12	0.17	ND
9	DFlood	06/08/2017 00:14	600	33.8	1.9	17.6	88.8	79.2	69.6	58.8	47.6	31.2	ND	0.10	0.15	ND
10	DFlow	05/09/2018 17:49	2500	22.2	0.4	53.3	117.6	106.8	85.6	66	44.4	22.2	0.24	0.17	0.21	0.15
11	DFlow	21/06/2019 15:23	2000	13	0.6	22.3	55.2	52.8	45.6	36.6	25.6	13	0.22	0.17	0.20	0.16
12	DFlow	06/06/2020 19:13	9600	29.5	2.75	10.7	79.1	63.6	53.8	45.6	32.7	19.2	0.26	0.25	0.28	0.24
13	DFlow	12/07/2020 12:00	10000	28.8	2.75	10.5	74.7	60.1	50.8	43	34.2	22.4	0.2	0.19	0.23	0.19
14	DFlood	14/07/2020 14:42	700	8.8	1.5	5.9	48.4	38.9	32.9	27.8	22.1	14.5	0.23	0.22	0.25	0.20
15	DFlood	28/08/2020 16:21	1200	27.4	2	13.7	96.7	77.7	65.7	55.7	45	27.2	0.18	0.07	0.13	0.09

Figure 5.5 presents a detailed view of soil water content (VWC) time evolution at infiltration stations INF-SCARP1 and INF-SCARP2 during three selected events. The first two events (first two columns in Figure 5.5) correspond to short duration and relatively high intensity rainfalls that triggered a debris flow (June 6, 2020) and debris flood (August 28, 2020), respectively. The third event (third column in Figure 5.5) corresponds to a long duration and low intensity rainfall, which did not trigger any torrential flow. Soil is quite wet in the 1st and 3rd event and drier in the 2nd event.

Figure 5.5c and Figure 5.5f evidence that triggering rainfall intensity is lower for initially wetter than dryer soil conditions. In case of the non-triggering rainfall event (Figure 5.5i), intensity is low and certainly not enough to initiate a torrential flow, although initial VWC are relatively high and accumulated rainfall almost three times higher than for the triggering events. These results confirm that triggering rainfall intensity is strongly related to soil hydrological conditions, while total precipitation seems not to be a critical parameter.

Figure 5.5a,b and Figure 5.5d,e provide insights into the hydrologic response of the slope under the short duration/high intensity rainfall events. VWCs at shallow depths (5 and 10 cm) appear to react quickly to rainfall while deeper sensors (15cm to 30 cm for INF-SCARP1, 15cm to 20cm for INF-SCARP2) exhibit an attenuated response. This generally expressed the propagation of a sharp front of higher water saturation within the shallowest soil layer. Deepest sensors (50 cm at INF-SCARP1, 30 cm at INF-SCARP2) present curiously higher changes than the ones at intermediate depths, which has been interpreted by modelling as resulting from the establishment of a lateral flow in the underlying layer [Luna, 2015]. Another interesting aspect is that the increase of water content is higher when the soil is initially in a drier state and rainfall intensity is higher. In such a case, soil will lose stability more quickly. As a final remark, the timing of torrential flow peak discharge at the FLOW-WR station matches in both cases the timing of maximum rainfall intensity and peak in shallow water content changes. Conversely, the variation in VWC is progressive for the low intensity non-triggering rainfall and shows slow increase of water content at all sensors depths (Figure 5.5g and Figure 5.5h).

These results confirm that initial hydrologic soil condition and short duration rainfall are important controlling factors for the triggering of torrential flows. In the following part

of the work, we will study the hydro-meteorological threshold by using VWCs at 15 cm and 30 cm as representative of slope hydrologic state before rainfall occurrence and rainfall maximum intensity for several short durations as trigger variable.

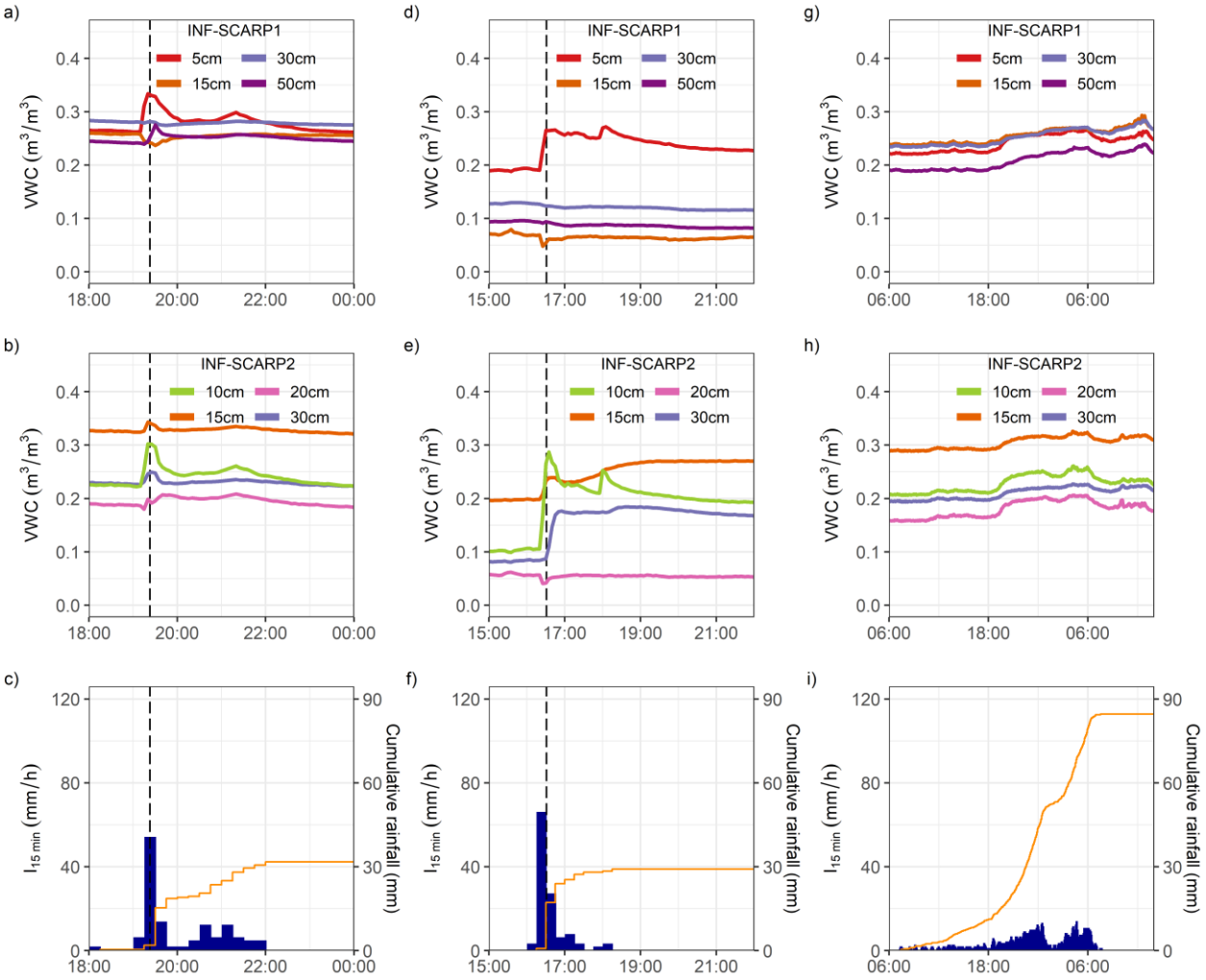

Figure 5.5: Time series of soil volumetric water content (VWC) and rainfall showing the slope hydrologic response at the initiation zone of torrential flows during three rainfall events: (a) debris flow of June 6, 2020, (b) debris flood of August 28, 2020, and (c) non-triggering rainfall of April 24, 2019. First and second rows: VWC at the infiltration stations INF-SCARP1 and INF-SCARP2, respectively. Third row: rainfall intensity in 15 minutes duration (I_{15min}) and cumulative rainfall. The vertical dashed lines indicate the timing of torrential flow peak discharge at the FLOW-WR monitoring station.

5.3.2. Threshold analysis

5.3.2.1. Scoring metrics, ROC and PRC curves

The scoring metrics of the thresholds with highest performance are listed in Table 5.4 for both the rainfall thresholds (I_{mean}-D and I_{max_dur} for the 2009-2020 and 2013-2020 datasets) and the hydro-meteorological thresholds ($I_{max\_durVWCdepth}$ regarding the 2013-2020 dataset). These thresholds have been selected on the premise that more than 85% of the torrential events are correctly predicted as TPs (TPR> 0.85) and by maximizing the F_1-score. The threshold equation with the best performance is highlighted for each type of threshold. In addition, some of the selected thresholds are presented in the ROC and PRC space (Figure 5.6) in order to visualize and better interpret their performance.

At the beginning, we analyzed the rainfall I_{mean}-D thresholds and realized that a high number of FPs (false alarms) were predicted; although more than 85% of the torrential flow events were correctly classified as TPs (Table 5.4). As a result, the precision (ratio between true alarms and the total triggered alarms) is low and around 18% and 15% for the 2009-2020 and 2013-2020 datasets, respectively. In the following, we focused on the comparison of the I_{mean}-D and I_{max_dur} rainfall thresholds. The first thing that stands out is the important reduction of FPs when considering maximum rainfall intensities instead of mean rainfall intensities. Hence, the rainfall I_{max_dur} thresholds mainly revealed higher precision and TPR values relative to the I_{mean}-D thresholds, when the same dataset is considered (Table 5.4 and Figure 5.6). Therefore, the results point out that maximum rainfall intensities are more appropriate for assessing the triggering rainfall conditions in the Rebaixader catchment, compared to mean rainfall intensities. Furthermore, the best performance is attained with the maximum rainfall intensity for a duration of 15 minutes (I_{max_15min} threshold) for the 2009-2020 dataset, and of 20 minutes (I_{max_20min} threshold) for the 2013-2020 dataset. As a result, the precision increased to 30% and 54%, respectively.

In continuation, we checked whether the rainfall thresholds defined by maximum rainfall intensities, I_{max_dur}, could further improve the performance by including VWC measurements. For this reason, the hydro-meteorological thresholds, $I_{max\_durVWCdepth}$, and rainfall I_{max_dur} thresholds are compared in Figure 5.6 for the same dataset (2013-2020). The results clearly highlight that adding subsurface hydrology decreases the number of FPs or

false alarms compared to the rainfall I_{max_dur} thresholds, while the number of TPs remains mainly equal. This produces increased precision and similar TPR compared to the rainfall I_{max_dur} threshold (Figure 5.6c-Figure 5.6d and Table 5.4). In any case, the combination of VWC and maximum rainfall intensities improved the thresholds performance and hence its prediction capabilities. Furthermore, one can see that the highest performance is achieved by linking the maximum rainfall intensity in 10-15 minutes duration with the VWC observations at 15 cm depth (which correspond to the $I_{max\_10minVWC15cm}$ and $I_{max\_15minVWC15cm}$ hydro-meteorological thresholds), and by combining the maximum rainfall intensity in 15 minutes duration with VWC at 30 cm depth ($I_{max\_15minVWC30cm}$). In this situation, the precision increased up to 65% and 63%, considering VWC at 15 and 30 cm depth, respectively. Nevertheless, the hydro-meteorological thresholds defined by the VWC at 30 depth scored slightly higher than those defined at 15 cm depth, even though both predicted better results compared to the rainfall I_{max_dur} thresholds. Anyway, the results confirm that, for such high permeable soils, similar performance is obtained regardless the VWC depth.

In addition, it can be seen that ROC curves of Figure 5.6 show less variability and are thus less informative than PRC curves when dealing with imbalanced datasets and high numbers of TN events. In this scenario, the FPRs are low and consequently the ROC curves seem quite optimistic and present similar results. For this reason, the rainfall and hydro-meteorological thresholds defined by maximum rainfall intensities are harder to compare (Figure 5.6a and Figure 5.6c), in contrast to the higher variability shown in the PRC curves (Figure 5.6b and Figure 5.6d). In essence, the PRC curves in Figure 5.6d clearly illustrate the higher performance of the rainfall I_{max_dur} thresholds relative to the I_{mean}-D rainfall thresholds, and which is further improved by the inclusion of VWC observations in the hydro-meteorological thresholds.

Table 5.4: Comparison of the equations and scoring metrics for the selected rainfall (I_{mean}-D and I_{max_dur}) and hydro-meteorological ($I_{max\_durVWCdepth}$) thresholds. The optimal equations for each threshold type and each dataset are highlighted focusing on the F_1-score. See Eq. (*7-9*) in the text for more details on equations. The total number of rainfall events are 1000 non-triggering and 37 triggering events for the 2009-2020 dataset, and 470-non triggering and 15 triggering events for the 2013-2020 dataset.

	Threshold type	***Equation***	***Dataset***	***TP***	***FN***	***TN***	***FP***	***TPR***	***FPR***	***Precision***	***F_1-score***
	Rainfall: I_{mean}-D (Eq. *7*)	$I_{\mathrm{mean}} = 11.03 Duration^{-0.75}$	2009 – 2020	32	5	858	142	0.865	0.142	0.184	0.303
	Rainfall: I_{max_dur} (Eq. *8*)	$I_{\mathrm{max\_5}min} = 31$	2009 – 2020	32	5	915	85	0.865	0.085	0.274	0.416
		$I_{\mathrm{max\_10}min} = 25$		32	5	923	77	0.865	0.077	0.294	0.438
		$I_{\mathrm{max\_15}min} = 21$		32	5	926	74	0.865	0.074	0.302	0.448
		$I_{\mathrm{max\_20}min} = 18$		32	5	923	77	0.865	0.077	0.294	0.438
		$I_{\mathrm{max\_30}min} = 16$		32	5	942	58	0.865	0.058	0.356	0.504
		$I_{\mathrm{max\_60}min} = 9$		33	4	892	108	0.892	0.108	0.234	0.371
	Rainfall: I_{mean}-D (Eq. *7*)	$I_{\mathrm{mean}} = 11.39 Duration^{-0.71}$	2013 – 2020	13	2	397	73	0.867	0.155	0.151	0.257
	Rainfall: I_{max_dur} (Eq. *8*)	$I_{\mathrm{max\_5}min}$ =48	2013 – 2020	14	1	448	22	0.933	0.047	0.389	0.549
		$I_{\mathrm{max\_10}min}$ =42		13	2	454	16	0.867	0.034	0.448	0.591
		$I_{\mathrm{max\_15}min}$ =36		13	2	457	13	0.867	0.028	0.500	0.634
		$I_{\mathrm{max\_20}min}$ =32		13	2	459	11	0.867	0.023	0.542	0.667
		$I_{\mathrm{max\_30}min}$ =23		13	2	456	14	0.867	0.030	0.481	0.619
		$I_{\mathrm{max\_60}min}$ =12		14	1	438	32	0.933	0.068	0.304	0.459
15cm depth	Hydro – meteorological: $I_{max\_durVWCdepth}$ (Eq. *9*)	$I_{\mathrm{max\_5min}} VWC_{15cm} = -110VWC + 72$	2013 – 2020	14	1	452	18	0.933	0.038	0.438	0.596
		$I_{\mathrm{max\_10}min} VWC_{15cm} = -103VWC + 70$		13	2	463	7	0.867	0.015	0.650	0.743
		$I_{\mathrm{max\_15}min} VWC_{15cm} = -88VWC + 60$		13	2	463	7	0.867	0.015	0.650	0.743
		$I_{\mathrm{max\_20}min} VWC_{15cm} = -62VWC + 47$		13	2	462	8	0.867	0.017	0.619	0.722
		$I_{\mathrm{max\_30}min} VWC_{15cm} = -57VWC + 35$		13	2	458	12	0.867	0.026	0.520	0.650
		$I_{\mathrm{max\_60}min} VWC_{15cm} = -35VWC + 22$		13	2	452	18	0.867	0.038	0.419	0.565
30cm depth	Hydro – Meteorological: $I_{max\_durVWCdepth}$ (Eq. *9*)	$I_{\mathrm{max\_5}min} VWC_{30cm} = -182VWC + 92$	2013 – 2020	14	1	455	15	0.933	0.032	0.483	0.636
		$I_{\mathrm{max\_10}min} VWC_{30cm} = -169VWC + 81$		14	1	461	9	0.933	0.019	0.609	0.737
		$I_{\mathrm{max\_15}min} VWC_{30m} = -161VWC + 73$		14	1	462	8	0.933	0.017	0.636	0.757
		$I_{\mathrm{max\_20}min} VWC_{30m} = -145VWC + 66$		13	2	463	7	0.867	0.015	0.650	0.743
		$I_{\mathrm{max\_30}min} VWC_{30cm} = -76VWC + 41$		14	1	458	12	0.933	0.026	0.538	0.683
		$I_{\mathrm{max\_60}min} VWC_{30cm} = -103VWC + 40$		13	2	453	17	0.867	0.036	0.433	0.578

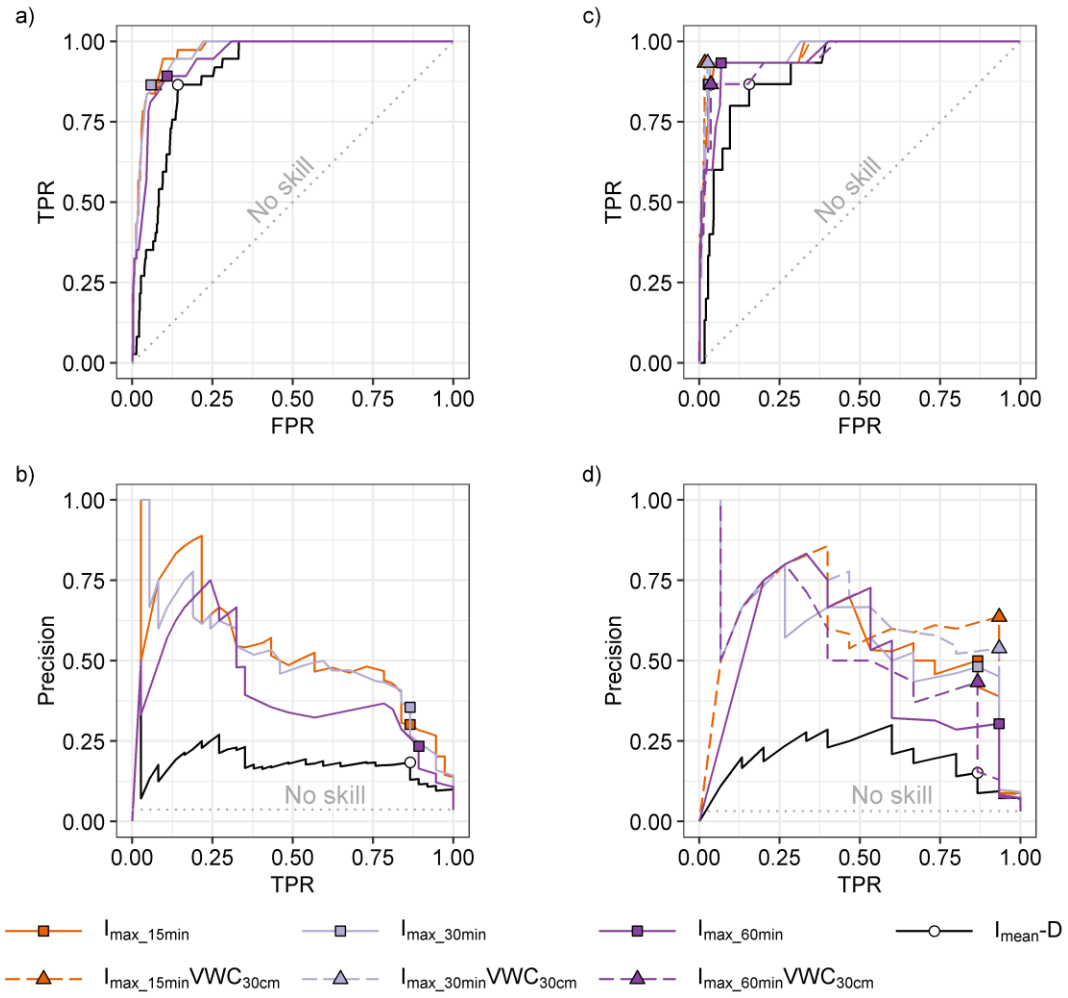

Figure 5.6: Receiver operating characteristic (ROC) curves and precision-recall (PRC) curves comparing rainfall thresholds (I_{mean}-D and I_{max_dur}) and hydro-meteorological thresholds ($I_{max\_durVWC30cm}$) regarding the VWC readings at 30 cm depth. (a) ROC curves and (b) PRC curves considering the rainfall thresholds for the 2009-2020 dataset. (c) ROC curves and (d) PRC curves considering the rainfall thresholds and the hydro-meteorological threshold for the 2013-2020 dataset. Note that the hydro-meteorological thresholds, $I_{max\_durVWC30cm}$, and the rainfall thresholds, I_{max_dur}, are represented by the maximum rainfall intensities in 15, 30 and 60 minutes duration.

5.3.2.2. Torrential flow thresholds

Finally, the selected rainfall and hydro-meteorological thresholds are plotted for a better visualization and interpretation of the results. In a first step, the rainfall I_{mean}-D thresholds with the highest performance are presented for the 2009-2020 and 2013-2020 dataset (Figure 5.7a and Figure 5.7b, respectively). In the next stage, we compare the best fitting rainfall I_{max_dur} thresholds and hydro-meteorological thresholds considering the VWC

at 15 cm depth (Figure 5.8a) and the VWC at 30 cm depth (Figure 5.8b) for the 2013-2020 dataset.

Regarding the rainfall I_{mean}-D thresholds (Figure 5.7), a high number of FPs events are predicted relative to the number of TPs for both datasets. Nevertheless, the thresholds performance could be increased if the rainfall events with a duration longer than 10 hours were not considered, since none of them triggered a torrential flow. Even so, the number of FPs would be higher compared to the rainfall I_{max_dur} and hydro-meteorological thresholds. In any case, the majority of torrential flows events exceed the threshold line and only 5 and 2 debris floods with small volumes (< 1000 m^3) did not fulfill the threshold condition for the 2009-2020 and 2013-2020 dataset, respectively. Therefore, the results in Figure 5.7 demonstrate that, regardless of the longer (2009-2020) or shorter (2013-2020) dataset, similar thresholds equations are obtained for the rainfall I_{mean}-D dataset. It is worth to note that very close threshold results were also described in a previous study spanning the period 2009-2018 [Oorthuis et al., 2021]. Furthermore, the results in Figure 5.7 confirm the hypothesis that torrential flows in the Rebaixader catchment are triggered by short lasting rainfalls, generally shorter than 3 hours in duration.

In relation to the rainfall I_{max_dur} and hydro-meteorological thresholds (Figure 5.8), the results clearly illustrate that, in general, higher maximum rainfall intensities are necessary for the triggering of torrential flows when compared to the non-triggering rainfalls. Moreover, one may distinguish a slight trend when looking closer at the hydro-meteorological thresholds: generally, higher rainfall intensities are required for the triggering of torrential flows when the soil is initially dryer, while lower rainfall intensities are necessary for initially wetter soil conditions. In conclusion, the results in Figure 5.8 confirm the hypothesis that including the soil hydrologic conditions (VWC in this study) prior to the triggering rainfall reduces the number of FPs compared to thresholds relying exclusively on rainfall parameters.

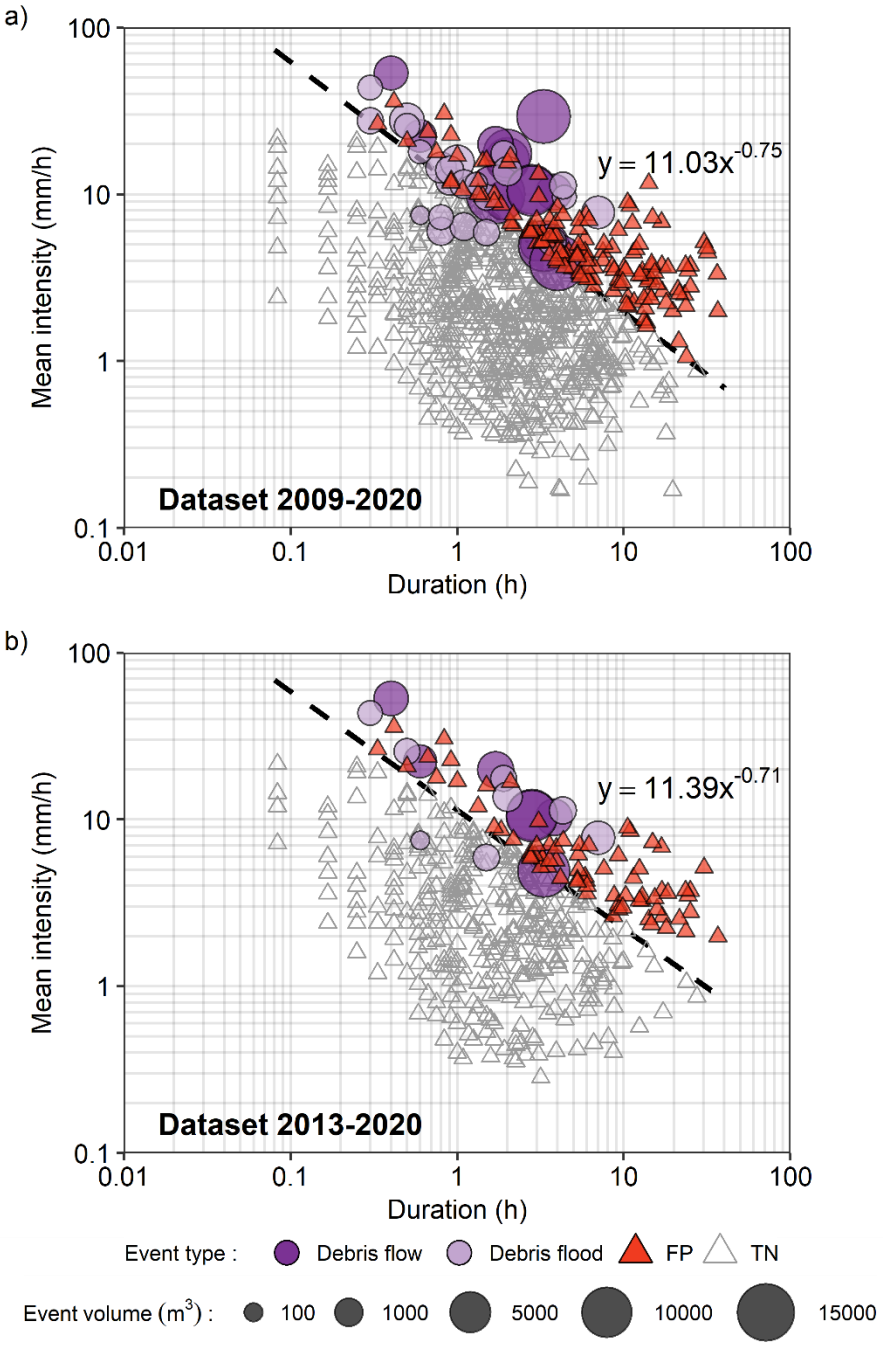

Figure 5.7: Mean intensity vs duration (I_{mean}-D) rainfall thresholds regarding the 2009-2020 dataset (a) and 2013-2020 dataset (b). Dashed line and equation indicate the threshold with best performance, selected by maximizing the F_1-score. FP and TN stand for false positive and true negative, respectively.

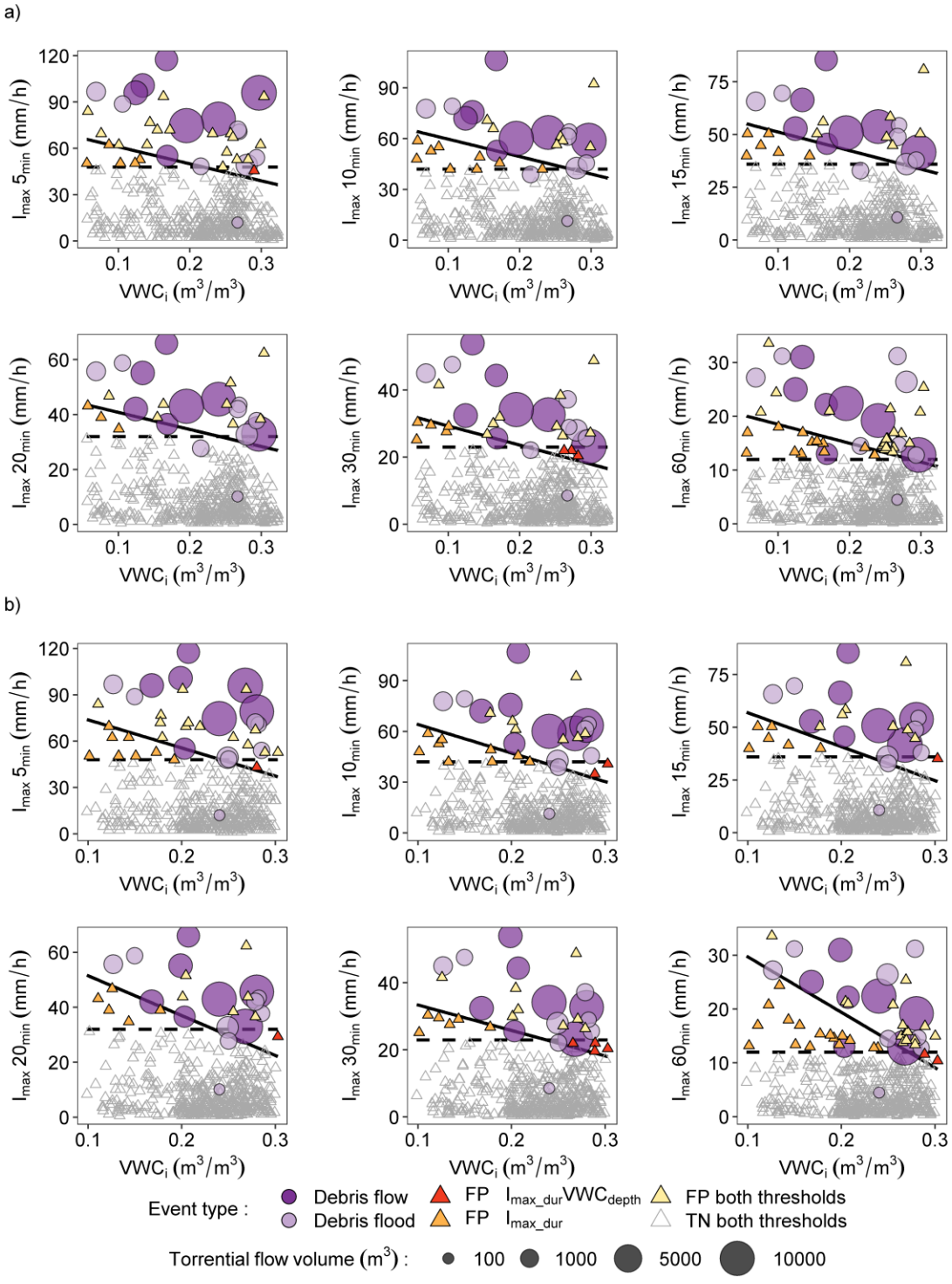

Figure 5.8: Comparison of the rainfall I_{max_dur} thresholds (dashed lines) and the hydro-meteorological $I_{max\_durVWCdepth}$ thresholds (solid lines) regarding the VWC prior to the rainfall event (VWC_i) at (a) 15 cm depth and (b) 30 cm depth. FP and TN stand for false positive and true negative, respectively.

5.3.2.3. Implementation in a landslide early warning system

Landslide early warning systems (LEWSs) are a significant option among the diverse mitigation solutions available to reduce the risk related to landslides [Segoni et al., 2018]. In contrast to active measures or structural engineering works, the installation of a LEWS is often a cost-effective and sustainable risk mitigation strategy [Glade & Nadim, 2014]. LEWSs are used to monitor one or more variable related to landslide triggering in order to generate and disseminate timely and meaningful warning information to enable authorities and communities to act appropriately and in sufficient time to reduce the landslide risk [UN/ISDR, 2006]. LEWSs can be classified into alarm, warning and forecasting systems, depending on the lead time between alarm and landslide triggering [Sättele et al., 2012]. Warning and forecasting systems monitor the precursors or predisposing factors in order to predict landslide triggering (e.g. rainfall and/or soil hydrologic conditions) and have higher lead times [Sättele et al., 2015]. An important part of LEWS is the definition of thresholds for landslide initiation.

Here, we check the implementation of our previous results into a LEWS by means of rainfall and hydro-meteorological thresholds. This is an exercise for research purposes, since there are no significant risks related to torrential activity in the catchment. The performance of the two thresholds is compared using the year 2019 as example (Figure 5.9). Both thresholds were defined considering the 2013-2020 dataset (see Table 5.4).

Regarding rainfall thresholds, the analysis of the I_{mean}-D threshold predictions (Figure 5.9a) reveals a high number of false positives, 16 in total, despite correctly predicting the occurrence of the only torrential flow detected on that year. This trade-off between correct and incorrect predictions limits the success of implementing the rainfall I_{mean}-D threshold in a LEWS, since with a high number of false alarms the so-called cry-wolf effect may induce populations to ignore the issued alarms [Barnes et al., 2007; Peres et al., 2018]. Conversely, the rainfall thresholds defined with maximum intensities of 5 and 15 minutes duration (Figure 5.9b and Figure 5.9c) reduce the false positives to 6 and 4, respectively, while torrential flow occurrence is still correctly predicted. Hence, when relying on rainfall measurements or rainfall forecasts, the maximum rainfall intensity threshold should be considered for a LEWS

in front of traditional rainfall I_{mean}-D thresholds. Nevertheless, the precision of the predicted alarms is still low which may be a drawback for implementing these thresholds into a LEWS.

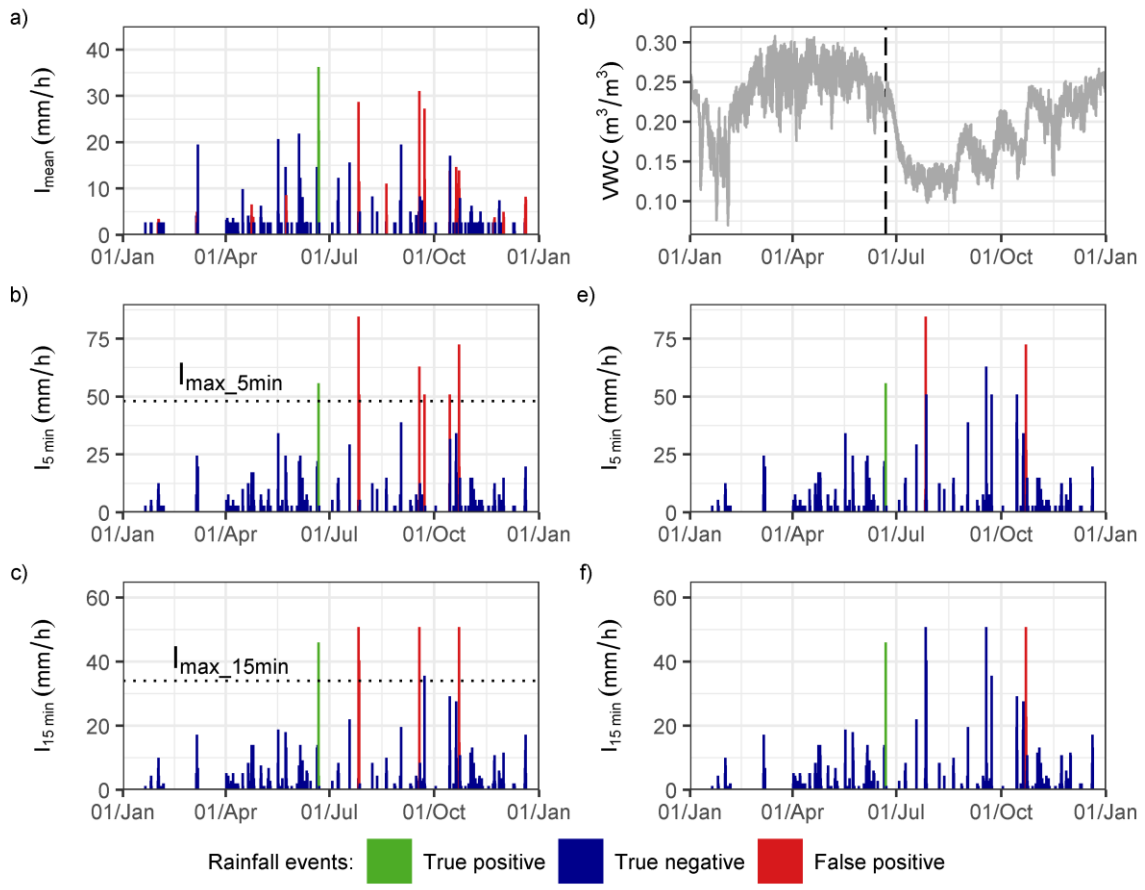

Figure 5.9: Time series of rainfall and volumetric water content (VWC) showing landslide occurrence and threshold exceedance in 2019. Predictions of rainfall thresholds in left column and hydro-meteorological thresholds in right column. Rainfall thresholds predictions for the I_{mean}-D threshold (a) and maximum rainfall intensity thresholds for 5 minutes (b) and 15 minutes (c) of duration. (d) VWC at INF-SCARP1 infiltration station and at 30 cm depth. Hydro-meteorological threshold predictions combining VWC at 30 cm at INF-SCARP1 and maximum rainfall intensities at 5 minutes (e) and 15 minutes (f) of duration. The horizontal dotted line in (b) and (c) shows the maximum intensities defined in the maximum rainfall intensity thresholds. The vertical dashed line in (d) indicates the timing of torrential flow detection at the FLOW-WR monitoring station.

Regarding the hydro-meteorological thresholds, the results demonstrate that including VWC measurements improves the predictions compared to rainfall-only thresholds. False positives reduce to 2 and 1 when considering maximum rainfall intensities in 5 and 15 minutes of duration in combination with the VWC at 30 cm depth (Figure 5.9e and Figure 5.9f). This reduction in the FPs occurs mainly during the summer and with initially low VWCs, which is especially favorable for the correct prediction of torrential

flows in the Rebaixader catchment, since debris flows and floods are mainly triggered between June and September [Oorthuis et al., 2021].

These results encourage further investigation of the role that soil hydrologic conditions play in triggering torrential flows or other slope mass movements and justify the definition of hydro-meteorological thresholds for landslide warning. We suggest considering the hydrological soil conditions in combination with rainfall in other catchments or landslide-prone areas to improve or implement new or existing LEWS.

5.4. Conclusions

Our study evaluates the role of hydrologic soil conditions and rainfall characteristics in the triggering of torrential flows at the Rebaixader catchment through monitoring close to the initiation zone of these flows. The results highlight the advances of considering both soil hydrologic conditions and rainfall characteristics for torrential flows initiation. The contributions of combining the hydrologic soil state with rainfall characteristics are compared in terms of predictive capability with rainfall thresholds based solely on the rainfall as triggering factor. As rainfall-based thresholds neglect the antecedent hydrologic soil conditions, their predictive performance is often low and results in many false positives, which may induce to ignore the issued alarms.

Regarding the hydrologic soil measurements (VWC and suction in this study), the results show that soil moisture can range from dry (VWC ≈ 0.10 m^3/m^3 and suction ≥ 1000 kPa) to wet (VWC ≈ 0.34 m^3/m^3 and suction ≈ 0 kPa) conditions prior to the initiation of triggering rainfalls. Therefore, the complete saturation of the sediment debris layer is not necessary for the initiation of these flows. The analysis of rainfall characteristics demonstrates that short duration (less than 3 hours) and high intensity (4-10 mm in 5 minutes duration, which corresponds to 48-120 mm/h) summer rainfalls between 12:00 and 18:00 h UTC triggered most of torrential flows. Conversely, long duration (e.g. more than 10 hours) rainfalls did not trigger torrential flows. In addition, the three largest debris flows (volume > 9000 m^3) were preceded by medium to high VWCs (0.18 to 0.30 at all depths) and were not triggered by the heaviest precipitations in terms of rainfall intensity and total rainfall amount,

which suggests that both hydrologic soil conditions and rainfall characteristics affect the triggering of torrential flows.

The implications of rainfall and VWC measurements in the definition of only-rainfall and hydro-meteorological thresholds for torrential flow prediction have been evaluated and the performance of each threshold has been analyzed. With respect to rainfall thresholds based exclusively on precipitation parameters, the maximum rainfall intensity thresholds obtained higher prediction accuracy compared to the traditional rainfall mean intensity – duration (I_{mean}-D) threshold. The rainfall I_{mean}-D threshold is not really the most suitable for the prediction of torrential flows in the Rebaixader catchment due to the elevated number of false positives. This confirms that peak rainfall intensities better represent the triggering rainfall characteristics compared to mean rainfall intensity which clearly diminishes for long duration rainfalls. Finally, the combination of VWC and maximum rainfall intensities in the hydro-meteorological thresholds provides an improved precision compared to only-rainfall thresholds, as important antecedent conditions and rainfall intensity variations or bursts are taken into account. The improved precision of hydro-meteorological thresholds justifies the testing of this approach in other torrential catchments or landslide-prone areas where continuous hydrologic soil conditions are being monitored.

Our results justify the definition of hydro-meteorological thresholds for application in LEWS including VWC. The hydro-meteorological thresholds confirm that the hydrologic conditions of the soil affect the maximum rainfall intensity necessary for torrential flow triggering. Generally, lower rainfall peak intensities are required for torrential flow triggering when the soil is initially wetter at the start of a rainfall event, and vice versa. This confirms that soil moisture is an important predisposing factor for torrential flows initiation, and therefore, a key parameter in LEWSs for torrential flow warning.

Chapter 6

CONCLUSIONS AND FUTURE RESEARCH WORK

In this last chapter, the most relevant conclusions and findings of this research are presented and future research works are described.

6.1 General conclusions

This research work started from two monitoring stations at different scales (slope and catchment scale) with the aim of increasing the knowledge related to soil-vegetation-atmosphere (SVA) interactions and its implications in the processes of slope mass-wasting (SMW). For this purpose, a full-scale embankment experiment has been instrumented to monitor atmospheric and soil hydrological and thermal variables at slope scale. Considering the catchment scale, the monitoring system in a torrential watershed for torrential flows research (debris flows and debris floods) has been maintained and upgraded to analyze the rainfall and soil hydrologic conditions necessary and favorable for torrential flows initiation. The main and overall conclusion of this work is that SVA interactions are complex and should not be neglected as they have many implications on the processes of SMW. In the following, the most relevant conclusions referring to the major objectives (see Chapter 1.4 Objectives) are summarized and presented for each research scale, whereas more detailed conclusions are specified at the end of each chapter.

Conclusions regarding slope scale:

During this thesis, the development and setup of a complex monitoring system in a full-scale embankment with different orientations (North and South) and slope covers (bare and vegetated) was performed. The aim of this embankment experiment was to improve our knowledge on soil-vegetation-atmosphere (SVA) interactions and analyze the effects of different orientations and slope covers on the hydrological and-thermal slope response to climatic actions.

The monitoring system focused on the recording of meteorological and soil hydro-thermal parameters by means of more than 60 sensors. The sensors were tested and calibrated, whereas the data acquisition system was programmed, before field installation. In addition, continuous maintenance was performed on both the sensor network and the turf grass species sowed on the vegetated slopes. The technical issues during the setup and the maintenance of the monitoring system prior to the analysis of the recorded data were high time-consuming tasks but necessary to obtain accurate and long-term monitoring data on SVA interactions. As a result, a dataset with more than 4 years of recordings related to SVA interactions is available for future research. Indeed, long-term time series of atmospheric and soil hydro-thermal parameters are necessary to better understand SVA interactions and the slope response to climatic actions. Furthermore, they provide the necessary input data for numerical modelling simulations and predictions of the thermo-hydro-mechanical slope response. Therefore, monitoring data are essential and provide valuable information when it comes to validate SVA models and to assess both the development and hazards of SMW. However, experiments monitoring SVA interactions on multiple variables over a long time-period are scarce and not very common.

A detailed laboratory characterization of soil hydrological and strength parameters is crucial to understand the slope failure mechanisms and SMW phenomena, which are mainly related to infiltration processes. The embankment soil consists of clayey sand with an estimated relative low permeability in the order of 10^{-8} and 10^{-7} m/s. Direct shear tests on partially saturated samples clearly highlight the contribution of matric suction to soil shear strength. However, field conditions may present larger heterogeneities due to fissures and cracks developed by climatic actions on clayey embankments and/or due root-growth. These features create preferential flow paths of water, which increase soil permeability and enhances rainfall infiltration, and therefore, reduces suction and soil strength. Consequently, the embankment stability and serviceability may be jeopardized. Therefore, permeability at the embankment slopes is probably much higher than the one measured in homogeneous laboratory soil samples.

Analysis of soil thermal data revealed that orientation has a strong effect in bare slopes due to solar radiation and solar angle incidence: soil temperature, and thus heat fluxes

and evaporation rates, are higher on South-facing slopes than on North-facing slopes, as expected. The effects of solar radiation produce higher surface temperatures (up to 55 °C at 1 cm depth on South non-vegetated slopes) compared to air temperature, while this effect decreases on the North-facing slopes. It is worth to note that the highest differences in surface temperature between North and South slopes are accounted during winter months and are related to the decrease of solar angle incidence during this season. In fact, the normal component of solar radiation to the slope surface totally cancels during autumn-winter on the North-slopes, and thus, heat flux into the ground is solely related to heat atmosphere diffraction. The variations in soil temperature on North slopes between autumn and winter months reflects the importance of heat atmosphere diffraction on the soil-atmosphere heat inflow exchange. Furthermore, daily fluctuations are attenuated with depth and are not significant below 50 cm. Concerning vegetation, the effects of solar radiation and orientation are clearly diminished by vegetation cover, which reduces the incidence of net solar radiation. This reduces the incoming heat fluxes up to 75% on the South-facing slopes, and thus, reduces soil-atmosphere heat exchange, while this effect decreases on the North-facing slopes. As a result, vegetation decreases soil evaporation rates.

Regarding soil hydrological state, higher soil drying rates and dryer slope conditions (lower VWCs and higher suctions) are observed in the vegetated slopes, below 6 cm depth, regardless of its orientation. This is clearly observed when comparing the North-facing vegetated slope, with dryer soil conditions and higher drying rates, and the South-facing bare slope, with wetter soil conditions and lower drying rates. Even between autumn and winter, when evaporation decreases on north-facing slopes due to the lower angle of solar incidence, dryer soil conditions are developed on the North vegetated slope than on the South bare slope. These results highlight the importance of in-depth evapotranspiration due to root growth and demonstrates that vegetation transpiration is much more efficient than orientation in developing dryer soil states, and thus, increases soil strength and slope stability, in absence of rainfall.

As seen, vegetation plays an important role on both thermal and hydrologic slope response in absence of rainfall, increasing matric suction and, consequently, slope stability. Nevertheless, the effect of vegetation on SMW during a rainfall event is more controversial

and not straightforward. First, the results demonstrate that vegetation enhances rainfall infiltration below 6 cm depth compared to bare slopes, and thus lowers rainfall runoff, regardless of its orientation. This evidence shows the effect of in-depth root penetration during dry periods with no rainfall: as roots penetrate the soil layer, they create fissures and preferential water paths through macropores, enhancing the hydraulic soil conductivity, and hence, rainfall infiltration. This results in larger variations of VWC and suction on vegetated slopes during a rainfall event below 6cm depth compared to a bare slope. As a consequence of increasing rainfall infiltration, vegetation reduces matric suction, which decreases shear strength and may jeopardize slope stability. In contrast, bare slopes present a slower and more attenuated hydrological response to rainfall infiltration. This effect is clearly observed on non-vegetated slopes during short duration rainfalls, which in most cases resulted in no significant variations of VWC nor suction. Conversely, most of the long duration rainfalls caused variations in both VWC and suction on non-vegetated or bare slopes, while this effect decreased with depth and is consistent with the infiltration process in the soil layer. These results mainly reveal higher infiltration rates at vegetated slopes, and thus, suggest lower runoff rates compared to bare slopes. Hence, lower surficial erosion rates are expected on slopes covered by vegetation, although this should be quantitatively confirmed in future research steps (see 6.2 Future research work for more details).

These results highlight the role of slope cover and rainfall duration and intensity on slope infiltration and runoff processes, and thus on SMW mechanisms. However, the increase in rainfall infiltration on vegetated slopes, which reduces suction and thus soil strength and slope stability, should be compared with other vegetation effects not studied in this research and clearly related to SMW. Such effects range from raindrop impact protection due to canopy interception and decrease of runoff and sediment trap, which are known to reduce surficial erosion, or others such as root mechanical reinforcement, which increases soil strength and slope stability.

In view of these outcomes, further research is needed to understand all the processes involved in SVA interactions and its effects on SMW, as well as to promote vegetation as a sustainable solution to mitigate SMW. See 6.2 Future research work for more details on future research steps.

Conclusions regarding catchment scale:

This work contributed to improving the knowledge on the initiation mechanisms of torrential flows (debris flows and debris floods) in the Rebaixader torrent (Central Pyrenees). The main aim was to characterize both torrential flow properties (type of flow, flow depth, estimated volume, average flow velocity, etc.), the triggering rainfall characteristics, as well as the effects of soil hydrologic conditions on torrential flows initiation, by means of a sophisticated monitoring system. In addition, this work contributed to developing meteorological thresholds, solely based on rainfall parameters, and hydro-meteorological thresholds, combining rainfall and hydrologic soil conditions, for torrential flow initiation and prediction. Thresholds for debris flows and debris floods initiation are an important tool when it comes to assess and reduce torrential flow hazards. In this sense, the definition of hydro-meteorological thresholds by in situ monitoring is a novel approach in the field of torrential flows prediction. In the following, the specific conclusions of this work are presented.

Since the start of the monitoring in 2009 and until December 2020, more than 1000 rainfalls have been recorded, of which 37 triggered a torrential flow. The dataset comprehends 12 years of torrential flows occurrence and rainfall characteristics (2009-2020) and 8 years of soil hydrologic conditions (2013-2020). The monitoring system has proved to be reliable for debris flows and debris floods detection and necessary to better understand the rainfall characteristics and the role of hydrologic soil conditions in the triggering of torrential flows.

Analysis of the rainfall characteristics shows that debris flows and debris floods are mainly triggered in summer (between June and August) by short duration (<3 hours) and high intensity (4-10 mm in 5 minutes duration corresponding to 48-120 mm/h) rainfalls and between 12:00 and 18:00 UTC. In contrast, rainfalls lasting more than 10 hours, characterized by low intensities, did not trigger any torrential flow. These outcomes highlight the influence of rainfall duration and intensity on torrential flows initiation and supports the hypothesis that antecedent rainfall and/or snowmelt, and thus hydrologic soil conditions, may affect the triggering of torrential flows in the Rebaixader catchment.

The monitoring of soil hydrologic conditions was performed by means of volumetric water content (VWC) and suction observations close to the initiation area of the torrential flows. The recordings show that the complete saturation of the sediment debris layer is not a required condition for torrential flow initiation. In addition, the hydrologic soil conditions prior to the start of a triggering rainfall range from initially dry conditions, (corresponding to VWC ≈ 0.10 and suction ≈ 1000 kPa) to initially wet conditions (corresponding to VWC ≈ 0.34 m3/m3 and suction ≈ 0 kPa). Another interesting point is the fact that the three largest debris flow events, with a mobilized volume greater than 9000 m^3, started from initially medium to high VWCs at all monitored depths (between 0.18 and 0.30 m^3/m^3). Furthermore, these debris flows were not triggered by the heaviest rainfalls in terms of total precipitation or intensity. These results suggest that both rainfall and soil moisture affect torrential flows initiation in the Rebaixader catchment.

Analysis of rainfall triggering characteristics and soil hydrologic conditions shows that, generally, higher rainfall intensities are required for torrential flow initiation when the soil is in an initially rather dry condition. Contrarily, lower triggering rainfall intensities are necessary with initially wetter conditions. In addition, higher VWC increments were observed when the soil was dryer at the start of a rainfall, and vice versa. These results support the hypothesis that both rainfall characteristics and soil hydrologic conditions affect torrential flows initiation in the Rebaixader catchment.

This work further evaluated the implications of rainfall and VWC measurements in the definition of only-rainfall and hydrometeorological thresholds for torrential flows prediction. Thresholds for torrential flow initiation are common tools in LEWSs hazard assessment. The performance of rainfall and hydrometeorological thresholds has been evaluated in terms of predictive capability by means of ROC and Precision-Recall curves analysis. For this purpose, the 2013-2020 dataset has been considered, which includes 15 torrential flows and long-term time series of both rainfall and soil hydrologic conditions,. The following conclusions were obtained:

First, the traditional I_{mean}-D rainfall threshold shows a poor performance: despite correctly identifying 13 torrential flows as true positives (and thus predicting 2 false negatives), it predicts a high number of false positives (73 in total). Hence, the issued alarms

of the I_{mean}-D rainfall threshold have a precision of 15.1%, which is low and may induce people to ignore the alarms on an operational LEWS.

Second, when considering maximum rainfall intensities (I_{max}) thresholds for different time intervals between 5 and 60 minutes, the performance increases with respect to the I_{mean}-D rainfall threshold. Consequently, the best I_{max} rainfall threshold is defined by a time interval of 20 minutes (I_{max_20min}) and predicts also 2 false negatives, but only 11 false positives, increasing the threshold precision to 54.2%. The I_{max_20min} rainfall threshold is characterized by the exceedance of 32 mm/h in 20 minutes duration. This confirms that rainfall intensities during a short time interval better represent the triggering rainfall intensities in the Rebaixader torrent as they account for rainfall intensity variations or rainfall bursts. In view of these results, maximum rainfall intensities should be considered instead of average rainfall intensity for the development of thresholds for torrential flows prediction in the Rebaixader catchment.

Third, the VWC measurements at 15 and 30 cm depth were combined with maximum rainfall intensities (I_{max}) in order to define the hydro-meteorological thresholds. The best hydro-meteorological threshold predicts 1 false negative and 8 false positives, which increases the precision to 63.6%, and is defined by combining VWC at 30 cm depth and maximum rainfall intensities for 15 minutes duration. Furthermore, increased precision was achieved when combining rainfall maximum intensities and VWC measurements at both 15 and 30 cm depth for the hydro-meteorological thresholds and when compared to rainfall I_{max} thresholds of same duration (5-60 minutes).

These results further confirm that soil hydrologic conditions affect the necessary triggering rainfalls. Furthermore, the results ratify that the monitoring of soil hydrological conditions improve torrential flows predictions in the Rebaixader catchment as moisture conditions preceding a rainfall are considered. The improved precision of hydro-meteorological thresholds endorses the continuous monitoring of rainfall and soil hydrologic conditions to develop and improve new or existing LEWSs for torrential flows prediction.

6.2 Future research work

This work contributed to better understand the effects of soil-vegetation-atmosphere (SVA) interactions on the processes of slope mass-wasting (SMW) at slope and catchment scales. After the development of this thesis there are still some points that remain unsolved and that should be addressed in future research:

Concerning the slope scale in the experimental embankment:

First, a system should be developed and implemented with the aim of measuring rainfall runoff and surficial soil erosion on each of the embankment slopes. More specifically, the effects of slope cover and orientation in terms of rainfall runoff and surficial erosion rates needs to be addressed in future research works. The measurement of runoff and surficial erosion rates are key parameters in the understanding of SMW mechanisms.

Second, the mechanical contribution of roots to soil shear strength is an important parameter on slope stability that has not been considered in this work. Therefore, laboratory experiments should be done in order to characterize root mechanical reinforcement and its effects on slope stability. The effects of root-reinforcement on soil mechanical properties should be counterbalanced in future research by others effects that jeopardize slope stability as increment of infiltration due to macropores created during root in-depth growth.

Third, future research work should assess the effects of decaying vegetation on slope hydro-mechanical response. Decaying roots are known to shrink and increase soil hydraulic conductivity, and thus increase rainfall infiltration and reduce slope stability. This task should be addressed in order to justify the importance of a correct and continuous vegetation maintenance or the selection of vegetation species adapted to the onsite climatic actions.

Forth, simulation of the embankment thermo-hydro-mechanical slope response on bare and vegetated slopes by means of FEM (e.g. Code_Bright) or DEM analysis should be carried out to contribute to the validation of SVA models and thermo-hydro-mechanical constitutive models. These models should include roots induced effects on soil strength and hydrologic soil properties. The calibration and validation of numerical models are an important task in views of application to other slopes subjected to climatic actions and SMW

processes. Such models when correctly calibrated allow simulating the thermo-hydro-mechanic response of slopes to climatic actions, and thus, may help to prevent soil losses or reduce the hazards of SMW. Therefore, the monitoring and gathering of atmospheric and soil hydrological and thermal parameters should be continued in future.

Concerning the catchment scale in the Rebaixader torrent:

First, future research should focus on the different causes for torrential flows initiation, and thus not only considering rainfall as triggering factor. More specifically, the effects of snowmelt on soil hydrologic conditions and on rainfall triggering characteristics should be addressed, as lower triggering rainfall intensities are expected. The effect of snowmelt may be considered by means of the definition of two different thresholds for periods with or without snowmelt affectation, especially for the rainfall-based thresholds where soil hydrologic conditions are not taken into account.

Second, the monitoring and gathering of soil hydrologic conditions and rainfall, as well as the characterization of the detected torrential flows (flow depth, volume, velocity, etc.), should be continued in future. This, on one hand, will allow the validation of thresholds (rainfall and hydrometeorological) developed during this thesis for the detection and prediction of future torrential flows events. A larger inventory of debris flows and debris floods, as well as rainfall and soil hydrologic conditions, will probably improve the characterization of both triggering rainfall and soil moisture conditions. Furthermore, future research steps should consider forecasted rainfalls as thresholds input values. Such methodology would increase the reaction time between the prediction and the triggering time of these hazardous flows. On the other hand, more monitored data may serve to relate the triggering rainfall and soil hydrologic conditions with other torrential flows characteristics, such as mobilized volume or flow depth. Since a complete dataset is only available for 15 torrential flows events, including soil hydrologic conditions and rainfall, additional data are necessary to relate such conditions with torrential flows characteristics.

Third, the methodology developed during this work for torrential flows prediction by means of rainfall and hydro-meteorological thresholds should be tested in other catchments prone to torrential activity. Therefore, rainfall maximum intensities thresholds should be

compared with the most frequently used mean rainfall intensity-duration (I_{mean}-D) threshold, and combined with hydrologic soil measurements when possible. For this purpose, it is necessary to dispose of long-term observations of both rainfall, soil hydrologic conditions and torrential flow occurrence.

Forth, numerical models should be applied to improve our knowledge on rainfall-infiltration-runoff processes and their effects in the triggering of torrential flows in the Rebaixader catchment. In this sense, physical-based models should be used to check or verify the previous defined rainfall and hydro-meteorological thresholds.

These different lines of research would provide further insights in the search to promote the adoption of vegetation as a sustainable, non-structural, and environmental-friendly mitigation strategy to prevent soil losses and SMW phenomena. They are also expected to give important hints for the correct maintenance of existing vegetated slopes and orient reforestation tasks in deep mountainous slopes.

REFERENCES

Abancó, C., Hürlimann, M., Fritschi, B., Graf, C., & Moya, J. (2012). Transformation of Ground Vibration Signal for Debris-Flow Monitoring and Detection in Alarm Systems. *Sensors*, *12*(4), 4870–4891.

Abancó, C., Hürlimann, M., & Moya, J. (2014). Analysis of the ground vibration generated by debris flows and other torrential processes at the Rebaixader monitoring site (Central Pyrenees, Spain). *Natural Hazards and Earth System Sciences*, *14*(4), 929–943. https://doi.org/10.5194/nhess-14-929-2014

Abancó, C., Hürlimann, M., Moya, J., & Berenguer, M. (2016). Critical rainfall conditions for the initiation of torrential flows. Results from the Rebaixader catchment (Central Pyrenees). *Journal of Hydrology*, *541*, 218–229. https://doi.org/10.1016/j.jhydrol.2016.01.019

Alcoverro, J., Corominas, J., & Gómez, M. (1999). The Barranco de Arás flood of 7 August 1996 (Biescas, Central Pyrenees, Spain). *Engineering Geology*, *51*(4), 237–255. https://doi.org/10.1016/S0013-7952(98)00076-3

Ali, F. H., & Osman, N. (2008). Shear Strength of a Soil Containing Vegetation Roots. *Soils and Foundations*, *48*(4), 587–596. https://doi.org/10.3208/sandf.48.587

Alonso, E., Gens, A., & Josa, A. (1990). A constitutive model for partially saturated soils. *Géotechnique*, *40*(3), 405–430. https://doi.org/10.1680/geot.1990.40.3.405

Alonso, E., Lloret, A., & Romero, E. (1999). Rainfall induced deformations of road embackments. *Rivista Italiana Di Geotecnica*, *33*(1), 8–15.

Alonso, E., Pinyol, N., & Puzrin, A. (2010). Catastrophic Slide: Vaiont Landslide, Italy. In *Geomechanics of Failures. Advanced Topics* (Issue October 2014, pp. 33–81). Springer Netherlands. https://doi.org/10.1007/978-90-481-3538-7_2

Arattano, M., & Marchi, L. (2008). Systems and Sensors for Debris-flow Monitoring and Warning. *Sensors*, *8*(4), 2436–2452. https://doi.org/10.3390/s8042436

Arisawa, T., & Suzuki, Y. (2013). Debris Flow in the Kitamatasawa Tributary of the Namekawa River in the Kiso River System. *International Journal of Erosion Control Engineering*, *6*(1), 13–22. https://doi.org/10.13101/ijece.6.13

Askarinejad, A., Akca, D., & Springman, S. M. (2018). Precursors of instability in a natural slope due to rainfall: a full-scale experiment. *Landslides*, *15*(9), 1745–1759. https://doi.org/10.1007/s10346-018-0994-0

ASTM International. (2011). *D3080 / D3080M - 11: Standard Test Method for Direct Shear Test of Soils Under Consolidated Drained Conditions*. www.astm.org

ASTM International. (2014). *D854 - 14: Standard Test Methods for Specific Gravity of Soil Solids by Water Pycnometer*. www.astm.org

ASTM International. (2017a). *D4318 - 17e1: Standard Test Methods for Liquid Limit, Plastic Limit, and Plasticity Index of Soils*. www.astm.org

ASTM International. (2017b). *D6913 / D6913M - 17: Standard Test Methods for Particle-Size Distribution (Gradation) of Soils Using Sieve Analysis*. www.astm.org

ASTM International. (2017c). *D7928 - 17: Standard Test Method for Particle-Size Distribution (Gradation) of Fine-Grained Soils Using the Sedimentation (Hydrometer) Analysis*. www.astm.org

ASTM International. (2018). *D7263 - 09(2018)e1 : Standard Test Methods for Laboratory Determination of Density (Unit Weight) of Soil Specimens*. www.astm.org

Bacon, C. W. (1993). Abiotic stress tolerances (moisture, nutrients) and photosynthesis in endophyte-infected tall fescue. *Agriculture, Ecosystems & Environment*, *44*(1–4), 123–141. https://doi.org/10.1016/0167-8809(93)90042-N

Badoux, A., Graf, C., Rhyner, J., Kuntner, R., & McArdell, B. W. (2009). A debris-flow alarm system for the Alpine Illgraben catchment: design and performance. *Natural Hazards*, *49*(3), 517–539. https://doi.org/10.1007/s11069-008-9303-x

Barnes, L. R., Gruntfest, E. C., Hayden, M. H., Schultz, D. M., & Benight, C. (2007). False Alarms and Close Calls: A Conceptual Model of Warning Accuracy. *Weather and Forecasting*, *22*(5), 1140–1147. https://doi.org/10.1175/WAF1031.1

Bel, C., Liébault, F., Navratil, O., Eckert, N., Bellot, H., Fontaine, F., & Laigle, D. (2017). Rainfall control of debris-flow triggering in the Réal Torrent, Southern French Prealps. *Geomorphology*, *291*, 17–32. https://doi.org/10.1016/j.geomorph.2016.04.004

Berger, C., McArdell, B. W., & Schlunegger, F. (2011). Sediment transfer patterns at the Illgraben catchment, Switzerland: Implications for the time scales of debris flow activities. *Geomorphology*, *125*(3), 421–432. https://doi.org/10.1016/j.geomorph.2010.10.019

Bernard, M. (2018). *Analysis and modelling of surface runoff triggering debris flows*. PhD thesis, Università degli Studi di Padova, Padua, Italy, 130 p. http://paduaresearch.cab.unipd.it/10682/

Berti, M., Genevois, R., LaHusen, R., Simoni, A., & Tecca, P. R. (2000). Debris flow monitoring in the acquabona watershed on the Dolomites (Italian alps). *Physics and Chemistry of the Earth, Part B: Hydrology, Oceans and Atmosphere*, *25*(9), 707–715. https://doi.org/10.1016/S1464-1909(00)00090-3

Berti, M., & Simoni, A. (2005). Experimental evidences and numerical modelling of debris flow initiated by channel runoff. *Landslides*, *2*(3), 171–182.

Bessason, B., Eiríksson, G., Thorarinsson, Ó., Thórarinsson, A., & Einarsson, S. (2007). Automatic detection of avalanches and debris flows by seismic methods. *Journal of Glaciology*, *53*(182), 461–472. https://doi.org/10.3189/002214307783258468

Bicalho, K. V., Boussafir, Y., & Cui, Y.-J. (2018). Performance of an instrumented embankment constructed with lime-treated silty clay during four-years in the Northeast of France. *Transportation Geotechnics*, *17*(April), 100–116. https://doi.org/10.1016/j.trgeo.2018.09.009

Bishop, A. W. (1959). The principle of effective stress. *Teknisk Ukeblad*, *106*(39), 859–863.

Bittelli, M., Valentino, R., Salvatorelli, F., & Rossi Pisa, P. (2012). Monitoring soil-water and displacement conditions leading to landslide occurrence in partially saturated clays. *Geomorphology*, *173–174*, 161–173. https://doi.org/10.1016/j.geomorph.2012.06.006

Blight, G. E. (1997). The Rankine Lecture: Interactions between the atmosphere and the Earth. *Géotechnique*, *47*(4), 713–767. https://doi.org/10.1680/geot.1997.47.4.713

Boardman, J., & Poesen, J. (2006). *Soil Erosion in Europe* (J. Boardman & J. Poesen (Eds.)). John Wiley & Sons, Ltd. https://doi.org/10.1002/0470859202

Bochet, E., Poesen, J., & Rubio, J. L. (2006). Runoff and soil loss under individual plants of a semi-arid Mediterranean shrubland: influence of plant morphology and rainfall intensity. *Earth Surface Processes and Landforms*, *31*(5), 536–549. https://doi.org/10.1002/esp.1351

Bogaard, T. A., & Greco, R. (2016). Landslide hydrology: from hydrology to pore pressure. *Wiley Interdisciplinary Reviews: Water*, *3*(3), 439–459. https://doi.org/10.1002/wat2.1126

Bogaard, T. A., & Greco, R. (2018). Invited perspectives: Hydrological perspectives on precipitation intensity-duration thresholds for landslide initiation: proposing hydro-meteorological thresholds. *Natural Hazards and Earth System Sciences*, *18*(1), 31–39. https://doi.org/10.5194/nhess-18-31-2018

Bogaard, T. A., & van Asch, T. W. J. (2002). The role of the soil moisture balance in the unsaturated zone on movement and stability of the Beline landslide, France. *Earth Surface Processes and Landforms*, *27*(11), 1177–1188. https://doi.org/10.1002/esp.419

Bordoni, M., Meisina, C., Valentino, R., Lu, N., Bittelli, M., & Chersich, S. (2015). Hydrological factors affecting rainfall-induced shallow landslides: From the field monitoring to a simplified slope stability analysis. *Engineering Geology*, *193*, 19–37. https://doi.org/10.1016/j.enggeo.2015.04.006

Brayshaw, D., & Hassan, M. A. (2009). Debris flow initiation and sediment recharge in gullies. *Geomorphology*, *109*(3–4), 122–131. https://doi.org/10.1016/j.geomorph.2009.02.021

Briggs, K. M., Loveridge, F. A., & Glendinning, S. (2017). Failures in transport infrastructure embankments. *Engineering Geology*, *219*, 107–117. https://doi.org/10.1016/j.enggeo.2016.07.016

Brocca, L., Melone, F., & Moramarco, T. (2008). On the estimation of antecedent wetness conditions in rainfall–runoff modelling. *Hydrological Processes*, *22*(5), 629–642. https://doi.org/10.1002/hyp.6629

Brunetti, M. T., Melillo, M., Peruccacci, S., Ciabatta, L., & Brocca, L. (2018). How far are we from the use of satellite rainfall products in landslide forecasting? *Remote Sensing of Environment*, *210*(March), 65–75. https://doi.org/10.1016/j.rse.2018.03.016

Caine, N. (1980). The rainfall intensity-duration control of shallow landslides and debris flows. *Geografiska Annaler*, *62A*, 23–27. http://links.jstor.org/sici?sici=0435-3676(1980)62:1/2%3C23:TRIDCO%3E2.0.CO;2-H

Capilleri, P. P., Motta, E., & Raciti, E. (2016). Experimental Study on Native Plant Root Tensile Strength for Slope Stabilization. *Procedia Engineering*, *158*, 116–121. https://doi.org/10.1016/j.proeng.2016.08.415

Casermeiro, M. A., Molina, J. A., de la Cruz Caravaca, M. T., Hernando Costa, J., Hernando Massanet, M. I., & Moreno, P. S. (2004). Influence of scrubs on runoff and sediment loss in soils of Mediterranean climate. *CATENA*, *57*(1), 91–107. https://doi.org/10.1016/S0341-8162(03)00160-7

Cassiani, G., Boaga, J., Rossi, M., Putti, M., Fadda, G., Majone, B., & Bellin, A. (2016). Soil–plant interaction monitoring: Small scale example of an apple orchard in Trentino, North-Eastern Italy. *Science of The Total Environment*, *543*, 851–861. https://doi.org/10.1016/j.scitotenv.2015.03.113

Chen, F., Zhang, J., Zhang, M., & Wang, J. (2015). Effect of Cynodon dactylon community on the conservation and reinforcement of riparian shallow soil in the Three Gorges Reservoir area. *Ecological Processes*, *4*(1), 3. https://doi.org/10.1186/s13717-014-0029-2

Chen, J., Chen, X., Zhao, W., & You, Y. (2019). Debris-flow mitigation measures and an

application case in a small-scale watershed in China. *Debris-Flow Hazards Mitigation: Mechanics, Monitoring, Modeling, and Assessment - Proceedings of the 7th International Conference on Debris-Flow Hazards Mitigation*, *2014*, 928–935. https://doi.org/10.25676/11124/173125

Chleborad, A. F., Baum, R. L., Godt, J. W., & Powers, P. S. (2008). A prototype system for forecasting landslides in the Seattle, Washington, area. In *Landslides and Engineering Geology of the Seattle, Washington, Area*. Geological Society of America. https://doi.org/10.1130/2008.4020(06)

Chok, Y. H., Jaksa, M. B., Kaggwa, W. S., & Griffiths, D. V. (2015). Assessing the influence of root reinforcement on slope stability by finite elements. *International Journal of Geo-Engineering*, *6*(1), 12. https://doi.org/10.1186/s40703-015-0012-5

Church, M., & Miles, M. J. (1987). *Meteorological antecedents to debris flow in southwestern British Columbia; Some case studies* (pp. 63–80). https://doi.org/10.1130/REG7-p63

Cleveland, W. S. (1979). Robust Locally Weighted Regression and Smoothing Scatterplots. *Journal of the American Statistical Association*, *74*(368), 829–836. https://doi.org/10.1080/01621459.1979.10481038

Coe, J. A., Godt, J. W., Parise, M., & Moscariello., A. (2003). Estimating debris-flow probability using fan stratigraphy, historic records, and drainage-basin morphology, Interstate 70 highway corridor, central Colorado, U.S.A. In D. Rickenmann & C. Chen (Eds.), *3rd International Conference on Debris-Flow Hazards Mitigation: Mechanics, Prediction, and Assessment* (pp. 1085–1096). Millpress.

Coe, J. A., Kean, J. W., McCoy, S. W., Staley, D. M., & Wasklewicz, T. A. (2010). Chalk Creek Valley: Colorado's natural debris-flow laboratory. In L. A. Morgan & S. L. Quane (Eds.), *Through the Generations: Geologic and Anthropogenic Field Excursions in the Rocky Mountains from Modern to Ancient: Geological Society of America Field Guide 18* (pp. 95–117). The Geological Society of America. https://doi.org/10.1130/2010.0018(05)

Coe, J. A., Kinner, D. A., & Godt, J. W. (2008). Initiation conditions for debris flows generated by runoff at Chalk Cliffs, central Colorado. *Geomorphology*, *96*(3–4), 270–297. https://doi.org/10.1016/j.geomorph.2007.03.017

Comiti, F., Marchi, L., Macconi, P., Arattano, M., Bertoldi, G., Borga, M., Brardinoni, F., Cavalli, M., D'Agostino, V., Penna, D., & Theule, J. (2014). A new monitoring station for debris flows in the European Alps: first observations in the Gadria basin. *Natural Hazards*, *73*(3), 1175–1198. https://doi.org/10.1007/s11069-014-1088-5

Cooper, M. R., Bromhead, E. N., Petley, D. J., & Grants, D. I. (1998). The Selborne cutting stability experiment. *Géotechnique*, *48*(1), 83–101. https://doi.org/10.1680/geot.1998.48.1.83

Coppin, N. J., & Richards, I. G. (1990). *Use of Vegetation in Civil Engineering* (N. J. Coppin & I. G. Richards (Eds.)). Construction Industry Research and Information Association (CIRIA). https://www.grad.unizg.hr/_download/repository/CIRIA_2007.pdf

Corominas, J. (2000). Landslides and climate. In Bromhead E, Dixon N, & M. Ibsen (Eds.), *8th International Symposium on Landslides* (pp. 1–33). A.A. Balkema.

Corominas, J., & Moya, J. (1999). Reconstructing recent landslide activity in relation to rainfall in the Llobregat River basin, Eastern Pyrenees, Spain. *Geomorphology*, *30*(1–2), 79–93. https://doi.org/10.1016/S0169-555X(99)00046-X

Cotecchia, F., Pedone, G., Bottiglieri, O., Santaloia, F., & Vitone, C. (2014). Slope-atmosphere interaction in a tectonized clayey slope: A case study. *Rivista Italiana Di Geotecnica*, *48*(1), 34–61.

Coviello, V., Arattano, M., & Turconi, L. (2015). Detecting torrential processes from a distance with a seismic monitoring network. *Natural Hazards*, *78*(3), 2055–2080. https://doi.org/10.1007/s11069-015-1819-2

Coyle, D. R., Nagendra, U. J., Taylor, M. K., Campbell, J. H., Cunard, C. E., Joslin, A. H., Mundepi, A., Phillips, C. A., & Callaham, M. A. (2017). Soil fauna responses to natural disturbances, invasive species, and global climate change: Current state of the science and a call to action. *Soil Biology and Biochemistry*, *110*(October), 116–133.

https://doi.org/10.1016/j.soilbio.2017.03.008

Crosta, G., & Frattini, P. (2001). Rainfall thresholds for triggering soil slips and debris flow. *2nd Plinius Conference, Mediterranean Storms*, 463–488.

Cui, P., Chen, X., Waqng, Y., Hu, K., & Li, Y. (2005). Jiangjia Ravine debris flows in south-western China. In M. Jakob & O. Hungr (Eds.), *Debris-flow Hazards and Related Phenomena* (pp. 565–594). Springer Berlin Heidelberg. https://doi.org/10.1007/3-540-27129-5_22

Cui, Y. J., Gao, Y. B., & Ferber, V. (2010). Simulating the water content and temperature changes in an experimental embankment using meteorological data. *Engineering Geology*, *114*(3–4), 456–471. https://doi.org/10.1016/j.enggeo.2010.06.006

Cui, Y. J., Lu, Y. F., Delage, P., & Riffard, M. (2005). Field simulation of in situ water content and temperature changes due to ground–atmospheric interactions. *Géotechnique*, *55*(7), 557–567. https://doi.org/10.1680/geot.2005.55.7.557

D'Odorico, P. (2005). Potential for landsliding: Dependence on hyetograph characteristics. *Journal of Geophysical Research*, *110*(F1). https://doi.org/10.1029/2004JF000127

Damiano, E., Olivares, L., & Picarelli, L. (2012). Steep-slope monitoring in unsaturated pyroclastic soils. *Engineering Geology*, *137–138*, 1–12. https://doi.org/10.1016/j.enggeo.2012.03.002

Day, S. R., & Daniel, D. E. (1985). Hydraulic Conductivity of Two Prototype Clay Liners. *Journal of Geotechnical Engineering*, *111*(8), 957–970. https://doi.org/10.1061/(ASCE)0733-9410(1985)111:8(957)

De Baets, S., Poesen, J., Reubens, B., Wemans, K., De Baerdemaeker, J., & Muys, B. (2008). Root tensile strength and root distribution of typical Mediterranean plant species and their contribution to soil shear strength. *Plant and Soil*, *305*(1–2), 207–226. https://doi.org/10.1007/s11104-008-9553-0

Decagon Devices. (2016). *MPS-2 & MPS-6 Dielectric Water Potential Sensor Operator's Manual (accessed on 16 December 2020)*. www.decagon.com

Deganutti, A. M., Marchi, L., & Arattano, M. (2000). Rainfall and debris-flow occurrence in the Moscardo basin (Italian Alps). In G. F. Wieczorek & N. D. Naeser (Eds.), *2nd International Conference on Debris-Flow Hazards Mitigation* (pp. 67–72). Balkema.

Donald H. Gray, R. B. S. (1996). *Biotechnical and Soil Bioengineering Slope Stabilization: A practical guide for erosion control*. John Wiley & Sons.

Drabo, A. (2017). Climate change mitigation and agricultural development models: Primary commodity exports or local consumption production? *Ecological Economics*, *137*, 110–125. https://doi.org/10.1016/j.ecolecon.2017.03.014

Duong, T. (2001). An Introduction to Kernel Density Estimation. *Weatherburn Lecture Series for the Department of Mathematics and Statistics, at the University of Western Australia*, 1–4.

Durán Zuazo, V. H., & Rodríguez Pleguezuelo, C. R. (2008). Soil-erosion and runoff prevention by plant covers. A review. *Agronomy for Sustainable Development*, *28*(1), 65–86. https://doi.org/10.1051/agro:2007062

Dyer, M., Utili, S., & Zielinski, M. (2009). Field survey of desiccation fissuring of flood embankments. *Proceedings of the Institution of Civil Engineers - Water Management*, *162*(3), 221–232. https://doi.org/10.1680/wama.2009.162.3.221

Eab, K. H., Likitlersuang, S., & Takahashi, A. (2015). Laboratory and modelling investigation of root-reinforced system for slope stabilisation. *Soils and Foundations*, *55*(5), 1270–1281. https://doi.org/10.1016/j.sandf.2015.09.025

Elia, G., Cotecchia, F., Pedone, G., Vaunat, J., Vardon, P. J., Pereira, C., Springman, S. M., Rouainia, M., Van Esch, J., Koda, E., Josifovski, J., Nocilla, A., Askarinejad, A., Stirling, R., Helm, P., Lollino, P., & Osinski, P. (2017). Numerical modelling of slope–vegetation–atmosphere interaction: an overview. *Quarterly Journal of Engineering Geology and Hydrogeology*, *50*(3), 249–270. https://doi.org/10.1144/qjegh2016-079

Elmi, A. A., & West, C. P. (1995). Endophyte infection effects on stomatal conductance, osmotic adjustment and drought recovery of tall fescue. *New Phytologist*, *131*(1), 61–67. https://doi.org/10.1111/j.1469-8137.1995.tb03055.x

Enrique, G., Braud, I., Jean-Louis, T., Michel, V., Pierre, B., & Jean-Christophe, C. (1999). Modelling heat and water exchanges of fallow land covered with plant-residue mulch. *Agricultural and Forest Meteorology*, *97*(3), 151–169. https://doi.org/10.1016/S0168-1923(99)00081-7

Evelpidou, N. (2012). Runoff erosion - The mechanisms. In N. Evelpidou, S. Cordier, A. Merino, T. Figuireido, & C. Centeri (Eds.), *(e-book)*.

Eyles, R. J. (1979). Slip-triggering rainfalls in Wellington City, New Zealand. *New Zealand Journal of Science*, *22*(2), 117–121.

Fawcett, T. (2006). An introduction to ROC analysis. *Pattern Recognition Letters*, *27*(8), 861–874. https://doi.org/10.1016/j.patrec.2005.10.010

Florides, G., & Kalogirou, S. (2004). Measurements of Ground Temperature at Various Depths. *Proceedings of the SET 2004, 3rd International Conference on Sustainable Energy Technologies*, 1–6. http://ktisis.cut.ac.cy/bitstream/10488/870/3/C55-PRT020-SET3.pdf

Fourie, A. B., Rowe, D., & Blight, G. E. (1999). The effect of infiltration on the stability of the slopes of a dry ash dump. *Géotechnique*, *49*(1), 1–13. https://doi.org/10.1680/geot.1999.49.1.1

Fraccica, A., Romero, E., & Fourcaud, T. (2019). Multi-scale effects on the hydraulic behaviour of a root-permeated and compacted soil. *E3S Web of Conferences*, *92*, 12014. https://doi.org/10.1051/e3sconf/20199212014

Fredlund, D. G., Morgenstern, N. R., & Widger, R. A. (1978). The shear strength of unsaturated soils. *Canadian Geotechnical Journal*, *15*(3), 313–321. https://doi.org/10.1139/t78-029

Fredlund, D. G., & Rahardjo, H. (1993). *Soil Mechanics for Unsaturated Soils*. John Wiley & Sons, Inc. https://doi.org/10.1002/9780470172759

Fredlund, D. G., Xing, A., Fredlund, M. D., & Barbour, S. L. (1996). The relationship of the unsaturated soil shear strength to the soil-water characteristic curve. *Canadian*

Geotechnical Journal, *33*(3), 440–448. https://doi.org/10.1139/t96-065

Froude, M. J., & Petley, D. N. (2018). Global fatal landslide occurrence from 2004 to 2016. *Natural Hazards and Earth System Sciences*, *18*(8), 2161–2181. https://doi.org/10.5194/nhess-18-2161-2018

Gabarrón-Galeote, M. A., Ruiz-Sinoga, J. D., & Quesada, M. A. (2013). Influence of aspect in soil and vegetation water dynamics in dry Mediterranean conditions: functional adjustment of evergreen and semi-deciduous growth forms. *Ecohydrology*, *6*(2), 241–255. https://doi.org/10.1002/eco.1262

Gallart, F., & Clotet, N. (1988). Some aspects of the geomorphic processes triggered by an extreme rainfall event: The November 1982 flood in The Eastern Pyrenees. *Catena Supplement*, *13*, 79–95.

Garg, A., Coo, J. L., & Ng, C. W. W. (2015). Field study on influence of root characteristics on soil suction distribution in slopes vegetated with Cynodon dactylon and Schefflera heptaphylla. *Earth Surface Processes and Landforms*, *40*(12), 1631–1643. https://doi.org/10.1002/esp.3743

Garg, A., Leung, A. K., & Ng, C. W. W. (2015). Comparisons of soil suction induced by evapotranspiration and transpiration of S. heptaphylla . *Canadian Geotechnical Journal*, *52*(12), 2149–2155. https://doi.org/10.1139/cgj-2014-0425

Gariano, S. L., & Guzzetti, F. (2016). Landslides in a changing climate. *Earth-Science Reviews*, *162*, 227–252. https://doi.org/10.1016/j.earscirev.2016.08.011

Genevois, R., Tecca, P. R., Berti, M., & Simoni, A. (2000). *Debris-flow in the Dolomites: Experimental data from a monitoring system*.

Gens, A. (2010). Soil–environment interactions in geotechnical engineering. *Géotechnique*, *60*(1), 3–74. https://doi.org/10.1680/geot.9.P.109

Germann, U., Galli, G., Boscacci, M., & Bolliger, M. (2006). Radar precipitation measurement in a mountainous region. *Quarterly Journal of the Royal Meteorological Society*, *132*(618), 1669–1692. https://doi.org/10.1256/qj.05.190

Glade, T., Crozier, M., & Smith, P. (2000). Applying probability determination to refine landslide-triggering rainfall thresholds using an empirical "Antecedent Daily Rainfall Model." *Pure and Applied Geophysics*, *157*(6–8), 1059–1079. https://doi.org/10.1007/s000240050017

Glade, T., & Nadim, F. (2014). Early warning systems for natural hazards and risks. *Natural Hazards*, *70*(3), 1669–1671. https://doi.org/10.1007/s11069-013-1000-8

Glendinning, S., Hughes, P., Helm, P., Chambers, J., Mendes, J., Gunn, D., Wilkinson, P., & Uhlemann, S. (2014). Construction, management and maintenance of embankments used for road and rail infrastructure: implications of weather induced pore water pressures. *Acta Geotechnica*, *9*(5), 799–816. https://doi.org/10.1007/s11440-014-0324-1

Godt, J. W., Baum, R. L., & Chleborad, A. F. (2006). Rainfall characteristics for shallow landsliding in Seattle, Washington, USA. *Earth Surface Processes and Landforms*, *31*(1), 97–110. https://doi.org/10.1002/esp.1237

Godt, J. W., & Coe, J. A. (2007). Alpine debris flows triggered by a 28 July 1999 thunderstorm in the central Front Range, Colorado. *Geomorphology*, *84*(1â€“2), 80–97. http://www.sciencedirect.com/science/article/pii/S0169555X06002868

Gofar, N., & Rahardjo, H. (2017). Saturated and unsaturated stability analysis of slope subjected to rainfall infiltration. *MATEC Web of Conferences*, *101*, 05004. https://doi.org/10.1051/matecconf/201710105004

Gonzalez-Ollauri, A., & Mickovski, S. B. (2017). Hydrological effect of vegetation against rainfall-induced landslides. *Journal of Hydrology*, *549*, 374–387. https://doi.org/10.1016/j.jhydrol.2017.04.014

Govi, M., & Sorzana, P. F. (1980). Landslide susceptibility as a function of critical rainfall amount in Piedmont Basin (North-Western Italy). *Studia Geomorphologica Carpatho-Balcanica, Krakow*, *14*, 43–61.

Goyal, R. K. (2004). Sensitivity of evapotranspiration to global warming: a case study of arid zone of Rajasthan (India). *Agricultural Water Management*, *69*(1), 1–11.

https://doi.org/10.1016/j.agwat.2004.03.014

Gray, D., & Barker, D. (2004). Root-soil mechanics and interactions. In S. J. Bennett & A. Simon (Eds.), *Riparian Vegetation and Fluvial Geomorphology* (pp. 113–123). American Geophysical Union. https://doi.org/10.1029/008WSA09

Gray, D., & Norum, D. (1967). The Effect of Soil Moisture on Infiltration As Related To Runoff and Recharge. *Proceedings of Hydrology Symposium*, *6*, 133–153. http://www.usask.ca/hydrology/papers/Gray_Norum_1967.pdf

Greenway, D. R. (1987). Vegetation and Slope Stability. In M. G. Anderson & K. S. Richards (Eds.), *Slope Stability: Geotechnical Engineering and Geomorphology* (pp. 187–230). John Wiley & Sons.

Greenwood, J. R., Norris, J. E., & Wint, J. (2004). Assessing the contribution of vegetation to slope stability. *Geotechnical Engineering*, *157*(4), 199–207. https://doi.org/10.1680/geng.157.4.199.51832

Gregoretti, C. (2012). *Monitoring of debris flows in the testbed Fiames Valley*. PARAmount Final Conference. http://www.paramount-project.eu

Gregoretti, C., Degetto, M., Bernard, M., Crucil, G., Pimazzoni, A., De Vido, G., Berti, M., Simoni, A., & Lanzoni, S. (2016). Runoff of small rocky headwater catchments: Field observations and hydrological modeling. *Water Resources Research*, *52*(10), 8138–8158. https://doi.org/10.1002/2016WR018675

Gregoretti, C., & Fontana, G. D. (2008). The triggering of debris flow due to channel-bed failure in some alpine headwater basins of the Dolomites: analyses of critical runoff. *Hydrological Processes*, *22*(13), 2248–2263. https://doi.org/10.1002/hyp.6821

Gregoretti, C., & Fontana, G. D. (2007). Rainfall threshold for the initiation of debris flows by channel bed failure of the Dolomites. *Debris-Flow Hazards Mitigation: Mechanics, Prediction and Assessment*, 11–21.

Guswa, A. J. (2010). Effect of plant uptake strategy on the water-optimal root depth. *Water Resources Research*, *46*(9), 1–5. https://doi.org/10.1029/2010WR009122

Guzzetti, F., Cardinali, M., Reichenbach, P., Cipolla, F., Sebastiani, C., Galli, M., & Salvati, P. (2004). Landslides triggered by the 23 November 2000 rainfall event in the Imperia Province, Western Liguria, Italy. *Engineering Geology*, *73*(3–4), 229–245. https://doi.org/10.1016/j.enggeo.2004.01.006

Guzzetti, F., Peruccacci, S., Rossi, M., & Stark, C. P. (2007). Rainfall thresholds for the initiation of landslides in central and southern Europe. *Meteorology and Atmospheric Physics*, *98*(3–4), 239–267. https://doi.org/10.1007/s00703-007-0262-7

Guzzetti, F., Peruccacci, S., Rossi, M., & Stark, C. P. (2008). The rainfall intensity–duration control of shallow landslides and debris flows: an update. *Landslides*, *5*(1), 3–17. https://doi.org/10.1007/s10346-007-0112-1

Hemmati, S., Gatmiri, B., Cui, Y.-J., & Vincent, M. (2012). Thermo-hydro-mechanical modelling of soil settlements induced by soil-vegetation-atmosphere interactions. *Engineering Geology*, *139–140*, 1–16. https://doi.org/10.1016/j.enggeo.2012.04.003

Highland, L. M., & Bobrowsky, P. (2008). The landslide Handbook - A guide to understanding landslides. In *US Geological Survey Circular* (Issue 1325). U.S. Geological Survey, Circular 1325. https://doi.org/10.3133/cir1325

Hilker, N., Badoux, A., & Hegg, C. (2009). The Swiss flood and landslide damage database 1972–2007. *Natural Hazards and Earth System Sciences*, *9*(3), 913–925. https://doi.org/10.5194/nhess-9-913-2009

Hirschberg, J., Badoux, A., McArdell, B. W., Leonarduzzi, E., & Molnar, P. (2021). Evaluating methods for debris-flow prediction based on rainfall in an Alpine catchment. *Natural Hazards and Earth System Sciences*, *21*(9), 2773–2789. https://doi.org/10.5194/nhess-21-2773-2021

Hong, Y., Wang, J. P., Li, D. Q., Cao, Z. J., Ng, C. W. W., & Cui, P. (2015). Statistical and probabilistic analyses of impact pressure and discharge of debris flow from 139 events during 1961 and 2000 at Jiangjia Ravine, China. *Engineering Geology*, *187*, 122–134. https://doi.org/10.1016/j.enggeo.2014.12.011

Horton, R. E. (1939). Analysis of runoff-plat experiments with varying infiltration-capacity.

Transactions, American Geophysical Union, *20*(4), 693. https://doi.org/10.1029/TR020i004p00693

Horton, R. E. (1940). An Approach Toward a Physical Interpretation of Infiltration-Capacity. *Soil Science Society of America Journal*, *5*(C), 399–417. https://doi.org/10.2136/sssaj1941.036159950005000C0075x

Hovius, N., Stark, C. P., & Allen, P. A. (1997). Sediment flux from a mountain belt derived by landslide mapping. *Geology*, *25*(3), 231. https://doi.org/10.1130/0091-7613(1997)025<0231:SFFAMB>2.3.CO;2

Hua, G. F., Zhao, Z. W., Kong, J., Guo, R., Zeng, Y. T., Zhao, L. F., & Zhu, Q. D. (2014). Effects of plant roots on the hydraulic performance during the clogging process in mesocosm vertical flow constructed wetlands. *Environmental Science and Pollution Research*, *21*(22), 13017–13026. https://doi.org/10.1007/s11356-014-3249-1

Huang, C.-C., & Yuin, S.-C. (2010). Experimental investigation of rainfall criteria for shallow slope failures. *Geomorphology*, *120*(3–4), 326–338. https://doi.org/10.1016/j.geomorph.2010.04.006

Huang, J., Wu, P., & Zhao, X. (2013). Effects of rainfall intensity, underlying surface and slope gradient on soil infiltration under simulated rainfall experiments. *CATENA*, *104*, 93–102. https://doi.org/10.1016/j.catena.2012.10.013

Hübl, J., & Kaitna, R. (2010). Sediment delivery from the Lattenbach catchment by debris floods and debris flows. *Geophysical Research Abstracts , EGU General Assembly 2010*, *12*(2-7 May, Vienna, Austria), 10585.

Hungr, O., Evans, S. G., Bovis, M. J., & Hutchinson, J. N. (2001). A review of the classification of landslides of the flow type. *Environmental and Engineering Geoscience*, *7*(3), 221–238. https://doi.org/10.2113/gseegeosci.7.3.221

Hungr, O., Leroueil, S., & Picarelli, L. (2014). The Varnes classification of landslide types, an update. *Landslides*, *11*(2), 167–194. https://doi.org/10.1007/s10346-013-0436-y

Hungr, O., Morgan, G. C., VanDine, D. F., & Lister, D. R. (1987). Debris flow defenses in

British Columbia. In G. F. W. John E. Costa (Ed.), *Debris Flows/Avalanches: Process, recognition, and mitigation* (pp. 201–222). Reviews in Engineering Geology. https://doi.org/10.1130/REG7-p201

Hur, J., Raghavan, S. V., Nguyen, N. S., & Liong, S.-Y. (2016). Evaluation of High-resolution Satellite Rainfall Data over Singapore. *Procedia Engineering*, *154*, 158–167. https://doi.org/10.1016/j.proeng.2016.07.437

Hürlimann, M., Abancó, C., & Moya, J. (2012). Rockfalls detached from a lateral moraine during spring season. 2010 and 2011 events observed at the Rebaixader debris-flow monitoring site (Central Pyrenees, Spain). *Landslides*, *3*, 385–393. https://doi.org/10.1007/s10346-011-0314-4

Hürlimann, M., Abancó, C., & Moya, J. (2010). Debris-flow initiation affected by snowmelt. Case study of the Senet monitoring site, Eastern Pyrenees. *Mountain Risks International Conference: Bringing Science to Society*, 81–86.

Hürlimann, M., Abancó, C., Moya, J., Raïmat, C., & Luis-Fonseca, R. (2011). Debris-flow monitoring stations in the Eastern Pyrenees. Description of instrumentation, first experiences and preliminary results. In R. Genevois, D. Hamilton, & A. Prestininzi (Eds.), *5th Int. Conf. on Debris-Flow Hazards Mitigation* (pp. 553–562). https://doi.org/10.4408/IJEGE.2011-03.B-061

Hürlimann, M., Abancó, C., Moya, J., & Vilajosana, I. (2014). Results and experiences gathered at the Rebaixader debris-flow monitoring site, Central Pyrenees, Spain. *Landslides*, *11*(6), 939–953. https://doi.org/10.1007/s10346-013-0452-y

Hürlimann, M., Corominas, J., Moya, J., & Copons, R. (2003). Debris-flow events in the Eastern Pyrenees. Preliminary study on initiation and propagation. In D. Rickenmann & C. Chen (Eds.), *3rd Int. Conf. on Debris-Flow Hazards Mitigation* (Vol. 1, pp. 115–126). Millpress.

Hürlimann, M., Coviello, V., Bel, C., Guo, X., Berti, M., Graf, C., Hübl, J., Miyata, S., Smith, J. B., & Yin, H.-Y. (2019). Debris-flow monitoring and warning: Review and examples. *Earth-Science Reviews*, *199*. https://doi.org/10.1016/j.earscirev.2019.102981

Hürlimann, M., Oorthuis, R., Abancó, C., Carleo, L., & Moya, J. (2019). Monitoring of rainfall and soil moisture at the Rebaixader catchment (Central Pyrenees). In J. W. Kean, J. A. Coe, P. M. Santi, & B. K. Guillen (Eds.), *International Conference on Debris-Flow Hazards Mitigation. "Debris-Flow Hazards Mitigation: Mechanics, Monitoring, Modeling, and Assessment: proceedings of the Seventh International Conference on Debris-Flow Hazards Mitigation* (pp. 131–137). Association of Environmental & Engineering Geologists (AEG). https://hdl.handle.net/11124/173227

Hürlimann, M., Rickenmann, D., & Graf, C. (2003). Field and monitoring data of debris-flow events in the Swiss Alps. *Canadian Geotechnical Journal*, *40*(1), 161–175. https://doi.org/10.1139/t02-087

Idso, S. B., Aase, J. K., & Jackson, R. D. (1975). Net radiation — soil heat flux relations as influenced by soil water content variations. *Boundary-Layer Meteorology*, *9*(1), 113–122. https://doi.org/10.1007/BF00232257

Igwe, P. U., Ezeukwu, J. C., Edoka, N. E., Ejie, O. C., & Ifi, G. I. (2017). A Review of Vegetation Cover as a Natural Factor to Soil Erosion. *International Journal of Rural Development, Environment and Health Research*, *1*(4), 21–28. https://doi.org/10.22161/ijreh.1.4.4

Image J software - Image Processing and Analysis in Java. Retrieved October 18, 2021, from https://imagej.nih.gov/ij/

Imaizumi, F., Ikeda, A., Yamamoto, K., & Ohsaka, O. (2021). Temporal changes in the debris flow threshold under the effects of ground freezing and sediment storage on Mt. Fuji. *Earth Surface Dynamics*, *9*(6), 1381–1398. https://doi.org/10.5194/esurf-9-1381-2021

Imaizumi, F., & Sidle, R. C. (2007). Linkage of sediment supply and transport processes in Miyagawa Dam catchment, Japan. *Journal of Geophysical Research*, *112*(F3). https://doi.org/10.1029/2006JF000495

Imaizumi, F., Tsuchiya, S., & Ohsaka, O. (2005). Behaviour of debris flows located in a mountainous torrent on the Ohya landslide, Japan. *Canadian Geotechnical Journal*,

42(3), 919–931. https://doi.org/10.1139/t05-019

Imeson, A. C., & Lavee, H. (1998). Soil erosion and climate change: the transect approach and the influence of scale. *Geomorphology*, *23*(2–4), 219–227. https://doi.org/10.1016/S0169-555X(98)00005-1

INADEF Project: INnovative eArly warning system for DEbris Flow events based on nowcasting and phenomenology. Retrieved October 22, 2021, from https://www.inadef.com/en/casi-studio/rio-rudan/

IPCC. (2014). *Climate Change 2013 – The Physical Science Basis: Working Group I Contribution to the Fifth Assessment Report of the Intergovernmental Panel on Climate Change* (Intergovernmental Panel on Climate Change (Ed.)). Cambridge University Press. https://doi.org/10.1017/CBO9781107415324

Itakura, Y., Inaba, H., & Sawada, T. (2005). A debris-flow monitoring devices and methods bibliography. *Natural Hazards and Earth System Sciences*, *5*(6), 971–977. https://doi.org/10.5194/nhess-5-971-2005

Iverson, R. M. (1997). The physics of debris flows. *Reviews of Geophysics*, *35*(3), 245–296. https://doi.org/10.1029/97RG00426

Iverson, R. M. (2000). Landslide triggering by rain infiltration. *Water Resources Research*, *36*(7), 1897–1910. https://doi.org/10.1029/2000WR900090

Iverson, R. M., Reid, M. E., & LaHusen, R. G. (1997). Debris-flow mobilization from landslides. *Annual Review of Earth and Planetary Sciences*, *25*(1), 85–138. https://doi.org/10.1146/annurev.earth.25.1.85

Jakob, M., & Hungr, O. (2005). *Debris-flow Hazards and Related Phenomena*. Springer Berlin Heidelberg. https://doi.org/10.1007/b138657

Joshi, V. U., & Tambe, D. T. (2010). Estimation of infiltration rate, run-off and sediment yield under simulated rainfall experiments in upper Pravara Basin, India: Effect of slope angle and grass-cover. *Journal of Earth System Science*, *119*(6), 763–773. https://doi.org/10.1007/s12040-010-0055-0

Jotisankasa, A., Mairaing, W., & Tansamrit, S. (2014). Infiltration and stability of soil slope with vetiver grass subjected to rainfall from numerical modeling. In *Unsaturated Soils: Research & Applications* (pp. 1241–1247). CRC Press. https://doi.org/10.1201/b17034-181

Katritzidakis, M., Liapis, A., Stathakopoulos, I., Pipinis, E., Kekis, G., Ververidou, E., & Sevastou, E. (2007). Erosion control by application of hydroseeding methods along the Egnatia Motorway (Greece). *Eco-and Ground Bio-Engineering: The Use of Vegetation to Improve Slope Stability*, *103*, 393–400. https://doi.org/10.1007/978-1-4020-5593-5_40

Kean, J. W., Staley, D. M., & Cannon, S. H. (2011). In situ measurements of post-fire debris flows in southern California: Comparisons of the timing and magnitude of 24 debris-flow events with rainfall and soil moisture conditions. *J. Geophys. Res.*, *116*(F4), F04019. https://doi.org/10.1029/2011jf002005

Kinnell, P. I. A. (2005). Raindrop-impact-induced erosion processes and prediction: a review. *Hydrological Processes*, *19*(14), 2815–2844. https://doi.org/10.1002/hyp.5788

Kirkham, M. B. (2014). Infiltration. In M. B. Kirkham (Ed.), *Principles of Soil and Plant Water Relations* (2nd ed., pp. 201–227). Elsevier. https://doi.org/10.1016/B978-0-12-420022-7.00013-6

Kjekstad, O., & Highland, L. (2009). Economic and Social Impacts of Landslides. In C. P. Sassa K. (Ed.), *Landslides – Disaster Risk Reduction* (pp. 573–587). Springer Berlin Heidelberg. https://doi.org/10.1007/978-3-540-69970-5_30

Kogelnig, A., Suriñach, E., Vilajosana, I., Hübl, J., Sovilla, B., Hiller, M., & Dufour, F. (2011). On the complementariness of infrasound and seismic sensors for monitoring snow avalanches. *Natural Hazards and Earth System Sciences*, *11*(8), 2355–2370. https://doi.org/10.5194/nhess-11-2355-2011

Le Bissonnais, Y., Lecomte, V., & Cerdan, O. (2004). Grass strip effects on runoff and soil loss. *Agronomie*, *24*(3), 129–136. https://doi.org/10.1051/agro:2004010

Leung, A. K., Garg, A., Coo, J. L., Ng, C. W. W., & Hau, B. C. H. (2015). Effects of the

roots of Cynodon dactylon and Schefflera heptaphylla on water infiltration rate and soil hydraulic conductivity. *Hydrological Processes*, *29*(15), 3342–3354. https://doi.org/10.1002/hyp.10452

Li, A. G., Yue, Z. Q., Tham, L. G., Lee, C. F., & Law, K. T. (2005). Field-monitored variations of soil moisture and matric suction in a saprolite slope. *Canadian Geotechnical Journal*, *42*(1), 13–26. https://doi.org/10.1139/t04-069

Li, J. H., Li, L., Chen, R., & Li, D. Q. (2016). Cracking and vertical preferential flow through landfill clay liners. *Engineering Geology*, *206*, 33–41. https://doi.org/10.1016/j.enggeo.2016.03.006

Lozano-Parra, J., Pulido, M., Lozano-Fondón, C., & Schnabel, S. (2018). How do Soil Moisture and Vegetation Covers Influence Soil Temperature in Drylands of Mediterranean Regions? *Water*, *10*(12), 1747. https://doi.org/10.3390/w10121747

Ludwig, J. A., Wilcox, B. P., Breshears, D. D., Tongway, D. J., & Imeson, A. C. (2005). Vegetation patches and runoff-erosion as interacting ecohydrological processes in semiarid landscapes. *Ecology*, *86*(2), 288–297. https://doi.org/10.1890/03-0569

Luna, B. Q. (2015). *Infiltración de lluvia en un suelo no saturado. Auscultación y simulación numérica en la Cuenca el Rebaixader (Pirineo Central)*. MSc thesis, Universitat Politècnica de Catalunya, Barcelona, Spain, 126 p.

Ma, D. (1994). General study on the development and current situation of glacial debris flow in Guxiang gully, south-east of Tibet. In J. Akamatsu & W. Zhang (Eds.), *Glacier Hazard System in Southeastern Tibet* (pp. 65–73). Disaster Prevention Research Institute, Kyoto Univ.

Maffra, C., Sousa, R., Sutili, F., & Pinheiro, R. (2019). The Effect of Roots on the Shear Strength of Texturally Distinct Soils. *Floresta e Ambiente*, *26*(3). https://doi.org/10.1590/2179-8087.101817

Maksimovic, M. (1989). Nonlinear Failure Envelope for Soils. *Journal of Geotechnical Engineering*, *115*(4), 581–586. https://doi.org/10.1061/(ASCE)0733-9410(1989)115:4(581)

Marchi, L., Arattano, M., & Deganutti, A. M. (2002). Ten years of debris-flow monitoring in the Moscardo Torrent (Italian Alps). *Geomorphology*, *46*(1–2), 1–17. https://doi.org/10.1016/S0169-555X(01)00162-3

Marchi, L., Cazorzi, F., Arattano, M., Cucchiaro, S., Cavalli, M., & Crema, S. (2021). Debris flows recorded in the Moscardo catchment (Italian Alps) between 1990 and 2019. *Natural Hazards and Earth System Sciences*, *21*(1), 87–97. https://doi.org/10.5194/nhess-21-87-2021

Marchi, L., Comiti, F., Arattano, M., Cavalli, M., Macconi, P., & Penna, D. (2012). A new debris-flow monitoring system in an Alpine catchment. *Geophysical Research Abstracts*, *14*, 6104.

Marino, P., Peres, D. J., Cancelliere, A., Greco, R., & Bogaard, T. A. (2020). Soil moisture information can improve shallow landslide forecasting using the hydrometeorological threshold approach. *Landslides*, *17*(9), 2041–2054. https://doi.org/10.1007/s10346-020-01420-8

McArdell, B., & Badoux, A. (2007). Influence of rainfall on the initiation of debris flows at the Illgraben catchment, canton of Valais, Switzerland. *Geophysical Research Abstracts*, *9*, 8804.

McArdell, B., Bartelt, P., & Kowalski, J. (2007). Field observations of basal forces and fluid pore pressure in a debris flow. *Geophysical Research Letters*, *34*(7). https://doi.org/10.1029/2006GL029183

McCoy, S. W., Kean, J. W., Coe, J. A., Staley, D. M., Wasklewicz, T. A., & Tucker, G. E. (2010). Evolution of a natural debris flow: In situ measurements of flow dynamics, video imagery, and terrestrial laser scanning. *Geology*, *38*(8), 735–738. https://doi.org/10.1130/G30928.1

McCoy, S. W., Kean, J. W., Coe, J. A., Tucker, G. E., Staley, D. M., & Wasklewicz, T. A. (2012). Sediment entrainment by debris flows: In situ measurements from the headwaters of a steep catchment. *Journal of Geophysical Research: Earth Surface*, *117*(F3). https://doi.org/10.1029/2011JF002278

McDougall, S. (2017). 2014 Canadian Geotechnical Colloquium: Landslide runout analysis — current practice and challenges. *Canadian Geotechnical Journal*, *54*(5), 605–620. https://doi.org/10.1139/cgj-2016-0104

Mickovski, S. B., Hallett, P. D., Bransby, M. F., Davies, M. C. R., Sonnenberg, R., & Bengough, A. G. (2009). Mechanical Reinforcement of Soil by Willow Roots: Impacts of Root Properties and Root Failure Mechanism. *Soil Science Society of America Journal*, *73*(4), 1276–1285. https://doi.org/10.2136/sssaj2008.0172

Mirus, B. B., Becker, R. E., Baum, R. L., & Smith, J. B. (2018). Integrating real-time subsurface hydrologic monitoring with empirical rainfall thresholds to improve landslide early warning. *Landslides*, *15*(10), 1909–1919. https://doi.org/10.1007/s10346-018-0995-z

Mirus, B. B., Morphew, M. D., & Smith, J. B. (2018). Developing hydro-meteorological thresholds for shallow landslide initiation and early warning. *Water (Switzerland)*, *10*(9), 1–19. https://doi.org/10.3390/W10091274

Moriwaki, H., Inokuchi, T., Hattanji, T., Sassa, K., Ochiai, H., & Wang, G. (2004). Failure processes in a full-scale landslide experiment using a rainfall simulator. *Landslides*, *1*(4), 277–288. https://doi.org/10.1007/s10346-004-0034-0

Mostbauer, K., Kaitna, R., Prenner, D., & Hrachowitz, M. (2018). The temporally varying roles of rainfall, snowmelt and soil moisture for debris flow initiation in a snow-dominated system. *Hydrology and Earth System Sciences*, *22*(6), 3493–3513. https://doi.org/10.5194/hess-22-3493-2018

Muñoz, J. A. (1992). Evolution of a continental collision belt: ECORS-Pyrenees crustal balanced cross-section. In K. R. McClay (Ed.), *Thrust Tectonics* (pp. 235–246). Springer Netherlands. https://doi.org/10.1007/978-94-011-3066-0_21

Navratil, O., Liébault, F., Bellot, H., Theule, J., Travaglini, E., Ravanat, X., Ousset, F., Laigle, D., Segel, V., & Fiquet, M. (2012). High-frequency monitoring of debris flows in the French alps. Preliminary results of a starting program. *INTERPRAEVENT*, 11pp. www.interpraevent.at

Nearing, M. A., Jetten, V., Baffaut, C., Cerdan, O., Couturier, A., Hernandez, M., Le Bissonnais, Y., Nichols, M. H., Nunes, J. P., Renschler, C. S., Souchère, V., & van Oost, K. (2005). Modeling response of soil erosion and runoff to changes in precipitation and cover. *Catena*, *61*(2–3), 131–154. https://doi.org/10.1016/j.catena.2005.03.007

Nearing, M. A., Polyakov, V. O., Nichols, M. H., Hernandez, M., Li, L., Zhao, Y., & Armendariz, G. (2017). Slope–velocity equilibrium and evolution of surface roughness on a stony hillslope. *Hydrology and Earth System Sciences*, *21*(6), 3221–3229. https://doi.org/10.5194/hess-21-3221-2017

Ng, C. W. W., Garg, A., Leung, A. K., & Hau, B. C. H. (2016). Relationships between leaf and root area indices and soil suction induced during drying–wetting cycles. *Ecological Engineering*, *91*, 113–118. https://doi.org/10.1016/j.ecoleng.2016.02.005

Ng, C. W. W., Ni, J. J., & Leung, A. K. (2019). Effects of plant growth and spacing on soil hydrological changes: a field study. *Géotechnique*, 1–15. https://doi.org/10.1680/jgeot.18.P.207

Ng, C. W. W., Springman, S. M., & Alonso, E. E. (2008). Monitoring the Performance of Unsaturated Soil Slopes. *Geotechnical and Geological Engineering*, *26*(6), 799–816. https://doi.org/10.1007/s10706-008-9203-6

Ng, C. W. W., Woon, K. X., Leung, A. K., & Chu, L. M. (2013). Experimental investigation of induced suction distribution in a grass-covered soil. *Ecological Engineering*, *52*, 219–223. https://doi.org/10.1016/j.ecoleng.2012.11.013

Ni, J. J., Leung, A. K., Ng, C. W. W., & Shao, W. (2018). Modelling hydro-mechanical reinforcements of plants to slope stability. *Computers and Geotechnics*, *95*, 99–109. https://doi.org/10.1016/j.compgeo.2017.09.001

Ni, J. J., Leung, A. K., Ng, C. W. W., & So, P. S. (2017). Investigation of plant growth and transpiration-induced matric suction under mixed grass–tree conditions. *Canadian Geotechnical Journal*, *54*(4), 561–573. https://doi.org/10.1139/cgj-2016-0226

Ochsner, T. E., Cosh, M. H., Cuenca, R. H., Dorigo, W. A., Draper, C. S., Hagimoto, Y., Kerr, Y. H., Larson, K. M., Njoku, E. G., Small, E. E., & Zreda, M. (2013). State of the

Art in Large-Scale Soil Moisture Monitoring. *Soil Science Society of America Journal*, *77*(6), 1888–1919. https://doi.org/10.2136/sssaj2013.03.0093

Oliver, S. A., Oliver, H. R., Wallace, J. S., & Roberts, A. M. (1987). Soil heat flux and temperature variation with vegetation, soil type and climate. *Agricultural and Forest Meteorology*, *39*(2–3), 257–269. https://doi.org/10.1016/0168-1923(87)90042-6

Olsson, L., H. Barbosa, S. Bhadwal, A. Cowie, K. Delusca, D. Flores-Renteria, K. Hermans, E. Jobbagy, W. Kurz, D. Li, D.J. Sonwa, L. S. (2019). Land Degredation. In J. M. P.R. Shukla, J. Skea, E. Calvo Buendia, V. Masson-Delmotte, H.-O. Pörtner, D. C. Roberts, P. Zhai, R. Slade, S. Connors, R. van Diemen, M. Ferrat, E. Haughey, S. Luz, S. Neogi, M. Pathak, J. Petzold, J. Portugal Pereira, P. Vyas, E. Huntley, K. Kissick, M (Ed.), *Climate Change and Land: an IPCC special report on climate change, desertification, land degradation, sustainable land management, food security, and greenhouse gas fluxes in terrestrial ecosystems* (In Press, pp. 345–436).

Oorthuis, R., Hürlimann, M., Abancó, C., Moya, J., & Carleo, L. (2021). Monitoring of Rainfall and Soil Moisture at the Rebaixader Catchment (Central Pyrenees). *Environmental and Engineering Geoscience*, *27*(2), 221–229. https://doi.org/10.2113/EEG-D-20-00012

Oorthuis, R., Hürlimann, M., Fraccica, A., Lloret, A., Moya, J., Puig-Polo, C., & Vaunat, J. (2018). Monitoring of a Full-Scale Embankment Experiment Regarding Soil–Vegetation–Atmosphere Interactions. *Water*, *10*(6), 688. https://doi.org/10.3390/w10060688

P. Orense, R., Shimoma, S., Maeda, K., & Towhata, I. (2004). Instrumented Model Slope Failure due to Water Seepage. *Journal of Natural Disaster Science*, *26*(1), 15–26. https://doi.org/10.2328/jnds.26.15

Pagano, L., Reder, A., & Rianna, G. (2019). Effects of vegetation on hydrological response of silty volcanic covers. *Canadian Geotechnical Journal*, *56*(9), 1261–1277. https://doi.org/10.1139/cgj-2017-0625

Palau, R. M., Hürlimann, M., Pinyol, J., Moya, J., Victoriano, A., Génova, M., & Puig-Polo,

C. (2017). Recent debris flows in the Portainé catchment (Eastern Pyrenees, Spain): analysis of monitoring and field data focussing on the 2015 event. *Landslides*, *14*(3), 1161–1170. https://doi.org/10.1007/s10346-017-0832-9

Panagos, P., Meusburger, K., Ballabio, C., Borrelli, P., & Alewell, C. (2014). Soil erodibility in Europe: A high-resolution dataset based on LUCAS. *Science of The Total Environment*, *479–480*, 189–200. https://doi.org/10.1016/j.scitotenv.2014.02.010

Pastorello, R., D'Agostino, V., & Hürlimann, M. (2020). Debris flow triggering characterization through a comparative analysis among different mountain catchments. *CATENA*, *186*, 104348. https://doi.org/10.1016/j.catena.2019.104348

Pathirage, U., Indraratna, B., Pallewattha, M., & Heitor, A. (2019). A theoretical model for total suction effects by tree roots. *Environmental Geotechnics*, *6*(6), 353–360. https://doi.org/10.1680/jenge.15.00065

Peres, D. J., & Cancelliere, A. (2014). Derivation and evaluation of landslide-triggering thresholds by a Monte Carlo approach. *Hydrology and Earth System Sciences*, *18*(12), 4913–4931. https://doi.org/10.5194/hess-18-4913-2014

Peres, D. J., Cancelliere, A., Greco, R., & Bogaard, T. A. (2018). Influence of uncertain identification of triggering rainfall on the assessment of landslide early warning thresholds. *Natural Hazards and Earth System Sciences*, *18*(2), 633–646. https://doi.org/10.5194/nhess-18-633-2018

Petley, D. (2012). Global patterns of loss of life from landslides. *Geology*, *40*(10), 927–930. https://doi.org/10.1130/G33217.1

Pierson, T. C. (1980). Erosion and deposition by debris flows at Mt Thomas, North Canterbury, New Zealand. *Earth Surface Processes*, *5*(3), 227–247. https://doi.org/10.1002/esp.3760050302

Pinyol, J., Hürlimann, M., Furdada, G., Moysset, M., Palau, R. M., Victoriano, A., González, M., Moya, J., Guinau, M., Raïmat, C., & Fañanás, C. (2017). El barranco de Portainé (Pirineo Central): un laboratorio in situ completo para el estudio de la actividad torrencial. In E. Alonso, J. Corominas, & M. Hürlimann (Eds.), *IX Simposio Nacional*

sobre Taludes y Laderas Inestables (pp. 1165–1176). CIMNE, Barcelona.

Pollen-Bankhead, N., & Simon, A. (2010). Hydrologic and hydraulic effects of riparian root networks on streambank stability: Is mechanical root-reinforcement the whole story? *Geomorphology*, *116*(3–4), 353–362. https://doi.org/10.1016/j.geomorph.2009.11.013

Ponziani, F., Pandolfo, C., Stelluti, M., Berni, N., Brocca, L., & Moramarco, T. (2012). Assessment of rainfall thresholds and soil moisture modeling for operational hydrogeological risk prevention in the Umbria region (central Italy). *Landslides*, *9*(2), 229–237. https://doi.org/10.1007/s10346-011-0287-3

Portilla, M., Chevalier, G., & Hürlimann, M. (2010). Description and analysis of the debris flows occurred during 2008 in the Eastern Pyrenees. *Natural Hazards and Earth System Science*, *10*(7), 1635–1645. https://doi.org/10.5194/nhess-10-1635-2010

Prenner, D., Hrachowitz, M., & Kaitna, R. (2019). Trigger characteristics of torrential flows from high to low alpine regions in Austria. *Science of The Total Environment*, *658*, 958–972. https://doi.org/10.1016/j.scitotenv.2018.12.206

Preti, F., & Giadrossich, F. (2009). Root reinforcement and slope bioengineering stabilization by Spanish Broom (Spartium junceum L.). *Hydrology and Earth System Sciences*, *13*, 1713–1726. https://doi.org/10.5194/hessd-6-3993-2009

Rahardjo, H., Leong, E. C., & Rezaur, R. B. (2008). Effect of antecedent rainfall on pore-water pressure distribution characteristics in residual soil slopes under tropical rainfall. *Hydrological Processes*, *22*(4), 506–523. https://doi.org/10.1002/hyp.6880

Rahardjo, H., Lim, T. T., Chang, M. F., & Fredlund, D. G. (1995). Shear-strength characteristics of a residual soil. *Canadian Geotechnical Journal*, *32*(1), 60–77. https://doi.org/10.1139/t95-005

Rahardjo, H., Rezaur, R. B., Leong, E. C., Alonso, E. E., Lloret, A., & Gens, A. (2008). Monitoring and modeling of slope response to climate changes. In C. Press (Ed.), *Landslides and Engineered Slopes. From the Past to the Future, Two Volumes + CD-ROM* (Issue 1996, pp. 89–106). CRC Press. https://doi.org/10.1201/9780203885284-8

Rahardjo, H., Satyanaga, A., & Leong, E. C. (2012). Unsaturated soil mechanics for slope stabilization. *Geotechnical Engineering Journal of the SEAGS & AGSSEA*, *43*(1), 48–58.

Rahardjo, H., Satyanaga, A., Leong, E. C., Santoso, V. A., & Ng, Y. S. (2014). Performance of an instrumented slope covered with shrubs and deep-rooted grass. *Soils and Foundations*, *54*(3), 417–425. https://doi.org/10.1016/j.sandf.2014.04.010

Raïmat, C. (2018). *Dinámica y peligrosidad de las corrientes de derrubios: aplicación en el barranco de Erill, Pirineo catalán.* PhD thesis, Universitat Politècnica de Catalunya, Barcelona, Spain, 509 p. http://hdl.handle.net/2117/121043

Ran, Q., Su, D., Li, P., & He, Z. (2012). Experimental study of the impact of rainfall characteristics on runoff generation and soil erosion. *Journal of Hydrology*, *424–425*, 99–111. https://doi.org/10.1016/j.jhydrol.2011.12.035

Remondo, J., Bonachea, J., & Cendrero, A. (2008). Quantitative landslide risk assessment and mapping on the basis of recent occurrences. *Geomorphology*, *94*(3–4), 496–507. https://doi.org/10.1016/j.geomorph.2006.10.041

Rivas, V., Remondo, J., Bonachea, J., & Sánchez-Espeso, J. (2020). Rainfall and weather conditions inducing intense landslide activity in northern Spain (Deba, Guipúzcoa). *Physical Geography*, *February*, 1–21. https://doi.org/10.1080/02723646.2020.1866790

Saco, P. M., Willgoose, G. R., & Hancock, G. R. (2007). Eco-geomorphology of banded vegetation patterns in arid and semi-arid regions. *Hydrology and Earth System Sciences*, *11*(6), 1717–1730. https://doi.org/10.5194/hess-11-1717-2007

Saito, T., & Rehmsmeier, M. (2015). The Precision-Recall Plot Is More Informative than the ROC Plot When Evaluating Binary Classifiers on Imbalanced Datasets. *PLoS ONE*, *10*(3), e0118432. https://doi.org/10.1371/journal.pone.0118432

Sajjan, A. K., Gyasi-Agyei, Y., & Sharma, R. H. (2013). Rainfall–runoff modelling of railway embankment steep slopes. *Hydrological Sciences Journal*, *58*(5), 1162–1176. https://doi.org/10.1080/02626667.2013.802323

Sakai, M., Jones, S. B., & Tuller, M. (2011). Numerical evaluation of subsurface soil water evaporation derived from sensible heat balance. *Water Resources Research*, *47*(2), 1–17. https://doi.org/10.1029/2010WR009866

Sánchez Castilla, M. (2004). *Thermo-Hydro-Mechanical Coupled Analysis in Low Permeability Media*. PhD thesis, Universitat Politècnica de Catalunya, Barcelona, Spain, 304p. http://hdl.handle.net/10803/405514

Sättele, M., Bründl, M., & Straub, D. (2015). Reliability and effectiveness of early warning systems for natural hazards: Concept and application to debris flow warning. *Reliability Engineering & System Safety*, *142*, 192–202. https://doi.org/10.1016/j.ress.2015.05.003

Sättele, M., Bründl, M., & Straub, D. (2012). Classification of warning systems for natural hazards. In C. Moormann, M. Huber, & D. Proske (Eds.), *Proceedings of the 10th International Probabilistic Workshop* (Issue November 2014, pp. 257–270). Institut für Geotechnik der Universitt Stuttgart. https://books.google.co.id/books/about/Proceedings_of_the_10th_International_Pr.html?id=m1oukgEACAAJ&redir_esc=y

Sauer, T. J., & Horton, R. (2015). Soil Heat Flux. In *Micrometeorology in Agricultural Systems. Agronomy Monograph no. 47* (pp. 131–154). https://doi.org/10.2134/agronmonogr47.c7

Scheevel, C. R., Baum, R. L., Mirus, B. B., & Smith, J. B. (2017). *Precipitation thresholds for landslide occurrence near Seattle, Mukilteo, and Everett, Washington: U.S. Geological Survey Open-File Report 2017–1039*. https://doi.org/10.3133/ofr20171039

Schenk, H. J., & Jackson, R. B. (2002). The global biogeography of roots. *Ecological Monographs*, *72*(3), 311–328. https://doi.org/10.1890/0012-9615(2002)072

Schmidt, K., Roering, J., Stock, J. D., Dietrich, W. E., Montgomery, D. R., & Schaub, T. (2001). The variability of root cohesion as an influence on shallow landslide susceptibility in the Oregon Coast Range. *Canadian Geotechnical Journal*, *38*(5), 995–1024. https://doi.org/10.1139/cgj-38-5-995

Schöffl, T., Koschuch, R., Jocham, P., & Hübl, J. (2021). Application of a combined and

automated monitoring and early warning system for debris flows at the Dawinbach. *EGU General Assembly 2021*, *Online*, EGU21-10280. https://doi.org/10.5194/egusphere-egu21-10280

Schrefler, B. A. (1984). *The finite element method in soil consolidation (with applications to surface subsidence)*. University College of Swansea.

Schuster, R. L., & Highland, L. M. (2001). Socioeconomic and environmental impacts of landslides in the Western Hemisphere. In *U.S. Geological Survey* (Issue August). https://doi.org/10.3133/ofr01276

Scott, K. M., & Yuyi, W. (2004). Debris flows: geologic process and hazard, illustrated by a surge sequence at Jiangjia Ravine, Yunnan, China. *USGS Professional Paper*, *1671*, 1–20. https://doi.org/10.3133/pp1671

Scotton, P., Genevois, R., Moro, F., Zorzi, L., Girardi, G., & Praticelli, N. (2011). The debris-flows monitoring system of acquabona torrent (Cortina d'Ampezzo, Belluno, Italy). In R. Genevois, D. Hamilton, & A. Prestininzi (Eds.), *5th Int. Conf. on Debris-Flow Hazards Mitigation* (pp. 595–603). https://doi.org/10.4408/IJEGE.2011-03.B-065

Segoni, S., Piciullo, L., & Gariano, S. L. (2018). Preface: Landslide early warning systems: monitoring systems, rainfall thresholds, warning models, performance evaluation and risk perception. *Natural Hazards and Earth System Sciences*, *18*(12), 3179–3186. https://doi.org/10.5194/nhess-18-3179-2018

Sidle, R. C., & Bogaard, T. A. (2016). Dynamic earth system and ecological controls of rainfall-initiated landslides. *Earth-Science Reviews*, *159*, 275–291. https://doi.org/10.1016/j.earscirev.2016.05.013

Simon, A., & Collison, A. J. C. (2002). Quantifying the mechanical and hydrologic effects of riparian vegetation on streambank stability. *Earth Surface Processes and Landforms*, *27*(5), 527–546. https://doi.org/10.1002/esp.325

Simoni, A., Bernard, M., Berti, M., Boreggio, M., Lanzoni, S., Stancanelli, L. M., & Gregoretti, C. (2020). Runoff-generated debris flows: Observation of initiation conditions and erosion–deposition dynamics along the channel at Cancia (eastern Italian

Alps). *Earth Surface Processes and Landforms*, *45*(14), 3556–3571. https://doi.org/10.1002/esp.4981

Skempton, A. W. (1964). Long-Term Stability of Clay Slopes. *Géotechnique*, *14*(2), 77–102. https://doi.org/10.1680/geot.1964.14.2.77

Smethurst, J. A., Clarke, D., & Powrie, W. (2012). Factors controlling the seasonal variation in soil water content and pore water pressures within a lightly vegetated clay slope. *Géotechnique*, *62*(5), 429–446. https://doi.org/10.1680/geot.10.P.097

Song, L., Li, J. H., Zhou, T., & Fredlund, D. G. (2017). Experimental study on unsaturated hydraulic properties of vegetated soil. *Ecological Engineering*, *103*(June 2017), 207–216. https://doi.org/10.1016/j.ecoleng.2017.04.013

Spiker, E. C., & Gori, P. L. (2003). National landslide hazards mitigation strategy: a framework for loss reduction. In *USGS Numbered Series, Circular1244*. https://doi.org/10.3133/cir1244

Springman, S. M., Jommi, C., & Teysseire, P. (2003). Instabilities on moraine slopes induced by loss of suction: a case history. *Géotechnique*, *53*(1), 3–10. https://doi.org/10.1680/geot.2003.53.1.3

Stoffel, M., Tiranti, D., & Huggel, C. (2014). Climate change impacts on mass movements - Case studies from the European Alps. *Science of the Total Environment*, *493*, 1255–1266. https://doi.org/10.1016/j.scitotenv.2014.02.102

Sun, Q., Miao, C., Duan, Q., Ashouri, H., Sorooshian, S., & Hsu, K. (2018). A Review of Global Precipitation Data Sets: Data Sources, Estimation, and Intercomparisons. *Reviews of Geophysics*, *56*(1), 79–107. https://doi.org/10.1002/2017RG000574

Suwa, H., Okano, K., & Kanno, T. (2009). Behavior of debris flows monitored on test slopes of Kamikamihorizawa Creek, Mount Yakedake, Japan. *International Journal of Erosion Control Engineering*, *2*(2), 33–45. https://doi.org/10.13101/ijece.2.33

Takahashi, T. (1981). Debris Flow. *Annual Review of Fluid Mechanics*, *13*(1), 57–77. https://doi.org/10.1146/annurev.fl.13.010181.000421

Takahashi, T. (2007). *Debris Flow: Mechanics, Prediction and Countermeasures*. Taylor & Francis Group.

Takahashi, T. (2014). *Debris Flow. Mechanics, Prediction and Countermeasures, 2nd edition*. CRC Press. https://doi.org/10.1201/b16647

Takeshi, T. (2011). Evolution of Debris-flow Monitoring Methods on Sakurajima. *International Journal of Erosion Control Engineering*, *4*(1), 21–31. https://doi.org/10.13101/ijece.4.21

Tang, A. M., Hughes, P. N., Dijkstra, T. A., Askarinejad, A., Brenčič, M., Cui, Y. J., Diez, J. J., Firgi, T., Gajewska, B., Gentile, F., Grossi, G., Jommi, C., Kehagia, F., Koda, E., ter Maat, H. W., Lenart, S., Lourenco, S., Oliveira, M., Osinski, P., … Van Beek, V. (2018). Atmosphere–vegetation–soil interactions in a climate change context; impact of changing conditions on engineered transport infrastructure slopes in Europe. *Quarterly Journal of Engineering Geology and Hydrogeology*, *51*(2), 156–168. https://doi.org/10.1144/qjegh2017-103

Tecca, P. R., Galgaro, A., Genevois, R., & Deganutti, A. M. (2003). Development of a remotely controlled debris flow monitoring system in the Dolomites (Acquabona, Italy). *Hydrological Processes*, *17*(9), 1771–1784. https://doi.org/10.1002/hyp.1212

Tohari, A., Nishigaki, M., & Komatsu, M. (2007). Laboratory Rainfall-Induced Slope Failure with Moisture Content Measurement. *Journal of Geotechnical and Geoenvironmental Engineering*, *133*(5), 575–587. https://doi.org/10.1061/(ASCE)1090-0241(2007)133:5(575)

Tsiampousi, A., Zdravkovic, L., & Potts, D. M. (2016). Soil-atmosphere interaction in unsaturated cut slopes. *E3S Web of Conferences*, *9*, 08004. https://doi.org/10.1051/e3sconf/20160908004

Tsunetaka, H., Shinohara, Y., Hotta, N., Gomez, C., & Sakai, Y. (2021). Multi-decadal changes in the relationships between rainfall characteristics and debris-flow occurrences in response to gully evolution after the 1990–1995 Mount Unzen eruptions. *Earth Surface Processes and Landforms*, *46*(11), 2141–2162.

https://doi.org/10.1002/esp.5148

Turconi, L., Coviello, V., Arattano, M., Savio, G., & Tropeano, D. (2015). Monitoring Mud-Flows for Investigative and Warning Purposes: The Instrumented Catchment of Rio Marderello (North-Western Italy). In G. Lollino, M. Arattano, M. Rinaldi, O. Giustolisi, J. Marechal, & G. Grant (Eds.), *Engineering Geology for Society and Territory - Volume 3* (Issue September, pp. 85–90). Springer International Publishing. https://doi.org/10.1007/978-3-319-09054-2_17

Underwood, S. J., Schultz, M. D., Berti, M., Gregoretti, C., Simoni, A., Mote, T. L., & Saylor, A. M. (2016). Atmospheric circulation patterns, cloud-to-ground lightning, and locally intense convective rainfall associated with debris flow initiation in the Dolomite Alps of northeastern Italy. *Natural Hazards and Earth System Sciences*, *16*(2), 509–528. https://doi.org/10.5194/nhess-16-509-2016

United Nations International Strategy for Disaster Reduction (UN/ISDR). (2006). Developing Early Warning Systems: A Checklist. *Third International Conference on Early Warning (EWC III), March*, 1–13. Retrieved October 18, 2021, from https://www.unisdr.org/2006/ppew/info-resources/ewc3/checklist/English.pdf

Vaezi, A. R., Ahmadi, M., & Cerdà, A. (2017). Contribution of raindrop impact to the change of soil physical properties and water erosion under semi-arid rainfalls. *Science of The Total Environment*, *583*, 382–392. https://doi.org/https://doi.org/10.1016/j.scitotenv.2017.01.078

Valenzuela, P., Domínguez-Cuesta, M. J., Mora García, M. A., & Jiménez-Sánchez, M. (2018). Rainfall thresholds for the triggering of landslides considering previous soil moisture conditions (Asturias, NW Spain). *Landslides*, *15*(2), 273–282. https://doi.org/10.1007/s10346-017-0878-8

van Beek, R., Cammeraat, E., Andreu, V., Mickovski, S. B., & Dorren, L. (2008). Hillslope Processes: Mass Wasting, Slope Stability and Erosion. In Norris J.E. et al. (Ed.), *Slope Stability and Erosion Control: Ecotechnological Solutions* (pp. 17–64). Springer Netherlands. https://doi.org/10.1007/978-1-4020-6676-4_3

Vanapalli, S. K., Fredlund, D. G., Pufahl, D. E., & Clifton, A. W. (1996). Model for the prediction of shear strength with respect to soil suction. *Canadian Geotechnical Journal*, *33*(3), 379–392. https://doi.org/10.1139/t96-060

Vardon, P. J. (2015). Climatic influence on geotechnical infrastructure: a review. *Environmental Geotechnics*, *2*(3), 166–174. https://doi.org/10.1680/envgeo.13.00055

Vergani, C., & Graf, F. (2016). Soil permeability, aggregate stability and root growth: a pot experiment from a soil bioengineering perspective. *Ecohydrology*, *9*(5), 830–842. https://doi.org/10.1002/eco.1686

Walker, J. P., Willgoose, G. R., & Kalma, J. D. (2004). In situ measurement of soil moisture: a comparison of techniques. *Journal of Hydrology*, *293*(1–4), 85–99. https://doi.org/10.1016/j.jhydrol.2004.01.008

Wallemacq, P. (2018). *UNISDR and CRED report: Economic Losses, Poverty and Disasters 1998-2017*. https://doi.org/10.13140/RG.2.2.35610.08643

Wang, Y., Liu, Y., & Jin, J. (2018). Contrast Effects of Vegetation Cover Change on Evapotranspiration during a Revegetation Period in the Poyang Lake Basin, China. *Forests*, *9*(4), 217. https://doi.org/10.3390/f9040217

Weiss, G. M. (2013). Foundations of Imbalanced Learning. In Y. M. Haibo He (Ed.), *Imbalanced Learning: Foundations, Algorithms, and Applications* (pp. 13–41). John Wiley & Sons, Inc. https://doi.org/10.1002/9781118646106.ch2

Wieczorek, G. F. (1996). Landslide Triggering Mechanisms. In R. L. Turner, A.K. and Schuster (Ed.), *Landslides: Investigation and Mitigation. Transportation Research Board Special Report* (Special Re, pp. 76–90). National Research Council.

Wieczorek, G. F., & Glade, T. (2005). Climatic factors influencing occurrence of debris flows. In M. Jakob & O. Hungr (Eds.), *Debris-flow Hazards and Related Phenomena* (Issue February, pp. 325–362). Springer Berlin Heidelberg. https://doi.org/10.1007/3-540-27129-5_14

Wilman, D., Gao, Y., & Leitch, M. H. (1998). Some differences between eight grasses within

the Lolium-Festuca complex when grown in conditions of severe water shortage. *Grass and Forage Science*, *53*(1), 57–65. https://doi.org/10.1046/j.1365-2494.1998.00104.x

Wu, W., Switala, B. M., Acharya, M. S., Tamagnini, R., Auer, M., Graf, F., te Kamp, L., & Xiang, W. (2015). Effect of Vegetation on Stability of Soil Slopes: Numerical Aspect. In W. Wu (Ed.), *Springer Series in Geomechanics and Geoengineering* (Vol. 2015, Issue June, pp. 163–177). Springer International Publishing. https://doi.org/10.1007/978-3-319-11053-0_15

Xue, J., & Gavin, K. (2008). Effect of Rainfall Intensity on Infiltration into Partly Saturated Slopes. *Geotechnical and Geological Engineering*, *26*(2), 199–209. https://doi.org/10.1007/s10706-007-9157-0

Yildiz, A., Graf, F., Rickli, C., & Springman, S. M. (2019). Assessment of plant-induced suction and its effects on the shear strength of rooted soils. *Proceedings of the Institution of Civil Engineers - Geotechnical Engineering*, *172*(6), 507–519. https://doi.org/10.1680/jgeen.18.00209

Yin, H. Y., Huang, C. J., Fang, Y. M., Lee, B. J., Chou, T. Y., Chen, C. Y., Fang, Y. M., Lee, B. J., & Chou, T. Y. (2011). The present development of debris flow monitoring technology in Taiwan - A case study presentation. In R. Genevois, D. Hamilton, & A. Prestininzi (Eds.), *5th International Conference on Debris-Flow Hazard Mitigation: Mechanics, Prediction, and Assessment* (pp. 623–631). https://doi.org/10.4408/IJEGE.2011-03.B-068

Yoshioka, M., Takakura, S., Ishizawa, T., & Sakai, N. (2015). Temporal changes of soil temperature with soil water content in an embankment slope during controlled artificial rainfall experiments. *Journal of Applied Geophysics*, *114*, 134–145. https://doi.org/10.1016/j.jappgeo.2015.01.009

Zha, T., Barr, A. G., van der Kamp, G., Black, T. A., McCaughey, J. H., & Flanagan, L. B. (2010). Interannual variation of evapotranspiration from forest and grassland ecosystems in western canada in relation to drought. *Agricultural and Forest Meteorology*, *150*(11), 1476–1484. https://doi.org/10.1016/j.agrformet.2010.08.003

Zhang, J., Lu, M., Zhang, L., & Xue, Y. (2021). Assessing indirect economic losses of landslides along highways. *Natural Hazards*, *106*(3), 2775–2796. https://doi.org/10.1007/s11069-021-04566-3

Zhang, M., Chen, F. Q., & Zhang, J. X. (2013). The Temporal Dynamics of Cynodon Dactylon Soil - Root System in Soil Conservation and Slope Reinforcement. *Advanced Materials Research*, *838–841*, 675–679. https://doi.org/10.4028/www.scientific.net/AMR.838-841.675

Zhao, B., Dai, Q., Han, D., Zhang, J., Zhuo, L., & Berti, M. (2020). Application of hydrological model simulations in landslide predictions. *Landslides*, *17*(4), 877–891. https://doi.org/10.1007/s10346-019-01296-3

Zhao, Q., Zhang, Y., Xu, S., Ji, X., Wang, S., & Ding, S. (2019). Relationships between Riparian Vegetation Pattern and the Hydraulic Characteristics of Upslope Runoff. *Sustainability*, *11*(10), 2966. https://doi.org/10.3390/su11102966

Zhao, S., Yang, Y., Qiu, G., Qin, Q., Yao, Y., Xiong, Y., & Li, C. (2010). Remote detection of bare soil moisture using a surface-temperature-based soil evaporation transfer coefficient. *International Journal of Applied Earth Observation and Geoinformation*, *12*(5), 351–358. https://doi.org/10.1016/j.jag.2010.04.007

Zhu, H., & Zhang, L. M. (2015). Evaluating suction profile in a vegetated slope considering uncertainty in transpiration. *Computers and Geotechnics*, *63*, 112–120. https://doi.org/10.1016/j.compgeo.2014.09.003

LIST OF PUBLICATIONS

The thesis contributed in several workshops, conferences and international ranked journals (chronologically listed):

Workshops and conference publications

Oorthuis, R., Hürlimann, M., Moya, J., & Vaunat, J. (2017). In-situ monitoring of slope mass-wasting. Examples from the Pyrenees. In E. Alonso & N. Pinyol (Eds.), *First JTC1 Workshop on Advances in Landslide Understanding*, *4*. International Center for Numerical Methods in Engineering (CIMNE), 24–26 May 2017 Barcelona, Spain. https://hdl.handle.net/2117/108777

Hürlimann, M., Vaunat, J., Oorthuis, R., Lloret, A., Moya, J., Puig-Polo, C., Fraccica, A., Gonzalez, M., Pinyol, J., Buill, F., Nuñez-Andrés, A., Romero, E., Abancó, C., Martínez, J., Raïmat, C., & Copons, R. (2017). Pérdida de suelo en laderas bajo cambio climático. Estrategias de mitigación - El proyecto de investigación "SMUCPHY". In E. Alonso, J. Corominas, & M. Hürlimann (Eds.), *IX Simposio Nacional sobre Taludes y Laderas Inestables* (pp. 1200–1211). International Center for Numerical Methods in Engineering (CIMNE), 27–30 June 2017, Santander, Spain. https://hdl.handle.net/2117/106105

Hürlimann, M., Oorthuis, R., Fraccica, A., Shu, H., Palau, R. M., Vaunat, J., Moya, J., Lloret, A., Puig, C., González, M., & Pinyol, J. (2018). Multi-scale analysis of slope-mass wasting under climate change: from laboratory tests to regional assessment in the Pyrenees. *EGU General Assembly 2018: Geophysical Research Abstracts*, *20*, EGU2018-444, 8–13 April 2018, Vienna, Austria. https://meetingorganizer.copernicus.org/EGU2018/EGU2018-4444.pdf

Oorthuis, R., Hürlimann, M., Shu, H., Puig-Polo, C., Fraccica, A., Moya, J., Vaunat, J., González, M., & Pinyol, J. (2019). Effect of land cover and climate change on slope mass-wasting at different scales. Preliminary results from a multidisciplinary project in the Pyrenees (Spain). Symposium on *Climate Change and Natural Hazards: Coping with and Managing Hazards in the Context of a Changing Climate*, 1, 25–26 February 2019, Padova, Italy.

Hürlimann, M., Oorthuis, R., Abancó, C., Carleo, L., & Moya, J. (2019). Monitoring of rainfall and soil moisture at the Rebaixader catchment (Central Pyrenees). 7th International Conference on Debris-Flow Hazards Mitigation, 7, 10–13 June 2019, Colorado, USA. https://doi.org/10.25676/11124/173227

Oorthuis, R., Hürlimann, M., Vaunat, J., Lloret, A., Moya, J., Puig-Polo, C., & Fraccica, A. (2019). Influence of orientation and vegetation cover on soil thermo-hydraulic behaviour: a monitored embankment study. *Multi-Scale Analysis of Slope under Climate Change. A Cross Disciplinary Workshop – MUSLOC 2019* -, 19–20 September 2019, Barcelona, Spain. https://congress.cimne.com/MUSLOC2019/admin/files/fileabstract/a528.pdf

Oorthuis, R., Hürlimann, M., Abancó, C., Moya, J., Lloret, A., & Vaunat, J. (2020). Rainfall and soil moisture conditions for the triggering of torrential flows at the Rebaixader catchment (Central Pyrenees). *EGU General Assembly 2020: Online*, 4–8 May 2020, EGU2020-427. https://doi.org/10.5194/egusphere-egu2020-427

Oorthuis, R., Vaunat, J., Hürlimann, M., Lloret, A., Moya, J., Puig-Polo, C., & Fraccica, A. (2021). Effect of vegetation and slope orientation on water infiltration in a monitored embankment. *EGU General Assembly 2021: Online*, 19–30 April 2021, EGU21-7599. https://doi.org/10.5194/egusphere-egu21-7599

Publications in ranked international journals

Oorthuis, R., Hürlimann, M., Fraccica, A., Lloret, A., Moya, J., Puig-Polo, C., & Vaunat, J. (2018). Monitoring of a Full-Scale Embankment Experiment Regarding Soil–

Vegetation–Atmosphere Interactions. *Water*, *10*(6), 688. https://doi.org/10.3390/w10060688

Oorthuis, R., Vaunat, J., Hürlimann, M., Lloret, A., Moya, J., Puig-Polo, C., & Fraccica, A. (2020). Slope Orientation and Vegetation Effects on Soil Thermo-Hydraulic Behavior. An Experimental Study. *Sustainability*, *13*(1), 14. https://doi.org/10.3390/su13010014

Oorthuis, R., Hürlimann, M., Abancó, C., Moya, J., & Carleo, L. (2021). Monitoring of Rainfall and Soil Moisture at the Rebaixader Catchment (Central Pyrenees). *Environmental and Engineering Geoscience*, *27*(2), 221–229. https://doi.org/10.2113/EEG-D-20-00012

Articles pending of publication

Oorthuis, R., Hürlimann, M., Vaunat, J., Moya, J., & Lloret, T. Monitoring the role of soil hydrologic conditions and rainfall for the triggering of torrential flows in the Rebaixader catchment (Central Pyrenees, Spain).